

NORTHWESTERN UNIVERSITY

**Using Predictive Models in Engineering Design: Metamodeling,
Uncertainty Quantification, and Model Validation**

A DISSERTATION

**SUBMITTED TO THE GRADUATE SCHOOL
IN PARTIAL FULFILLMENT OF THE REQUIREMENTS**

for the degree

DOCTOR OF PHILOSOPHY

Field of Mechanical Engineering

By

Ying Xiong

EVANSTON, ILLINOIS

November 2008

© Copyright by Ying Xiong 2008
All Rights Reserved

ABSTRACT

Using Predictive Models in Engineering Design: Metamodeling, Uncertainty Quantification, and Model Validation

Ying Xiong

Predictive modeling has emerged as a new research subject that studies a broad range of modeling techniques to provide confident prediction of the phenomenon of interest by integrating scientific principles together with both computer models and observed physical experiments. Motivated by overcoming the existing challenges, the objective in this dissertation is to develop methodology and techniques to facilitate the use of predictive models in engineering design.

To develop an improved metamodeling technique that better captures changing smoothness behavior in high-dimensional engineering applications, a Kriging method with sparse yet flexible parameterization of non-stationary covariance is investigated.

To efficiently yield an improved predictive model, a bias-correction approach is examined considering two scenarios by combining either computer and physical experimental data or data from variable fidelity computer models. A Bayesian approach is applied to the Gaussian process model to assess the uncertainty of the bias-corrected model.

To achieve a better understanding of the various model updating strategies, we examine different model updating formulations as well as different solution methods. As opposed to traditional calibration approaches we pay particular attention to the situations in which certain computer model parameters vary from trial to trial. A maximum likelihood estimation approach

for parameter estimation s developed toward the best agreement between physical and computer observations.

Motivated by the need for validating predictive models in engineering design, a design-driven Bayesian model validation procedure is employed. With the quantified uncertainty of Bayesian prediction models, decision validation metrics are proposed to provide confidence measures in making a design choice.

To facilitate resource allocation in updating a predictive model, a new objective oriented sequential sampling approach is developed for computer experiments, by employing a periodical switching criterion in sampling for balancing the needs of optimizing a design objective versus reducing the metamodel uncertainty. A design confidence metric is proposed as the stopping criterion to facilitate design decision making.

Through various example problems, it is illustrated that the research developments in this dissertation are applicable to various engineering applications, thus providing useful techniques in metamodeling, uncertainty quantification, and model validation that are critical to using predictive models in engineering design.

ACKNOWLEDGEMENT

First, I would like to express my sincere and the greatest thanks to my advisor, Professor Wei Chen, for providing me with her guidance, extensive support, inspiration, and encouragement throughout my Ph.D. study and life at Northwestern University. She is one of the most outstanding advisors, active researchers, and excellent teachers I have ever known. I owe my special gratitude to Dr. Chen.

I am very thankful to my committee members: Professor Daniel Apley, Professor Kornel Ehmann, for their suggestions and contributions to my PhD research. I also owe my gratitude to Professor Kwok-Leung Tsui at Georgia Institute of Technology for his ongoing help and valuable advice during the past three years while working collaboratively on the research topics of sequential sampling, model updating, and model validation.

I am grateful to my great colleagues at the Integrated DEsign Automation Laboratory (IDEAL). Many thanks go to Dr. Huibin Liu (now working in BD Medical), Dr. Deepak Kumar Dileep Kumar (now working in Google), Mr. Xiaolei Yin, Mr. Chris Hoyle, Dr. Sanghoon Lee, Mr. Shikui Chen, Ms. Lin He, Ms. Fenfeng Xiong, Professor Hongzhong Huang, for their valuable discussions, advice, and help from various aspects. I enjoyed the friendly and collaborative environment in the IDEAL. This research was supported by the US National Science Foundation (NSF). The supports are gratefully acknowledged. I would also like to thank all the staff in the Department of Mechanical Engineering at Northwestern University for always being very friendly and helpful.

I am also very grateful to Dr. Xuru Ding in General Motors for providing simulation data of a vehicle crash model and co-authoring the paper on non-stationary Kriging method. The exposure to real industry problems through this collaboration were valuable experiences.

Finally, I am most grateful to my parents, my elder brother, and my parents-in-law for all they have done for me. They always encourage me to go after my dreams. I cannot imagine finishing my graduate study without their constant support. I also would like to thank my wife Lulu for her love, understanding, and support throughout my graduate study. Her encouragements always give me the confidence to continue to pursue my goals.

DEDICATION

This dissertation is dedicated to my parents Dawu Xiong and Chenghua Liu.

TABLE OF CONTENTS

CHAPTER 1. INTRODUCTION.....	12
1.1 Research Motivation.....	12
1.2 Predictive Modeling and Research Issues.....	14
1.3 Dissertation Outline	22
CHAPTER 2. TECHNICAL BACKGROUND	24
Nomenclature	24
2.1 Introduction.....	25
2.2 Kriging Techniques for Metamodeling.....	25
2.2.1 Overview of Kriging Techniques.....	25
2.2.2 Bayesian Interpretation of the Kriging Method.....	27
2.2.3 Determination of hyperparameters in Kriging model.....	29
2.2.4 General Bayesian Analysis of Kriging metamodeling.....	33
2.3 Optimal Design of Computer Experiments	34
2.4 Sequential Sampling Strategies	35
2.4.1 Sequential Sampling for Global Metamodeling	36
2.4.2 Objective-Oriented Sequential Sampling	38
2.5 Overview of Model Verification and Validation (V&V)	42
2.5.1 Definitions of Model Verification and Validation.....	42
2.5.2 Sources of Uncertainty in Verification and Validation.....	44
2.6 Model Validation Metrics.....	46
2.6.1 Traditional Metrics.....	46
2.6.2 Frequentist's Metrics	47
2.6.3 Hypothesis Testing based Metrics	48
2.6.4 Metrics based on Pooling Multiple Data	50
2.7 Concepts of Model Calibration and Bias-Correction	52
CHAPTER 3. A NEW KRIGING MODEL WITH NON-STATIONARY COVARIANCE STRUCTURE	55

	9
Nomenclature	55
3.1 Introduction.....	56
3.2. Technological Base.....	59
3.2.1 Kriging metamodeling with a stationary covariance function.....	59
3.2.2 Representing Non-stationary Covariance: The Nonlinear Map Approach.....	61
3.3. A Proposed Non-stationary Covariance Structure.....	63
3.3.1 Proposed Density Function.....	64
3.3.2 Determining Hyperparameters.....	66
3.4 Case Study	68
3.4.1 Improvement of Prediction Accuracy.....	68
3.4.2 Improvement of Uncertainty Quantification.....	77
3.5 Summary.....	80
 CHAPTER 4. MODEL BIAS-CORRECTION WITH UNCERTAINTY QUANTIFICATION	
.....	81
Nomenclature	81
4.1 Introduction.....	82
4.2 Bias-correction of Computer Model against Physical Experiment Data.....	84
4.3 Bias-Correction of Low Fidelity (LF) Computer Model against High Fidelity (HF)	
Computer Model	92
4.4 Case Studies.....	97
4.4.1 Combining Variable Fidelity Computer Models: A Single Dimensional Problem	97
4.4.2 Computer Model vs. Physical Experiment: Engine Piston Problem	99
4.4.3 Accuracy Comparison of Different Model Fusion Approaches	104
4.5 Summary.....	105
 CHAPTER 5. BETTER UNDERSTANDING OF MODEL UPDATING STRATEGIES IN	
VALIDATING ENGINEERING MODEL	107
Nomenclature	107
5.1 Introduction.....	107
5.2 Role of Model Updating in a Validation Procedure	110

	10
5.3 Examination of Existing Model Updating Methods	112
5.3.1 Model bias-correction approaches	112
5.3.2 Model calibration approaches	114
5.3.3 Limitations of Bayesian approaches	117
5.4 A Maximum Likelihood Estimation (MLE) Based Model Updating Methodology	118
5.4.1 Model updating formulations and parameters	118
5.4.2 Determining model updating parameters via MLE	120
5.4.3 Comparison of the MLE based model updating with traditional Bayesian approach ...	122
5.5 Prediction Using the Updated Model	124
5.6 Case Study: Comparative Studies Using the Thermal Challenge Problem	124
5.6.1 Problem description	124
5.6.2 Bayesian approaches to the thermal challenge problem	128
5.6.3 Three model updating formulations used for testing the MLE method.....	129
5.6.4 Results of model updating parameters of different formulations	130
5.6.5 Studing of the predictive capability of the updated models.....	131
5.6.6 Model validation metrics	135
5.6.7 Comparison of regulatory test results	137
5.7 Summary.....	138
 CHAPTER 6. DESIGN DRIVEN MODEL VALIDATION METRICS AND PROCEDURE	
.....	141
Nomenclature	141
6.1 Introduction.....	142
6.2 A Proposed Design-Driven Model Validation Procedure	145
6.3 Design-Driven Model Validation Metrics.....	149
6.4 Case Study: Engine Piston Design.....	154
6.5 Summary.....	158
 CHAPTER 7. OBJECTIVE ORIENTED SEQUENTIAL EXPERIMENTATION.....	160
Nomenclature	160
7.1 Introduction.....	160
7.2 A New Objective Oriented Sequential Sampling Approach.....	162

	11
7.3 Stopping Criteria for Sequential Sampling	164
7.4 Application of the Proposed Sequential Sampling Approach in Variable Fidelity Optimization	167
7.4.1 Background of variable-fidelity optimization.....	167
7.4.2 Sequential sampling based variable-fidelity optimization approach	168
7.5 Case Study	170
7.5.1 Computer Experiment: One Dimensional Problem	170
7.5.2 Computer Experiment: Two Dimensional Problem (the Modified Branin Function)...	171
7.6 A Framework of Sequential Physical Experimentation	179
7.7 Summary.....	185
CHAPTER 8. CONCLUSION.....	187
8.1 Contribution	187
8.2 Future work.....	189
REFERENCES.....	193
APPENDIX.....	203
VITA.....	212

Chapter 1. Introduction

1.1 Research Motivation

In many engineering fields, computer simulation models (simply called **computer models**) have been widely used for engineering analysis and design, to predict the behavior of a real system when the physical phenomenon is not accessible by direct measurements or the physical experiments are much more expensive than numerical simulations. Associated with the advancement of **simulation-based engineering and science (SBES)** (NSF report 2006) is the emergence of a new design paradigm called **simulation based design**, which takes an increased responsibility for the success of new “engineered” systems, in replacement of the present design practice that relies heavily on extensive testing of components, subsystems and prototype systems. In addition, **Predictive Modeling** has emerged as a new research subject that studies a broad range of modeling techniques to provide confident prediction of the phenomenon of interest by integrating scientific principles together with the information obtained from both computer models and observed physical experiments. There are several major challenges in using predictive models for engineering design:

(1) A computer model could be computationally very expensive, which largely downgrades the efficiency and effectiveness of using it for design analysis and synthesis. For designing new and complex “engineered” systems in various applications such as microsystems, biological systems, and energy generation and consumption systems, the computational cost of sophisticated multi-discipline and multi-physics simulations can be extremely expensive and the use of simulation-based design becomes prohibitive. It is impractical to rely exclusively on high-

fidelity simulation models for the purpose of engineering design. **Metamodeling** techniques are widely used to build cheap-to-compute surrogate models (called **metamodels**) to replace the original expensive models in simulation-based design. However, with most metamodeling techniques, a general assumption is that the smoothness of a response is uniform over the input space domain. This is a convenient assumption that simplifies the metamodeling analysis and lessens the amount of prior information required. However, for engineering systems with complex physical behavior, cases are common where the level of smoothness of a response changes over its input space. There is a need for developing flexible metamodeling techniques that are capable of capturing highly nonlinear behaviors with changing smoothness of responses.

(2) Various sources of uncertainty should be sufficiently taken into account when using predictive models for engineering design. To name a few, there are uncertainties due to the model/method error, design parameter uncertainty, lack of data, experimental uncertainty, metamodeling uncertainty, etc. Because uncertainties have a large impact on the credibility of any consequent decision making, it is important to quantify each source of uncertainty, to study its impact on the final prediction, and more importantly, to mitigate its effect on the final design performance. While methods are widely accessible for uncertainty quantification of model parameters, there does not exist a unified theory or approach to quantify model uncertainty. To yield confident predictions, reliable design, and to minimize the unforeseen risk of final decision making, uncertainty of a predictive model must be sufficiently quantified with a comprehensive treatment of uncertainties from different sources. Throughout this process, there is also a need for developing model updating techniques that effectively combine information from both physical and computer experiments to improve model prediction.

(3) Before a model can be used for prediction purpose, its validity should be critically assessed, which is called model validation. Recent years have seen growing interest in model validation from both government and industries. In most of the existing efforts, model validation is viewed as verifying the model accuracy through comparing the model predictions with physical experiment observations. Due to the lack of resource, validation metrics are assessed based on limited test points without considering the predictive capability at untested but potential design space and the various sources of uncertainties. Therefore, the existing approaches for validating analysis models are not directly applicable for assessing the confidence of using predictive models in engineering design. There is a need to define a new model validation framework and metrics from the perspective of engineering design, and to establish the mathematical procedure accordingly.

1.2 Predictive Modeling and Research Issues

Figure 1.1 depicts a general framework considered in this work for predictive modeling by combining the information from both computer experiments (simulations), and physical experiments. A brief explanation of the steps in this flowchart is provided as follows.

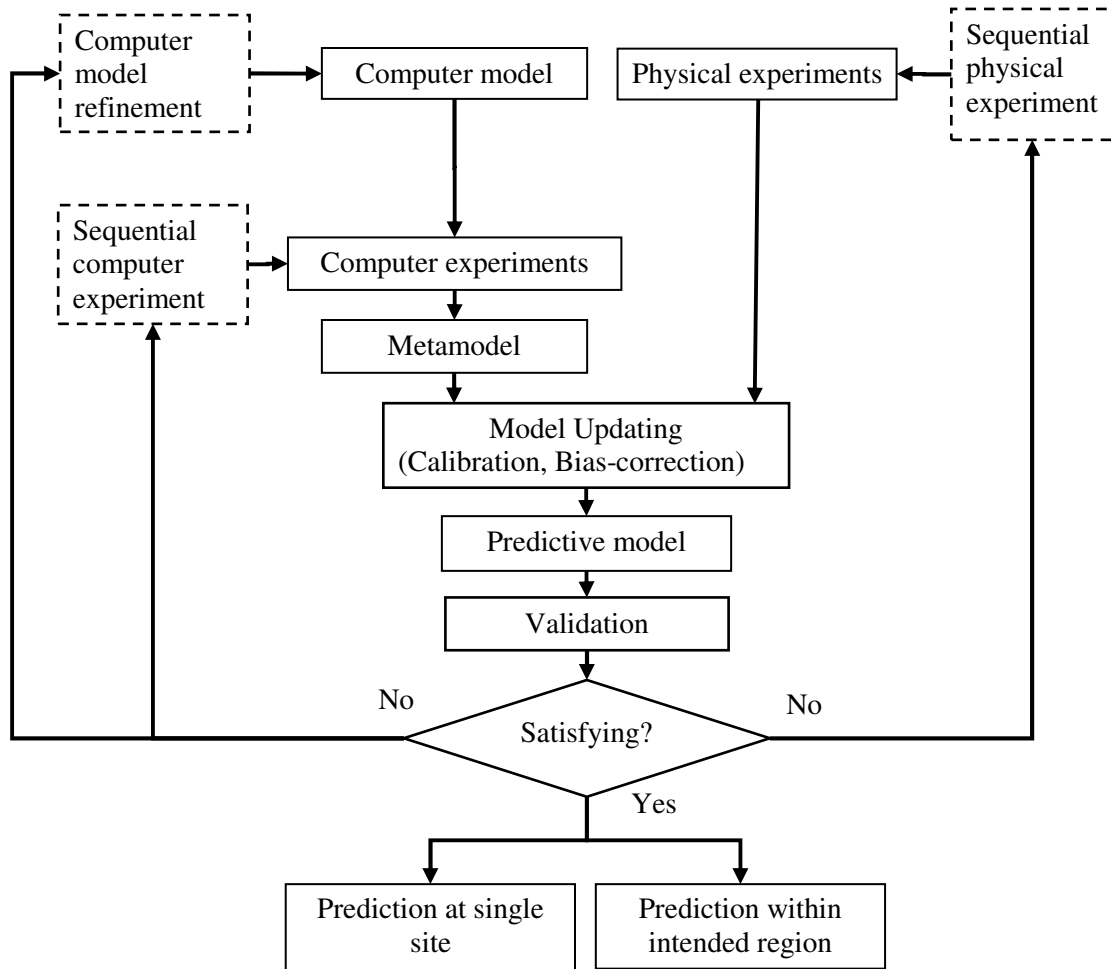


Figure 1.1 A general framework of predictive modeling based on computer model and physical experiment data

(1) If a given a computer model is expensive to simulate, computer experiments will be first designed to simulate the computer model and construct a metamodel to replace the expensive model in the later steps of the framework.

(2) In parallel to computer experiments, physical experiments are conducted to provide a better understanding of the system. Once the observational data is available, the computer model

will be updated by “fusing” both the original computer model and the new information obtained from physical experiments.

(3) This updated predictive model is then subject to a validation procedure that utilizes both existing and, more importantly, additional physical experiments associated with the intended region of interest in prediction. Note that unlike many contemporary model validation works that assess the validity of the original computer model, this proposed framework allows model validation to be applied to the predictive model, which is an updated computer model.

(4) If the predictive model passes the validation test, it will be further used for prediction and design purposes. The prediction may be associated with two scenarios: prediction at a single design site and prediction within an intended design region. In addition to the uncertainty of model itself, other sources of uncertainty must be considered (e.g., the input parameter uncertainty) in the final prediction.

(5) If the predictive model fails the validation test, remedy will be taken by refining the computer model, and collecting additional computer experimental data to further update and validate the computer model.

Associated with the above framework, the **overall objective** in this dissertation is to develop methodology and techniques to facilitate the use of predictive models in engineering design, with emphasis on techniques for metamodeling, model uncertainty quantification, and model validation. Five individual research tasks are identified in this work to accomplish this overall objective.

- **Task 1. Developing an improved Kriging metamodeling approach for capturing non-stationary behavior**

The research objective of this task is to develop an improved metamodeling technique that allows for high-dimensional engineering applications using the data from computer experiments. In addition to enhancing the prediction accuracy of model behavior with changing smoothness, the method is also expected to provide convenient assessments of “interpolation uncertainty” due to the use of metamodels.

Among the most widely used metamodeling techniques, Kriging model is well recognized for its capability of capturing nonlinear behavior and providing estimation of prediction error without using extra validation tests (Sacks et al., 1989). The latter feature makes Kriging model very attractive especially when the estimation of metamodel uncertainty is needed for purposes such as sequential sampling in multistage metamodeling. The assumption of a stationary covariance structure underlying ordinary Kriging does not hold in situations where the level of smoothness of a response varies significantly, which may downgrade the accuracy of Kriging prediction in terms of response prediction and error estimation. Although non-stationary Gaussian process models were put forward years ago in statistics and geostatistics communities, they are largely considered suitable in the scenario of physical experimental data with relatively low dimensions (Santner et al., 2003). Little prior work has been done on non-stationary covariance modeling for complex systems design based on deterministic computer experiments. This is mostly because complex design problems are often high dimensional, which leads to overparameterized non-stationary covariance functions. Therefore, the development of an efficient and effective non-stationary Gaussian process modeling approach for metamodeling is one of the research tasks undertaken in this work.

To be specific, a Kriging method with sparse yet flexible parameterization of non-stationary covariance, essentially a modified version of Gibbs (1997)’s nonlinear map approach,

is investigated. Through both mathematical and engineering examples, it is demonstrated that Kriging modeling based on the proposed non-stationary covariance representation is flexible enough to capture the changing smoothness behavior of a response, while providing a more accurate qualification of prediction uncertainty.

Details of the proposed method will be presented in **Chapter 3**.

▪ **Task 2. Developing a Bayesian Bias-Correction Approach for Model Fusion**

Although metamodeling techniques have been widely developed to construct a predictive model based on computer experiment data, very little research is on constructing a predictive model based on a combination of multiple sources of information with different fidelities and costs. Two scenarios of combining or fusing different sources of information are considered.

Scenario (a)

Multiple computer models are available but at different levels of model fidelity. No physical experiments are available.

Scenario (b)

Both computer simulations and physical experiment data are available.

Model fusion techniques have been developed to combine different sources of information under Scenarios (a) and (b). However, the existing approaches do not offer a unified mathematical framework for different scenarios, and lack the capability of quantifying the prediction uncertainty of the “fused” models.

The research objective under this task is to develop a generic model fusion approach that is able to effectively assess the uncertainty in model prediction by integrating data from different sources. More specifically, uncertainty associated with various levels of fidelity and

experimental error will be accounted for by a bias-function that models the difference between a low-fidelity and a high-fidelity model (Scenario (a)) or between computer predictions and physical experiments (Scenario (b)). The physical experiment data possesses the highest level of fidelity because it is the closest to reality. The approach is therefore generic to be applicable to both Scenarios (a) and (b) presented earlier.

In our approach, the Gaussian process model is used to represent the bias-function. A Bayesian approach is applied to the Gaussian process model to assess the uncertainty of the prediction error of the bias-corrected model. The approach provides a generic and flexible framework for drawing inferences for predictions in the intended but untested design domains, where data of physical experiments or high fidelity simulations are very limited. The Bayesian approach also provides a solid foundation for further research that may incorporate other, much broader, forms of uncertainty in engineering design.

Details of this task will be presented in **Chapter 4**.

▪ **Task 3. Achieving a Better Understanding of Model Updating Strategies**

Model updating is a strategy that utilizes mathematical means to update a computer model based on both physical and computer observations to improve the predictive capability of a computer model. Although various model updating techniques such as bias-correction and calibration are seen in literature, there is a need to achieve a better understanding of their merits. In this work, different model updating formulations, e.g., calibration and bias correction, as well as different solution methods are examined.. Traditional approaches to calibration treat certain computer model parameters as fixed over the physical experiment, but unknown, and the objective is to infer values for the so-called calibration parameters that provide a better match

between the physical and computer data. In many practical applications, however, certain computer model parameters vary from trial to trial over the physical experiment, in which case there is no single calibrated value for a parameter. We pay particular attention to this situation and develop a maximum likelihood estimation (MLE) approach for estimating the distributional properties of the randomly varying parameters which, in a sense, calibrates them to provide the best agreement between physical and computer observations. Furthermore, the newly developed u-pooling method (Ferson et al. 2008) is employed as a validation metric to assess the accuracy of an updated model over a region of interest. Using the benchmark thermal challenge problem as an example, several possible model updating formulations are studied using the proposed methodology. The effectiveness of the various formulations is examined. The benefits and limitations of using the MLE method versus the Bayesian approach are presented. Insights into various model updating strategies are provided through this study.

Details of this task will be presented in **Chapter 5**.

▪ **Task 4. Developing Design Driven Model Validation Framework and Metrics**

Even though there is a growing interest from both government and industries in developing fundamental concepts and terminology for model validation, model validation are still poorly understood in engineering design. Most of the existing model validation work is rooted in computational science where validation is viewed as verifying the model accuracy, i.e., a measure of the agreement between computational and experimental results. In most of the existing work, model validation has been primarily carried out from the perspective of model builders (or analysts), but not from that of designers (model users). They cannot provide

stochastic measurements with regard to the confidence (as well as the risk) in using a model for design purpose.

The research objective under this task is to develop a framework that combines both computer and physical experiments in validating the use of predictive models for engineering design. Different from the existing view in literature for assessing the model accuracy, model validation in this work is considered as a means to provide designer with statistical confidence measure while using predictive models in making a specific design decision. Built upon the techniques developed in Task 3 for uncertainty quantification of model prediction, the research objective here is to develop design-oriented model validation metrics to guide designers for achieving high confidence of using predictive models in making a specific design decision.

Appropriate metrics are developed to measure the confidence in using the predictive model for choosing one design candidate versus the other alternatives. Meanwhile, metrics are also intended to guide validation activities. If large uncertainty exists in predicting a design outcome and the validation requirement is not satisfied, new physical experiments will be designed and added sequentially to reduce the model uncertainty as well as improving the confidence of accepting a design solution.

Details of this task will be presented in **Chapter 6**.

▪ **Task 5. Developing A New Strategy in Objective Oriented Sequential Experiment**

Sequential experimentation has been shown to be a useful strategy in predictive modeling for engineering design because it helps maximize the information gained from experimental data sampled sequentially, especially when computer simulations are computationally expensive or physical experiments are resource taking. The interest in this task

is to research new strategies in sequential experiments in support of multistage metamodeling, model updating, and model validation in the context of engineering design. Considering that the end goal of using a predictive model in engineering design is to obtain a “true” optimal design solution with high level of confidence, an objective oriented sequential sampling approach is proposed for computer experiments towards improving a design objective as well as reducing the interpolation uncertainty due to the lack of experimentation data. In connection with the bias correction approach for combining variable-fidelity models developed under Task 2, the proposed objective oriented sequential sampling approach is applied to *variable fidelity optimization* where both the high-fidelity and low-fidelity simulations are integrated.

As an extension of the sequential sampling of computer experiments, a general framework that guides objective oriented sequential physical experimentation for updating predictive models in engineering design is also described.

Details of this task will be elaborated in **Chapter 7**.

1.3 Dissertation Outline

The outline of this dissertation can be illustrated in Figure 1.2. The technological bases related to the five research tasks are introduced in Chapter 2. The five research tasks are respectively presented in Chapters 3 – 7. Chapter 8 summarizes the contributions and presents the conclusion of this dissertation.

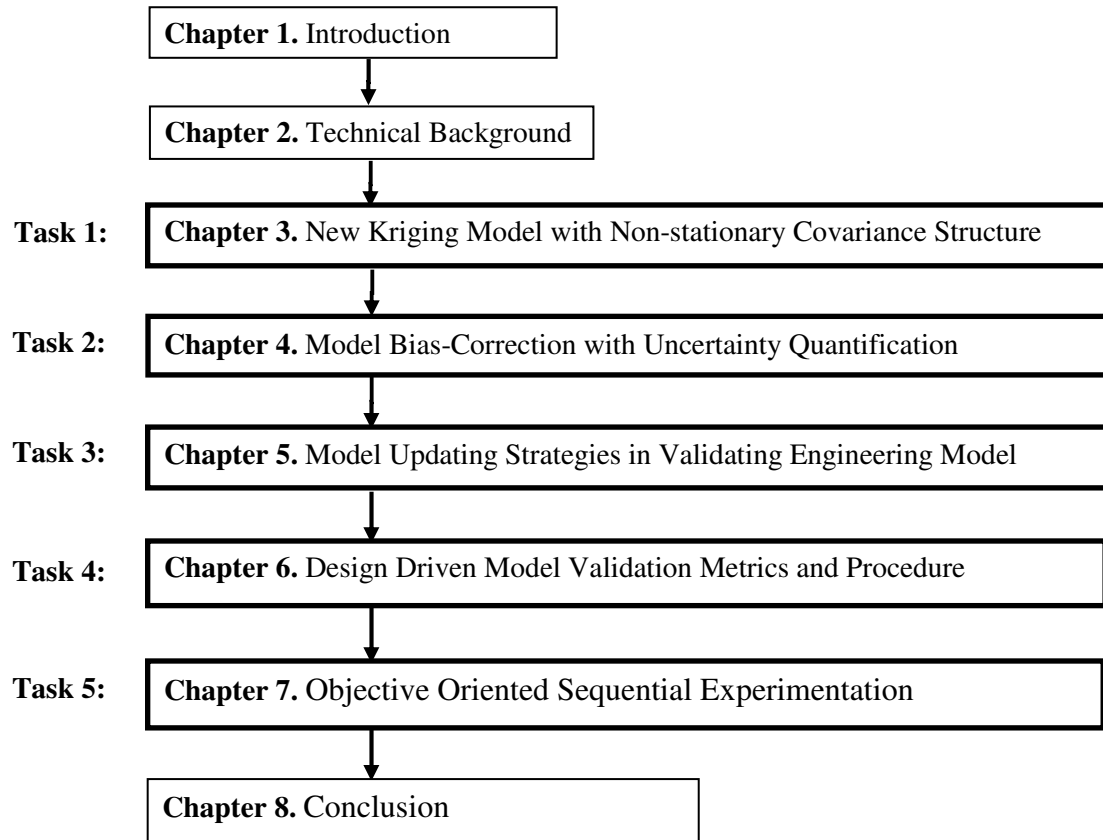


Figure 1.2 Outline of dissertation

Chapter 2. Technical Background

Nomenclature

$\mathbf{X}_D = [\mathbf{x}_1, \mathbf{x}_2, \dots, \mathbf{x}_n]^T$	sample points
$\mathbf{y}_D = [y_1, y_2, \dots, y_n]^T$	simulation outputs
$f_j(\mathbf{x})$	polynomial items
β_j	polynomial coefficients
$Z(\mathbf{x})$	Gaussian process
θ_m	correlation parameters
σ^2	variance of Gaussian process
\mathbf{R}	correlation matrix
EI, $EI(\mathbf{x})$	Expected Improvement
SLB, $SLB(\mathbf{x})$	Statistical Lower Bound
$y^e(\mathbf{x})$	Physical experiment
$y^m(\mathbf{x}, \boldsymbol{\theta})$	computer model
$\varepsilon_c(\mathbf{x})$	software coding errors
$\varepsilon_h(\mathbf{x})$	numerical errors
$\boldsymbol{\theta}$	calibration parameters, Model uncertainty parameter
$\delta(\mathbf{x})$	modeling error/bias (assessed by validation)
$\varepsilon_e(\mathbf{x})$	Experimental error (assessed by validation)
RMSE	Root Mean Square Error

R^2	R Square
RAME	Root Absolute Mean Error
$\delta(\mathbf{x})$	Bias function

2.1 Introduction

This chapter provides the technical background related to the several major research tasks in this dissertation. An overview of basic concepts and existing methods of metamodeling techniques is first provided in Section 2.2. In Section 2.3, techniques of optimal design of computer experiments are summarized, followed by the challenge and techniques in sequential sampling strategies in Section 2.4. In Section 2.5, fundamental concepts of model verification and validation are introduced, and the mathematical framework of model prediction based on both computer experiments and physical experiments is provided. In Section 2.6, general model validation approaches in literature are reviewed. Finally in Section 2.7, fundamental concepts in model calibration and bias-correction for model updating are described.

2.2 Kriging Techniques for Metamodeling

2.2.1 Overview of Kriging Techniques

Metamodels are widely applied in engineering design to facilitate the analysis and optimization of complex systems based on computationally expensive simulations. The simulation model studied here is assumed to be deterministic: if the simulation model is run twice (on the same computer) with the same value of input setting, the same value of output will result. The metamodeling problem can be formulated as: given n sample points $\mathbf{X}_D = [\mathbf{x}_1, \mathbf{x}_2, \dots, \mathbf{x}_n]^T$ and their simulation outputs (responses) $\mathbf{y}_D = [y_1, y_2, \dots, y_n]^T$, what is an

approximation for the functional relationship between input (design variables) \mathbf{x} and output (response) y of the simulation model? Each sample point is expressed as a vector of values of input variables, for k -dimensional problem, $\mathbf{x}_i = [x_{i1}, x_{i2}, \dots, x_{ik}]^T$. Various approaches have been widely used in engineering applications. The Response Surface Methodology (Box, et al.; 1978; Myers and Montgomery, 1995) is a well-known approach for constructing simple and fast approximations of complex computer codes. Kriging is a widely used interpolation method for the design and analysis of computer experiments (Sacks, et al., 1989; Currin, et al, 1991), as well as for design optimization (Booker, et al., 1999; Jones, et al., 1998). Other techniques, such as Artificial Neural Network (ANN) methods (Smith, 1993; Cheng and Titterington, 1994), Multivariate Adaptive Regression Splines (Friedman, 1991), and radial basis function methods (Hardy, 1971; Dyn, et al., 1986; Mullur and Messac, 2005) have drawn the attention of many researchers. Numerous comparative studies of metamodel types have been published over the years in an attempt to determine a “best” model (Jin et al. 2000, Simpson 2001; and Mullur et al. 2005; Turner et al. 2006).

Kriging model, named after the South African mining engineer D.G. Krige, was originally developed to analyze mining data (Krige, 1951). Krige’s work formed the foundation for an entire field of study now known as geostatistics (see, e.g., Cressie, 1997). Sacks, et al. (1989a, 1989b) extended the techniques of Kriging to deterministic computer experiments. Currin, et al. (1991) provided a Bayesian interpretation for the Kriging method. In the recent years, this new research avenue of using Kriging for metamodeling was quickly explored by engineering community as its potential for more general engineering applications became apparent (e.g., Simpson, et al., 2001a; Jones, 2001; Booker, 1998; Stinstra et al., 2001). One of the distinctive advantages of Kriging is that it provides not only the prediction of a response at

any site, but also the Mean Square Error (or the uncertainty) associated with the prediction. Currin et al. (1991) provided a comprehensive review of Kriging with a Bayesian interpretation.

Kriging method treats the simulation model $y(\mathbf{x})$ as a combination of a polynomial model (global trend) and a lack-of-fit part, i.e.,

$$y(\mathbf{x}) = \sum_{j=1}^P \beta_j f_j(\mathbf{x}) + z(\mathbf{x}) = \boldsymbol{\beta}^T \mathbf{f}(\mathbf{x}) + z(\mathbf{x}), \quad (2.1)$$

where $f_j(\mathbf{x})$ and β_j ($j=1,2,\dots,P$) are polynomial items and corresponding coefficients, respectively; $\mathbf{f}(\mathbf{x})=[f_1(\mathbf{x}),f_2(\mathbf{x}),\dots, f_p(\mathbf{x})]^T$ and $\boldsymbol{\beta}=[\beta_1,\beta_2,\dots,\beta_p]^T$; $z(\mathbf{x})$ is the lack of fit. Kriging method assumes that the lack-of-fit values at different locations are not independent; rather $z(\mathbf{x})$ is a systematic departure, which is a realization of a stochastic process $Z(\mathbf{x})$ with mean zero, variance σ^2 and non-zero covariance. The covariance of $Z(\mathbf{x})$ between two points \mathbf{t} and \mathbf{u} is expressed as:

$$\text{cov}(Z(\mathbf{t}), Z(\mathbf{u})) = \sigma^2 \rho(\mathbf{t}, \mathbf{u}; \boldsymbol{\theta}), \quad (2.2)$$

where ρ is the correlation function and $\boldsymbol{\theta} = [\theta_1, \theta_2, \dots, \theta_M]^T$ are correlation parameters. The correlation function can have many different forms (cf., Simpson, et al., 1998b), among which the most popular is the Gaussian correlation function. The correlation parameter is used to measure how fast the correlation between \mathbf{t} and \mathbf{u} decays with the increase of the distance between \mathbf{t} and \mathbf{u} in the direction of the corresponding coordinate. The smaller the correlation parameter is, the slower the correlation decays, which means the response is smooth in the corresponding direction.

2.2.2 Bayesian Interpretation of the Kriging Method

The Kriging method can be interpreted in a Bayesian point of view in many ways. Gaussian process (GP) prior over functions (Sacks et al. 1989, Currin et al. 1988, 1991).are

similar to the Bayesian approach to neural networks, where a prior is put on the weights of a network which represents a prior over functions. In Kriging method, such a prior is in the form Gaussian process. Compared to neural networks, Kriging model allows for analytical treatment because at least the lowest level of a Bayesian hierarchical model can be treated analytically (Li and Sudjanto, 2003).

The prior knowledge about a model can be expressed by a Gaussian process $Y(\mathbf{x}) = \boldsymbol{\beta}^T \mathbf{f}(\mathbf{x}) + Z(\mathbf{x})$ as in Eq. (2.1), with $\boldsymbol{\beta}^T \mathbf{f}(\mathbf{x})$ as its mean, σ^2 as its variance and Eq. (2.2) as the correlation function. The variance represents the uncertainty in the prior knowledge for the simulation model. After observing the responses on some sample points, more knowledge about the simulation model is obtained in the *posterior process*, reflecting the posterior knowledge. From the Bayesian viewpoint, the variance of posterior process is the *uncertainty* in the posterior knowledge on the simulation model. It has been shown that the mean and variance of the posterior process in Bayesian are exactly the Kriging predictor (Eq. 2.8) and the estimator of the prediction error (Eq. 2.9), respectively, when Gaussian process with improper uniform priors on $\boldsymbol{\beta}$'s.

Figure 2.1 shows the comparison between the prior and posterior distribution of Kriging metamodeling from the Bayesian point of view. As can be in (a) shows in the figure, the function of $Y(\mathbf{x})$ is assumed as a Gaussian process, where the *prior* distribution of function $Y(\mathbf{x})$ are identically distributed (with prior mean and covariance function). At the presence of two observations the function values (y_1 and y_i) at site \mathbf{x}_1 and \mathbf{x}_i , the *posterior* distribution of function $Y(\mathbf{x})$ (with posterior mean and covariance) is shown in Figure 2.1 (b).

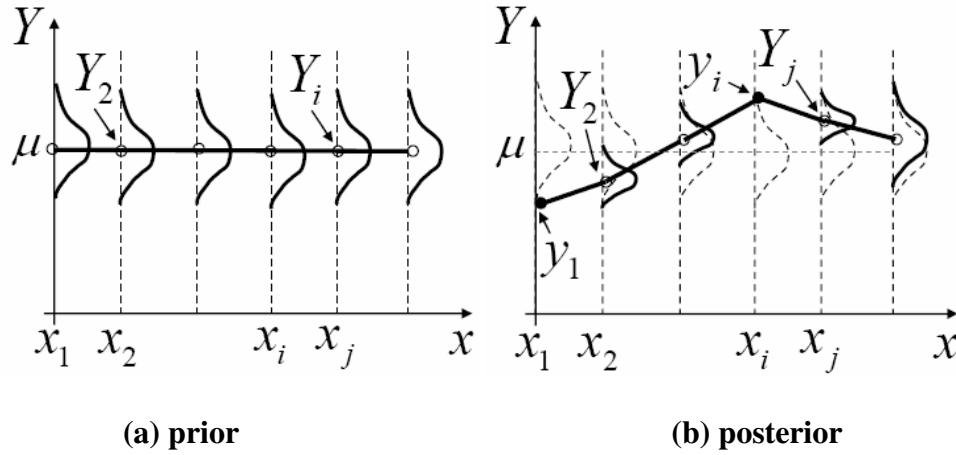


Figure 2.1 Bayesian view of Kriging metamodeling (Li and Azarm, 2006)

2.2.3 Determination of hyperparameters in Kriging mdoel

Given the form of the correlation function and the observations $y_D = [y(x_1), y(x_2), \dots, y(x_n)]^T$ of the unknown function $y(x)$, we need to identify the values of $\hat{\boldsymbol{\beta}}$, $\hat{\sigma}^2$, and $\hat{\boldsymbol{\theta}}$. One approach is to use the *maximum likelihood estimation* (MLE) method that maximizes the likelihood function (joint probability distribution function for y_D):

$$L(\boldsymbol{\beta}, \sigma^2, \boldsymbol{\theta}) = p(\mathbf{y}_D) = \frac{1}{(2\pi\sigma^2)^{n/2} |\mathbf{R}|^{1/2}} \exp\left\{-\frac{1}{2\sigma^2} [\mathbf{y}_D - \mathbf{F}\hat{\boldsymbol{\beta}}]^T \mathbf{R}^{-1} [\mathbf{y}_D - \mathbf{F}\hat{\boldsymbol{\beta}}]\right\}, \quad (2.3)$$

where $\mathbf{F} = [\mathbf{f}(\mathbf{x}_1), \mathbf{f}(\mathbf{x}_2), \dots, \mathbf{f}(\mathbf{x}_n)]^T$; \mathbf{R} is the correlation matrix, whose elements are $R_{ij} = \rho(\mathbf{x}_i, \mathbf{x}_j; \boldsymbol{\theta}), 1 \leq i, j \leq n$.

The values for $\boldsymbol{\beta}$ and σ are obtained by considering:

$$\frac{\partial L}{\partial \boldsymbol{\beta}} = 0 \Rightarrow \hat{\boldsymbol{\beta}} = (\mathbf{F}^T \mathbf{R}^{-1} \mathbf{F})^{-1} \mathbf{F}^T \mathbf{R}^{-1} \mathbf{y}_D \quad (2.4)$$

$$\text{and } \frac{\partial L}{\partial(\sigma^2)} = 0 \Rightarrow \hat{\sigma}^2 = \frac{1}{n} [\mathbf{y}_D - \mathbf{F}\hat{\boldsymbol{\beta}}]^T \mathbf{R}^{-1} [\mathbf{y}_D - \mathbf{F}\hat{\boldsymbol{\beta}}]. \quad (2.5)$$

The correlation coefficients $\boldsymbol{\theta}$, however, cannot be determined analytically. They are typically obtained numerically by solving the optimization problem, i.e., maximizing the likelihood function in Eq. (2.3). The values of $\hat{\boldsymbol{\beta}}$, $\hat{\sigma}^2$, and $\hat{\boldsymbol{\theta}}$ reflect the typical pattern of variations in the observations.

In general, σ^2 , $\boldsymbol{\beta}$ and the correlation parameters $\boldsymbol{\theta}$ are estimated by the maximum likelihood estimation (MLE) method. Furthermore, it can be proved that the following realization is the best predictor of $y(\mathbf{x})$ in terms of the maximum likelihood function:

$$\hat{y}(\mathbf{x}) = \hat{\boldsymbol{\beta}}^T \mathbf{f}(\mathbf{x}) + \mathbf{r}(\mathbf{x})^T \mathbf{R}^{-1} (\mathbf{y}_D - \mathbf{F}\hat{\boldsymbol{\beta}}), \quad (2.6)$$

where $\hat{\boldsymbol{\beta}}$ is the MLE of $\boldsymbol{\beta}$; \mathbf{F} denotes the matrix of the values of all the polynomial items at the sample points, i.e., $\mathbf{F} = [\mathbf{f}(\mathbf{x}_1), \mathbf{f}(\mathbf{x}_2), \dots, \mathbf{f}(\mathbf{x}_N)]^T$; $\mathbf{R} = [R_{ij}]_{N \times N}$ is a $N \times N$ matrix (correlation matrix), whose element $R_{ij} = \rho(\mathbf{x}_i, \mathbf{x}_j)$ is the correlation between sample points \mathbf{x}_i and \mathbf{x}_j ; $\mathbf{r}(\mathbf{x}) = [r_i(\mathbf{x})]_{N \times 1}$ is a $N \times 1$ vector, whose element $r_i(\mathbf{x}) = \rho(\mathbf{x}, \mathbf{x}_i)$ is the correlation between \mathbf{x} and \mathbf{x}_i . This prediction model is an interpolation model in that it passes through all the sample points.

In $Y(\mathbf{x})$, there are infinite realizations which pass through all the sample points. These realizations form a new stochastic process, which is denoted as $Y(\mathbf{x}) | \mathbf{y}_D$. In fact, the unknown function $y(\mathbf{x})$ is one of the realizations in the new stochastic process. The maximum likelihood method is used to obtain a predictor of $y(\mathbf{x})$ (Jones, 2001), i.e., the predictor should maximize:

$$L(y(\mathbf{x}) | \mathbf{y}_D) = \frac{p(y(\mathbf{x}), \mathbf{y}_D)}{p(\mathbf{y}_D)}. \quad (2.7)$$

By considering $\frac{\partial L}{\partial \mathbf{y}} = 0$, the maximum likelihood predictor of $y(\mathbf{x})$, i.e., the Kriging

metamodel prediction, can be expressed as

$$\hat{y}(\mathbf{x}) = \hat{\boldsymbol{\beta}}^T \mathbf{f}(\mathbf{x}) + \mathbf{r}^T \mathbf{R}^{-1} (\mathbf{y}_D - \mathbf{F} \hat{\boldsymbol{\beta}}). \quad (2.8)$$

The correlation of the errors will affect the estimate of prediction accuracy. Since $y(\mathbf{x})$ is unknown, it is impossible to obtain the prediction error of $\hat{y}(\mathbf{x}) - y(\mathbf{x})$. One way to estimate the prediction error is to use the variance of the new stochastic process $Y(\mathbf{x}) | \mathbf{y}_D$, i.e., the estimator of the prediction error can be expressed in Eq. (2.9), which is also called the mean squared error (MSE, Sacks et al., 1989).

$$s^2(\mathbf{x}) = E[(\hat{y}(\mathbf{x}) - Y(\mathbf{x}) | \mathbf{y}_D)^2] = \hat{\sigma}^2 (1 - \mathbf{r}^T \mathbf{R}^{-1} \mathbf{r}). \quad (2.9)$$

The covariance will be:

$$Cov(\mathbf{x}_i, \mathbf{x}_j) = \hat{\sigma}^2 \left(r(\mathbf{x}_i, \mathbf{x}_j) - \mathbf{r}^T(\mathbf{x}_i) \mathbf{R}^{-1} \mathbf{r}(\mathbf{x}_j) \right), \quad (2.10)$$

where \mathbf{x}_i and \mathbf{x}_j are any two sites.

Eq. (2.8) and Eq. (2.9) are the two major outputs yielded by Kriging modeling. It can be verified from these two equations that: (1) $\hat{y}(\mathbf{x}_i) = y_i$ (meaning that Kriging is interpolative); (2) $s^2(\mathbf{x}_i) = 0$, where \mathbf{x}_i is one of the sampling points.

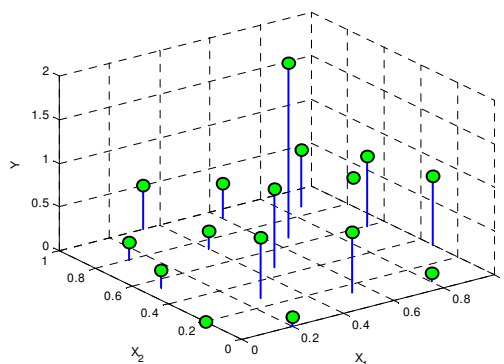
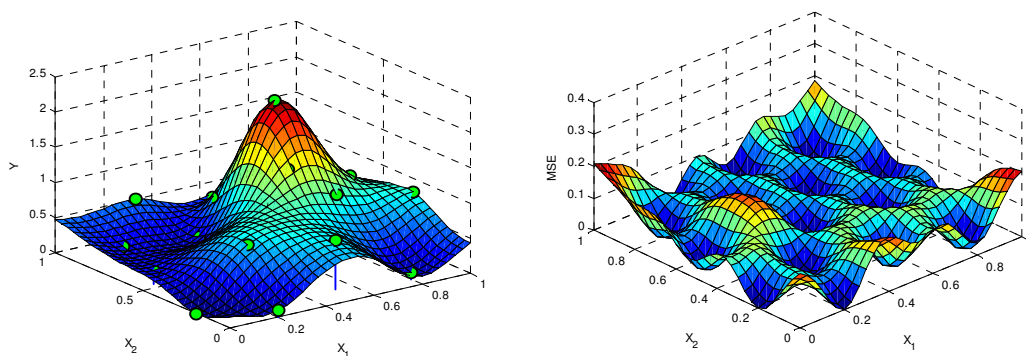


Figure 2.2 The sampling points (16) used in a Kriging model in two dimension



(a) Kriging predictor $\hat{y}(\mathbf{x})$ **(b) Kriging prediction uncertainty (variance)**

Figure 2.3 Kriging predictor and the prediction uncertainty

based on sixteen (16) sampling points

Figure 2.3 shows an example of the Kriging predictor and estimator of the prediction error for a two-dimensional function, based on sixteen sampling points shown in Figure 2.3. It is found that at any sample point, the estimation of the prediction error is exactly equal to 0 and at

any other locations the estimation of the prediction error is dependent on the distance between the point for prediction and the other sample points.

2.2.4 General Bayesian Analysis of Kriging metamodeling

As described in Section 2.2.3, the three unknown hyperparameters $\hat{\boldsymbol{\beta}}$, $\hat{\sigma}^2$, and $\hat{\boldsymbol{\theta}}$ are determined through the MLE approach. There are several deficiencies of using MLE approach to determine the hyperparameter in Kriging metamodel (Martin et al., 2005). One deficiency of this approach is that it is characterized as an optimization process that suffers from multiple maximum issues in many cases. To guarantee the selection of the global maximum likelihood, stochastic optimization and some penalty function based approaches (Li and Sudjanto, 2005) are required.

A second deficiency of using the MLE approaches is resulted from the treatment of the three unknown hyperparameters $\hat{\boldsymbol{\beta}}$, $\hat{\sigma}^2$, and $\hat{\boldsymbol{\theta}}$ as fixed parameters. However, under very rare cases can such parameters be known (e.g., from expert's advices or pervious experience). Therefore, the MLE treatment potentially leads to the underestimation of the stochastic process variability (Martin 2005). To mitigate this problem, a general Bayesian analysis can be applied to determine the hyperparameters $\hat{\boldsymbol{\beta}}$, $\hat{\sigma}^2$, and $\hat{\boldsymbol{\theta}}$ in Kriging model. Specifically, prior distributions are assigned to these parameters. Given observed experimental data, the posterior distributions of these parameters are viewed as the uncertainty of parameters and could be propagated through the deterministic predictor in further predictions.

2.3 Optimal Design of Computer Experiments

The selection of sample points, namely the design of experiments (DOE, also called experimental design or sampling technique), has direct impact on the performance of a metamodel. “Classical” DOE methods, such as full-factorial designs, fractional factorial designs, central composite designs, etc, are mainly developed for physical experiments, in which substantial random noise is assumed to be present.

However, the simulation yielded by computer model is deterministic and therefore able to replicate observations from running the code with the same inputs. Furthermore, with simulation models, it is common to allow the variables to vary over wider ranges than in physical experiments. The function behavior over such large ranges may be much more nonlinear than what is normally observed in physical experiments. It is argued by many researchers (e.g., Currin, et al., 1991; Sacks, 1989) that classical experimental designs are not well-suited for computer experiments. It is generally believed that a good design of computer experiments should have a good space-filling (Sacks et al., 1989) property and a good projective property (Fang et al., 2002). Numerous experimental designs have been developed in an effort to provide more efficient and effective means for deterministic computer experiments. Some examples of these experimental designs are the Latin Hypercube design, orthogonal arrays (OA) and maximin designs. Different experimental designs have distinctive features. However, with a limited number of sample points, a tradeoff often has to be made between the *space-filling properties* and the *projective properties* in low dimensional subspaces.

Optimal Design of Computer Experiment refers to designs constructed by algorithmic approaches under certain optimality criteria. Many different optimality criteria have been proposed for computer experiments are widely used in literature, such as the Minimax and

Maximin distance criterion, the maximum entropy criterion (Currin et al, 1991), integrated mean squared-error (IMSE) criterion (Sacks et al, 1989) and the uniformity criterion (Fang and Wang, 1994). Jin et al. (2005) proposed an efficient evolutionary optimization algorithm to search the optimal Latin Hypercube design (OLHD), by exchanging elements in the design matrix in a pair-wise manner. This approach is gaining popularity and is used as one of the standard DOE methods in some commercial software packages (e.g., iSIGHT).

2.4 Sequential Sampling Strategies

Sequential sampling procedures are extremely important in engineering problems when simulations are expensive, because they help obtain the most information from a limited number of simulations. Even though the following review on sequential sampling strategies focuses on their uses in designing computer experiments, they are not restricted to computer experiments. Similar ideas could be extended to the design of physical experiments.

The merits of sequential sampling strategies lie in the following aspects:

(1) They are akin to the common industry practice of conducting non-parallel simulations in a sequential or stage-by-stage manner, as opposed to single stage (one-shot).

(2) They provide a mechanism to monitor the accuracy of metamodels and to control the size of samples based on the accuracy of metamodels. This allows sampling process to be terminated as soon as the metamodel is deemed sufficiently accurate or dependable for the purpose of design (Sacks, et al., 1989).

(3) With appropriate criteria, they allow the sampling process to adapt to the metamodel previously obtained. The adaptivity of sequential sampling here has a two-fold meaning: a) it helps identify a design region of interest and thereby improve the accuracy of metamodel in a

narrowed design region of interest; b) it helps efficiently allocate sampling points: if the behavior of response varies dramatically throughout the input space, that regions of poor approximation could be allocated with more sampling points, while regions of enough accuracy would not be over-sampled.

(4) They help quickly identify the design variables with prominent or negligible influence to a response. The information can be used to reduce problem dimension in the later design process.

Depending on various purposes, two categories of strategies are seen in literature, which will be elaborated in Sections 2.4.1 and 2.4.2 that follow.

2.4.1 Sequential Sampling for Global Metamodeling

The goal of *global metamodeling* is to fit a metamodel that is accurate over the entire input space. Currin et al. (1988) proposed the maximum Entropy criterion for selecting the sequential sampling points. Because the information matrix used for entropy assessment is closely related to the covariance matrix of the samples, this method incorporates the covariance information (i.e. the estimated correlation parameters) gained from previous metamodels. However, Currin's method is limited to Kriging metamodel, since the adjusted covariance comes directly from the Kriging model. Lin et al. (2004) developed a SEED (Sequential Exploratory Experimental Design) method, together with two possible ways to adjust the covariance matrix of sampling. In Lin's method, additional sampling points are used for estimating the prediction error, which provides the basis of adjusting the covariance matrix. As a result, more sampling points are expected in regions of larger prediction error. The disadvantage of this method is that

it wastes some sampling points as test data for verifying the prediction error, rather than as training data. Similar to Lin's method, Farhang Mehr et al. (2005) incorporated the local fluctuation behavior of response surface into the covariance matrix. As a result, regions of higher fluctuation are filled with more sampling points. Osio and Amon (1996) proposed an adaptive sequential procedure based on the A-optimality criterion. These works utilized a common Bayesian view of sampling, with different adaptation criteria in selecting sample sites.

Sacks et al. (1989) proposed the Integrated Mean Squared Error (IMSE) criterion to guide the sampling, in which a new sampling point is selected so that the IMSE is minimized. A similar method is to select the new sampling point where the MSE prediction is maximized. These two methods are directly based on the MSE prediction provided by the Kriging model (see also Section 2.2).

Jin et al. (2002) used a scaled distance in the Maximin distance criteria, based on the Maximin Distance Criterion proposed by Johnson, et al. (1990). The scaling parameter in each dimension reflects the importance of each input variable, which could be obtained by the sensitivity indicator of global sensitivity analysis approaches, such as the variance-based approaches (Sobol 1993). Jin et al. (2002) also proposed a Cross-validation approach, in which a point with the largest cross-validation error is selected as the new sampling point. The above two approaches have no limitation on the metamodeling technique used.

Xiong et al. (2008) recently presented a sequential sampling approach called Quasi-LHD, considering simultaneously the space-filling property and the projection property. The method extends the Maximin distance criterion (i.e. space-filling) that is formulated as an unconstrained optimization problem, placing a constrained optimization problem with a minimum distance on each dimension of a design space.

2.4.2 Objective-Oriented Sequential Sampling

The Objective-oriented sequential sampling approach shows advantages in engineering design because it is driven by the intended purpose or objective in design optimization. It focuses on how to efficiently update a metamodel, while overlooking inferior or less promising design region and narrowing the sampling down to the most promising design region or site. Several major sampling approaches in this category are reviewed as follows.

(1) Expected Improvement

The concept of **Expected Improvement (EI)** was first applied in the Efficient Global Optimization (EGO) algorithm proposed by Jones et al. (1998). The algorithm selects the next sampling site to maximize the expected improvement of a design objective function with respect to the interpolation uncertainty. Two aspects of goals are achieved with traded-offs in the EI maximization: **local search** and **global search**. The **local search** tends to put the next sampling site at the location where the objective function is optimized (e.g., point \mathbf{x}_A in Figure 2.4), while the **global search** tends to put the next sampling at the location where the interpolation uncertainty is maximized (e.g., point \mathbf{x}_B in Figure 2.4). Considering the tradeoff between these two aspects, the EI function is formulated as $E[\max\{0, [y_{\min} - y^s(\mathbf{x}_{N+1})]\}]$ and further expanded as

$$EI(\mathbf{x}_{N+1}) = [y_{\min} - \mu_y] \Phi\left(\frac{y_{\min} - \mu_y}{\sigma_y}\right) + \sigma_y \phi\left(\frac{y_{\min} - \mu_y}{\sigma_y}\right), \quad (2.11)$$

where $\Phi(\cdot)$ and $\phi(\cdot)$ are the CDF and PDF functions, respectively, of the standard normal distribution, $y_{\min} = \hat{y}^s(\mathbf{x}_i^*)$, \mathbf{x}_i^* is the optimal design point based on the current metamodel,

$y^s(\mathbf{x}_{N+1})$ stands for the surrogate model at site \mathbf{x}_{N+1} with mean $\mu_y = \hat{y}^s(\mathbf{x}_{N+1})$ and standard deviation $\sigma_y = \text{Var}^{1/2}[y^s(\mathbf{x}_{N+1})]$. According to the study done in Sasena (2002) and Sekishiro et al. (2006), although the EI method is intended to balance between the local search and the global search, it may not converge in some cases. Sometimes, it is difficult to optimize the EI function because it may show extremely ‘bumpy’ behavior at existing sampling points and extremely ‘flat’ (close to zero) behavior in regions that are largely inferior to the optimum.

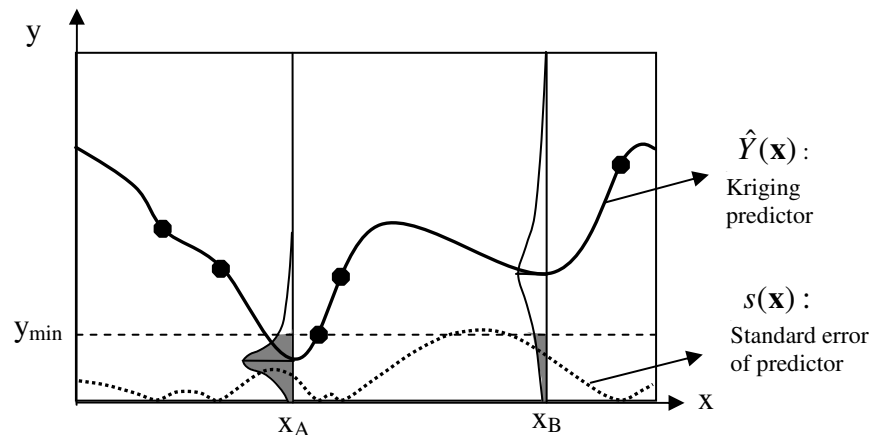


Figure 2.4 Expected improvements (EI, the shaded area) at two sites x_A and x_B .

$$E[I(x_A)] > E[I(x_B)].$$

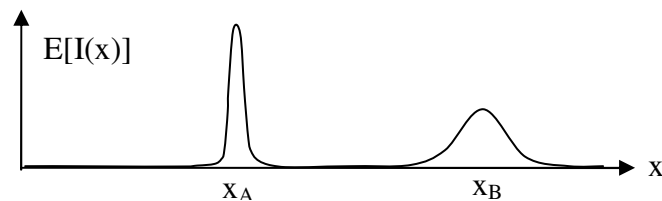


Figure 2.5 Plot of Expected Improvements across the whole design region

In Figure 2.4, the two PDF curves at sites \mathbf{x}_A and \mathbf{x}_B are determined by the prediction distribution of $\hat{Y}(\mathbf{x}_A)$ and $\hat{Y}(\mathbf{x}_B)$, indicating the uncertainty in model prediction. Figure 2.5 shows the expected $E[I(\mathbf{x})]$ function vs. design site \mathbf{x} . Since \mathbf{x}_A achieves the maximum EI, \mathbf{x}_A is chosen as the next sampling point. The advantage of EGO over a normal deterministic optimization approach based on a deterministic objective function lies in its capability of balancing the two objectives: to improve the accuracy of metamodel and to improve the objective, so regions that might contain potential optimal points will be explored more than those less promising. It is shown that EGO is an efficient global optimization approach even though it does not rely on a globally accurate metamodel.

(2) Prediction Interval Based Approaches

Given the uncertainty quantification associated with a metamodel, the prediction interval with a specified confidence level can also be utilized to formulate a sequential sampling problem. One of the approaches that utilize the information of the prediction interval is the Statistical Lower Bound (SLB) criterion (Cox et al., 1997), which has the following form:

$$\text{Minimize } SLB(\mathbf{x}_{N+1}) \equiv \mu_{y^s}(\mathbf{x}_{N+1}) - k\sigma_{y^s}(\mathbf{x}_{N+1}), \quad (2.12)$$

where $\mu_{y^s}(\mathbf{x}_{N+1}) = \hat{y}^s(\mathbf{x}_{N+1})$, $\sigma_{y^s}(\mathbf{x}_{N+1}) = Var^{1/2}[y^s(\mathbf{x}_{N+1})]$, and k is a user-defined parameter. A larger k value implies the emphasis on reducing interpolation uncertainty or the need for global search. The SLB criterion is easier to be controlled and interpreted than the EI criterion.

In Apley et al (2005), a promising design region is narrowed down by comparing the prediction interval of one design to that of the optimal design. The approach deals with the

robust design objective (rather than the deterministic optimization), i.e., $f = w_1 \mu_{y^s}(\mathbf{x}) + w_2 \sigma_{y^s}(\mathbf{x})$, where $y^s(\mathbf{x})$ is the metamodel with uncertainty, w_1 and w_2 are the weights defined in the robust design objective. The uncertainty of $f(\mathbf{x})$ is determined by propagating the uncertainty of $y^s(\mathbf{x})$. By doing so, the effect of prediction uncertainty is isolated from those caused by random design variables/parameters. In Figure 2.6, \mathbf{x}^* is the optimal design determined over $\mu_f(\mathbf{x})$. Points in regions marked by darker solid lines are of over 95% confidence that they are inferior to the optimal design \mathbf{x}^* , therefore, there is no need to further refine those regions by adding further sampling points.

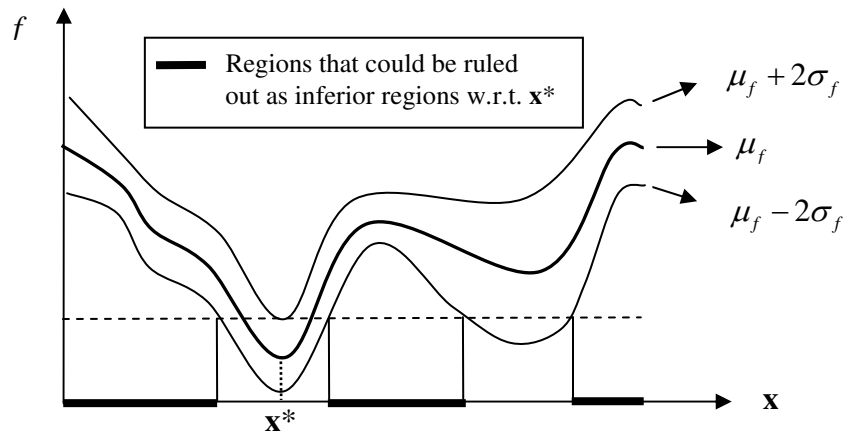


Figure 2.6 The prediction interval based approach to rule out inferior design region

In the recently developed multi-stage and multi-response sequential sampling approach proposed by Chen et al (2008), the idea of prediction intervals is used to identify the worst and best possible designs to determine the region of interest for both the design objective and design constraints. Distinct from the existing objective-oriented sequential sampling methods, where the design objective and constraints have to be combined into a single response of interest, this

method offers the flexibility of building metamodels for multiple responses (objective/constraints) simultaneously. Based on the extreme values of the optimal solution identified within the confidence interval, the level set representation, together with a series of Boolean operations, is used to synthesize the region(s) of interest with arbitrary topologies. The method possesses superior efficiency in design exploration and allows multiple sample points at each sampling stage.

2.5 Overview of Model Verification and Validation (V&V)

2.5.1 Definitions of Model Verification and Validation

Verification and validation (V&V) are the primary approaches to assess the accuracy and the reliability of computer models. The prediction by a computer model is used to simulate the physical event and is fundamental to decision-making. There is growing interest from both government and industries in developing fundamental concepts and terminology for model verification and validation. The definition of V&V by AIAA (1997) is adopted in this work as follows.

- ***Verification*** is the assessment of the accuracy of the solution to a computational model;
- ***Validation*** is the assessment of the accuracy of a computational simulation by comparison with experimental data.

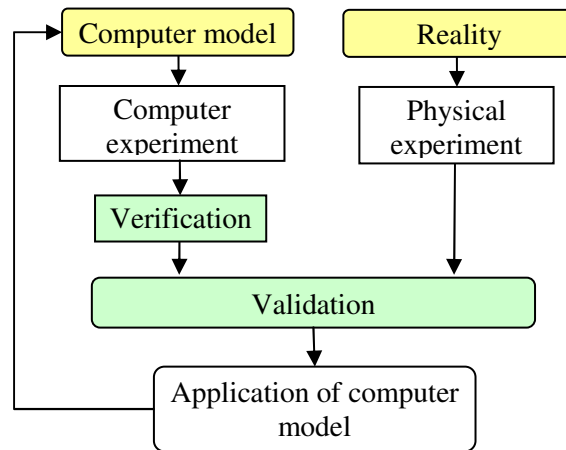


Figure 2.7 A general flowchart of Verification & Validation

To put into simple words, verification deals with the mathematics associated with the implementation of a model on computer, whereas validation deals with the physics associated with a model (Roach, 1998). Figure 2.7 shows a general flowchart of V&V, which explains the relationship between verification and validation. As shown, the comparison between the physical experiments and the computer outputs is the key element in V&V processes. It is often expected that the model verification needs to be implemented first before a model is validated.

Verification involves two basic components, namely, **code verification** and **solution verification**. *Code verification* deals with the error due to computer programming. In the process of code verification, two types of verifications are involved: Numerical Algorithm Verification (NAV); and Software Quality Assurance (SQA). *Solution verification* (also referred to as ‘numerical error estimation’) deals with four types of errors that can occur in a computer model: (1) error due to spatial discretization; (2) error due to temporal discretization; (3) error due to iterative procedure; and (4) computer round-off error. The first three types of errors are also called the ‘approximation error’ or ‘numerical error’. The numerical model (computer model)

must be carefully verified, including features of the model such as load functions, boundary and initial conditions, constitutive models. Numerical error is opposed to modeling error, which is due to natural imperfections of abstract models. Much effort in quantifying the numerical error has been devoted by Ainsworth et al. (1997), Oden et al. (2003), in which the solution verification is viewed as essentially an estimation of posteriori error.

Ideally, a computer model should be carefully verified before it can be passed to the validation process. The validation analyst should be aware of the magnitude or characteristics of possible numerical error, because the reliability of the validation would be decreased by the imperfection of the computer model. However, the focus of this work is on model validation. It is assumed that *the computer model has been verified with ignorable numerical error.*

2.5.2 Sources of Uncertainty in Verification and Validation

Predicting the amount by which a model output may differ from the true value is often complicated by the presence of uncertainties and errors from various sources, such as model (lack of knowledge), parametric, algorithmic, computational, and system variability, as well as testing data that are used to compare with the model prediction. Different ways of classifying uncertainties in model prediction are seen in the literature (Apostolakis 1994; Trucano, 1998; Hazelrigg, 1999; Oberkampf et al., 1999).

The following equation between $y^e(\mathbf{x})$ and $y^m(\mathbf{x}, \boldsymbol{\theta})$ is intended to encompass all sources of error/uncertainty that are involved in a model verification and validation process:

$$y^e(\mathbf{x}, \boldsymbol{\theta}) = y^m(\mathbf{x}, \boldsymbol{\theta}) + \mathcal{E} \{ \varepsilon_c, \varepsilon_h(\mathbf{x}), \delta(\mathbf{x}), \varepsilon_e(\mathbf{x}) \} \quad (2.13)$$

$y^e(\mathbf{x})$ - Physical experiment

$y^m(\mathbf{x}, \boldsymbol{\theta})$ - Computer model

$\varepsilon_c(\mathbf{x})$ - Software coding errors (assessed by verification)

$\varepsilon_h(\mathbf{x})$ - Numerical errors (assessed by verification)

$\boldsymbol{\theta}$ - Calibration parameters, Model uncertainty parameter (assessed by validation)

$\delta(\mathbf{x})$ - Modeling error/bias (assessed by validation)

$\varepsilon_e(\mathbf{x})$ - Experimental error (assessed by validation)

Assuming that $\varepsilon_c(\mathbf{x})$ and $\varepsilon_h(\mathbf{x})$ are already eliminated in verification, a simplified equation can be established:

$$y^e(\mathbf{x}, \boldsymbol{\theta}) = y^m(\mathbf{x}, \boldsymbol{\theta}) + \delta(\mathbf{x}) + \varepsilon_e(\mathbf{x}) \quad (2.14)$$

Statistical approaches for characterizing the probability distributions of $\delta(\mathbf{x})$ are generally divided into two categories, classical statistical (Easterling and Berger, 2002) and Bayesian (Bayarri et al., 2002) approaches. The fundamental difference between the two is that the former draws confidence intervals of prediction based on statistical data analysis, while the latter assumes that the model parameters themselves are random and follow a prior distribution, specified based on model builder/designers' prior knowledge. The prior distribution will be updated once data is available and becomes posterior distribution. The Bayesian approach is preferred to the classical statistical approach when it is too expensive to obtain statistically sufficient amount of data.

2.6 Model Validation Metrics

2.6.1 Traditional Metrics

Most of the earlier model validation work (e.g., Marczyk et al. 1997; Freese, 1960; Reynolds, 1984; Gregoire and Reynolds, 1988; Hills and Trucano, 1999) is rooted in computational science. In these works, validation is viewed as verifying the model accuracy, i.e., a measure of the agreement between computational results and experimental results. For instance, graphical comparisons through visual inspection of x-y plots, scatter plots and contour plots are often subjective and not sufficient (Oberkampf and Trucano, 2000). Quantitative comparisons (Marczyk et al. 1997) that rely on the measures of correlation coefficient and other weighted and non-weighted norms to quantify the distance between the two “clouds” cannot provide statistical judgment of model validity. Other techniques, such as χ^2 (Chi-square) test on residuals between model and experimental results (Freese, 1960; Reynolds, 1984; Gregoire and Reynolds, 1988) require multiple evaluations of the model and experiments, and many statistical assumptions that are difficult to satisfy.

An extensive discussion of traditional validation literature, and examples of statistical analysis of physics models and experiments are given in Hills, Trucano (1999) and Easterling and Berger (2002), Oberkampf and Trucano (2000). Among the traditionally used validation metrics in statistics community, we provide the formulations of several widely seen metrics, namely, **R²**(R-Square), **RMSE** (Root Mean Square Error), and **RAME** (Root Absolute Mean Error), Eqs. (2.15) – (2.17).

$$R^2 = 1 - \frac{\sum_{i=1}^N (y_i - \hat{y}_i)^2}{\sum_{i=1}^N (y_i - \bar{y})^2}, \quad (2.15)$$

$$RMSE = \sqrt{\frac{1}{N} \sum_{i=1}^N (y_i - \hat{y}_i)^2}, \quad (2.16)$$

$$RAME = \max_{i=1, \dots, N} |y_i - \hat{y}_i| / \sqrt{\frac{1}{N} \sum_{i=1}^N (y_i - \bar{y})^2}. \quad (2.17)$$

In the above equations, N represents the total number of validation points; y_i and \hat{y}_i represent the real and predicted value at the validation point, respectively; \bar{y} represents the mean of y_i . The above three validation metrics all consist a common term $(y_i - \hat{y}_i)$, which measures the individual error (lack of fit) at each experimental site.

The advantage of these three validation metrics is that they are easy to compute and interpret. However, they do not explicitly take into account the uncertainty of model prediction \hat{y}_i and the uncertainty of the physical data y_i .

2.6.2 Frequentist's Metrics

Recent approaches to quantitatively comparing computations and experiments can be roughly divided into two categories, namely classical frequentist approach (Oberkampf and Barone, 2004) and Bayesian approach (Kennedy and O'Hagan, 2001; Bayarri et al., 2002; Buslik, 1994; Hanson, 1999; Wang, et al., 2008).

One of the frequentist's validation approaches can be exemplified by the *confidence interval* based approach developed by Oberkampf and Barone (2004). The confidence intervals in Eq. (2.18) are used to assess the model accuracy separately at **individual tested points**, by comparing a maximum allowable error with the confidence interval.

$$\left(\hat{e}(x) - t_{-\alpha/2, n-1} \cdot \frac{s(x)}{\sqrt{n}}, \hat{e}(x) + t_{-\alpha/2, n-1} \cdot \frac{s(x)}{\sqrt{n}} \right), \quad (2.18)$$

where the confidence level is specified at $100(1-\alpha)\%$, and the confidence interval for the true prediction error e is defined at different values of design input, $e(x)$. The estimated prediction error is $\hat{e}(x) = \frac{1}{n} \sum_{i=1}^n [y_i^E(x) - y^M(x)]$, y^M is the deterministic outcome from the model, and $y_i^E, i = 1, \dots, n$ is the repetitive experimental observations at the same input, which are assumed to be independently, identically, and normally distributed, and s^2 be the sample variance. To assess the model within an entire test region, a single **global validation metric** based on the L_1 norm and the L_∞ norm (worst-case idea), with linear interpolation, is defined, respectively as (Oberkembf and Barone, 2004).

$$\left| \frac{\hat{e}}{\bar{y}^E} \right|_{avg} = \frac{1}{x_u - x_l} \int_{x_l}^{x_u} \left| \frac{y^M(x) - \bar{y}^E(x)}{\bar{y}^E(x)} \right| dx \quad (2.19)$$

$$\left| \frac{\hat{e}}{\bar{y}^E} \right|_{max} = \max_{x_l \leq x \leq x_u} \left| \frac{y^M(x) - \bar{y}^E(x)}{\bar{y}^E(x)} \right| \quad (2.20)$$

The advantage of the above metrics is that they offer the capability of validating over a region rather than individual design sites. However, one difficulty of this method is that it relies on good interpolation of error function $\bar{y}^E(x)$ from observed sites to non-observed sites, which might not be accurate. Secondly, in multi-dimensional cases, the evaluations of such interpolation can be computationally expensive.

2.6.3 Hypothesis Testing based Metrics

By assessing prediction confidence, the model validation problem can be treated as a hypothesis test. Classical hypothesis testing is a well-developed statistical method of choosing between two competing models of an experimental outcome.

In the hypothesis test approach developed by Chen et al. (2004) and Buranathiti et al. (2004), metamodels are utilized for uncertainty propagation of simulation models. The probability distributions of function performance at multiple design settings are used to generate the joint probability distributions. The contours of the joint probability distributions are then used to define the boundary of a given confidence level for model validation and compared with the results from physical tests. However, this approach is more useful for rejecting (invalidating) a model rather than accepting (validating) a model.

It has been argued that the classical hypothesis testing is difficult to interpret and sometimes misleading. As an alternative method, the Bayesian hypothesis testing which uses assumptions on the prior distribution for the hypothesis that the model is incorrect, could be useful.

Mahadevan and Rebba (2005) developed a Bayesian hypothesis testing approach. As a result of applying the Bayesian analysis when comparing two competing hypotheses, Bayes factor is a metric derived from the Bayesian hypothesis testing used to compare prior and posterior distributions (Mahadevan et al., 2005). By definition, **Bayes factor** is the ratio of posterior and prior density values at the predicted value of a given set of input data. The same input data are used in the model prediction as well as in the validation experiment, so that the predicted output may be compared with the measured output.

One important difference between the classical hypothesis test and the Bayesian hypothesis test is that the Bayesian approach focuses on model acceptance whereas classical hypothesis testing focuses on model rejection.

However, as pointed out by Romero (2007), one widely recognized problem with hypothesis tests is that hypothesis tests themselves have subjectivity in the level-of-significance

criteria. Furthermore, small perturbations in the level-of-significance threshold can switch between rejecting and accepting a model. Furthermore, a potential problem with hypothesis test is that the more noisy and uncertain the experiment, the easier it is to pass the validation test, and vice versa: the more precise the validation experiment, the more difficult to pass.

One possible way to solve this problem could be to allow a small amount of acceptable bias error between the model and data, and then test the hypothesis that the differences are likely less than this allowed error.

2.6.4 Metrics based on Pooling Multiple Data

The above validation metrics are limited to comparing the mean prediction of a computer model and the mean performance of a physical system. Although hypothesis testing based validation metrics can be used to compare the mean and variance of computer model output with that of experimental data, the metrics only apply for a specific input setting \mathbf{x} and requires a large amount of physical experimental data which is always difficult to gather in practice.

A *u-pooling method* recently developed by Ferson et al. is used to measure the difference between the physical experiments and the distribution of computer outputs. A nice feature of the u-pooling method is that it allows for integrating or pooling all available physical experiments over a validation domain at different input settings \mathbf{x} into a single aggregate metric. First, a value u_i is obtained for each experiment by calculating the CDF at y_i^e , i.e.,

$$u_i = F_{\mathbf{x}_i^e}(y_i^e) \quad (i=1, \dots, N^e), \quad (2.21)$$

where y_i^e represents a physical observation at the experimental site \mathbf{x}_i^e ($i=1, \dots, N^e$). $F_{\mathbf{x}_i^e}(y)$ represents the corresponding CDF function generated by the updated model $y^{m'}(\mathbf{x}, \Theta)$ at \mathbf{x}_i^e .

Figure 2.8 (a) provides an illustration of calculating the values u_i for three observations $y_1^e(\mathbf{x}_1^e)$, $y_2^e(\mathbf{x}_2^e)$, and $y_3^e(\mathbf{x}_3^e)$. After pooling all values of u_i for all physical experiments, a distribution of u_i could be characterized. According to Ferson et al., if each physical observation y_i^e hypothetically comes from the same ‘mother’ distribution $F_{\mathbf{x}_i^e}(y)$, all u_i ’s are expected to constitute a stranded uniform distribution on $[0, 1]$. An explanation of the u-pooling method is given in Figure 2.8, with three ($N^e=3$) experimental sites. By comparing the empirical distribution of u_i to that of the standard uniform distribution, the area difference (depicted as the shaded region in Figure 2.8 (b), henceforth termed ‘u-pooling’ metric (Ferson et al. 2008) can be used to quantify the mismatch between the dispersion of physical experiments and the distributions of model output. The larger the difference, the less agreement, and therefore less accuracy can be concluded.

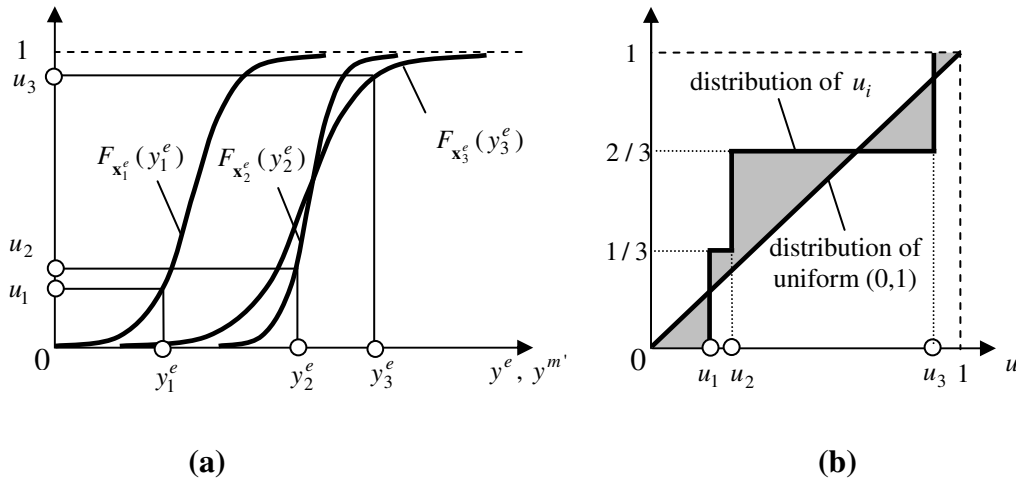


Figure 2.8 Illustration of the u-pooling method

From the above introduction, we note that the u-pooling method becomes especially handy when a sparse set of physical experiment data was collected over a wide region with limited or no repeated tests at each site. One drawback of the u-pooling approach is that it

assumes that the data can be reproduced with the predicted mother distribution, which may not be true if the predicted model distribution is resulted by uncertainty that is different from the cause of uncertainty observed in the experimental data.

2.7 Concepts of Model Calibration and Bias-Correction

Calibration and bias-correction are two approaches employed to improve the agreement between a computer model and the observed experiments. In this section the similarity and the difference between the concepts of model calibration and bias-correction are reviewed.

(1) Model Calibration

Computer models often have some uncertainty with the values of physical constants. These values can be determined by using the results from physical experiments to calibrate the simulation models. In model calibration, the goal is to adjust the value of the calibration parameters to bring the computer model outputs as close as possible to the physical observations. There is clear distinction between *calibration* and *tuning* (Higdon et al., 2005): calibration parameters have physical interpretation, while tuning parameters usually have little or no meaning in the physical system. In practice, the parameters are usually treated indifferently. Denote $y^m(\mathbf{x}, \boldsymbol{\theta})$ as the computer model output given input vector $(\mathbf{x}, \boldsymbol{\theta})$, where \mathbf{x} are observable inputs which are often controllable, and $\boldsymbol{\theta}$ are additional unobservable calibration and tuning parameters which are required to run the computer code.

For complex codes and corresponding experiments, one computation and one experiment can each yield thousands of data-values – traces of multiple response variables over time and

space. There may be many parameters in θ that could be adjusted to bring the computer model toward the data.

One simple approach is to minimize the mean squared error between the prediction from a simulation model and the results from physical experiments, i.e.,

$$\text{Minimize } \frac{1}{N} \sum_{i=1}^N [y^m(\mathbf{x}_i, \theta) - z_i]^2, \quad (2.22)$$

where $y^m(\mathbf{x}_i, \theta)$ is the simulation model, z_i ($i=1, 2, \dots, N$) are physical experiment results; $\mathbf{x}_i = [x_{i1}, x_{i2}, \dots, x_{ik}]^T$ ($i=1, 2, \dots, N$) are sample points, $\theta = [\theta_1, \theta_2, \dots, \theta_m]^T$ are m unknown physical constants, k is the number of model input variables \mathbf{x} . A metamodel (denoted as $\hat{\eta}(\mathbf{x}_i, \theta)$) could be used to replace the computationally expensive simulation model $y^m(\mathbf{x}_i, \theta)$. For example, Leoni, et al. (2000) used Kriging metamodels to calibrate heat transfer simulation models of wearable computers. In Figure 2.9, 16 sampling points for $y^m(\mathbf{x}_i, \theta)$ and 5 samples for z_i are used for calibrating the parameter θ . The best θ for calibrating (tuning) parameters could be around c_3 .

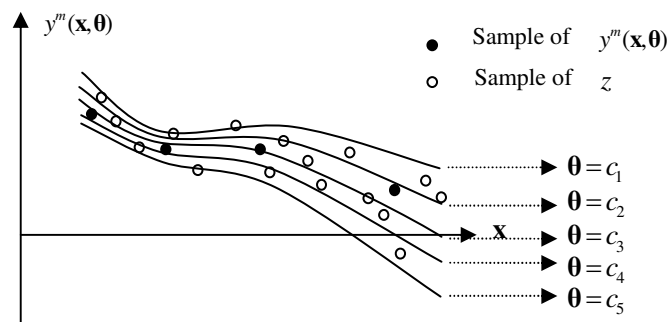


Figure 2.9 Concept of model calibration

(2) Model Bias-correction

Calibration approaches introduced earlier generally need a large amount of computer experiment data, especially when calibration parameters are high-dimensional. If there are no (affordably) correctable flaws in the computer model, and one still wants to use the computational model to make predictions, a second way in addition to calibration is the so-called model **bias-correction**, which adjusts a model by adding the estimated *bias function* (Easterling et al., 2002). As a result, with the added *bias function*, the adjusted model is based on the relation

$$y(\mathbf{x}) = y^m(\mathbf{x}) + \delta(\mathbf{x}), \quad (2.23)$$

where $y^m(\mathbf{x})$ is the output of computer model, and $\delta(\mathbf{x})$ denotes the *bias function*. Bias-correction focuses on characterizing the systematic bias $\delta(\mathbf{x})$ between the computer output and reality.

Bias is the evidence of correctable flaws in either the computational model or the experiments, which could be due to the wrong model assumption or wrong parameter values. For a model that has been calibrated, it is still possible that there is still residual of error that can not be remedied by calibration or other means. In such cases, a bias function can be applied to account for the remaining errors. The distribution of bias function $\delta(\mathbf{x})$ not only captures the correction made to the computer model, but also incorporates the uncertainty caused by the experiment error.

To quantify the uncertainty of a bias function due to the lack of sample points, various approaches could be used, e.g., the Gaussian process model and the linear regression. It is also possible to incorporate the bias-correction and calibration at the same time as we will further demonstrate in Chapter 5 that examines various model updating strategies.

Chapter 3. A New Kriging Model with Non-Stationary Covariance

Structure

Nomenclature

$Z(\mathbf{x})$	the Gaussian process indexed by \mathbf{x}
$\boldsymbol{\beta}^T \mathbf{h}(\mathbf{x})$	the polynomial regression part in Kriging model
C_{stat}	stationary covariance
ρ_{stat}	stationary correlation
$C_{nonstat}$	non-stationary covariance
$\rho_{nonstat}$	non-stationary correlation
Θ	hyperparameter set
J	number of function basis centers
L	number of input variables
l	index of input variable (i.e. dimension)
$\theta^{(l)}$	correlation parameter for input variable $x^{(l)}$
$f^{(l)}(\mathbf{x})$	general mapping function
$f^{(l)}(x^{(l)})$	mapping function (univariate)
$g^{(l)}(\mathbf{x})$	general density function
$g^{(l)}(x^{(l)})$	mapping function (univariate)
$\eta_k^{(l)}$	hyperparameter in the piecewise density function

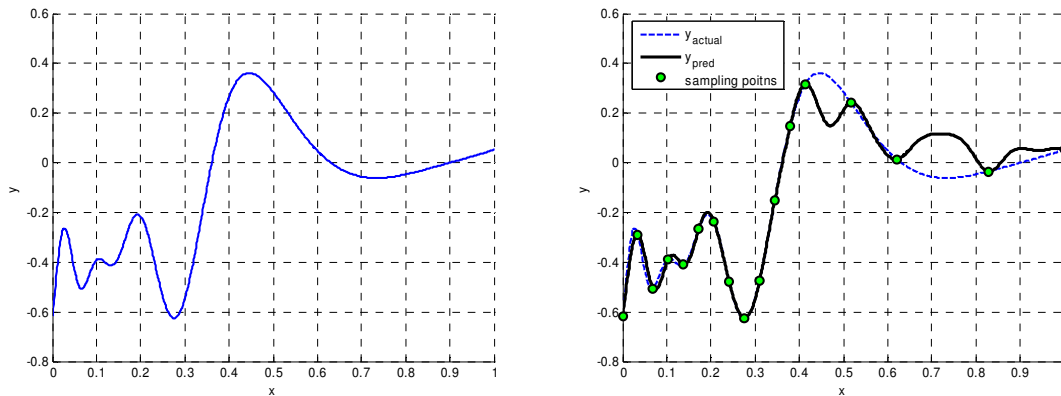
ξ_k	knot in the piecewise density function
K	number of pieces in the piecewise density function
k	index of function piece ($k=1,2,\dots,K$); index of knots or hyperparameters

3.1 Introduction

Among the widely used metamodeling techniques (Friedman, 1991, Box, et al., 1978, Hardy, 1971, Sack et al, 1989, Jin et al., 2001, Wang et al., 2001, Booker et al., 1999, Barthelemy and Haftka, 1993), Kriging is considered powerful and flexible for building surrogate models (or metamodels) of simulated response surfaces with different functional forms (Wang et al., 1999, Simpson, et al., 2001). As discussed in Section 2.2 in Chapter 2, one of the distinctive advantages of Kriging is that it provides not only the prediction of the response at any site, but also the Mean Square Error (or the uncertainty) associated with the prediction.

In a conventional Kriging model, a response is assumed to be a spatial random process with stationary covariance function. The stationary covariance, like the one in Eq. (3.2), implies that the smoothness of a response is fairly uniform in each region of the input space (Paciorek, 2003). This is a convenient assumption that simplifies the analysis and lessens the amount of prior information required (Currin et al., 1991). However, cases are common where the level of smoothness of a response could change dramatically throughout the whole design region. For example, in engineering design, when subsystem models with distinctive underlying physics are integrated, the system response behavior can differ greatly from one design region to another. Similar phenomena have been observed in geostatistics and environmental problems, where the geology of spatial locations greatly influences the correlation between responses (Schmidt and O'Hagan, 2003; Kim et al. 2005). In those cases, the assumption of the uniformity of smoothness

is not well satisfied. One such function is illustrated in Figure 3.1, in which the roughness in region $x \in [0, 0.3]$ is larger than in the region $[0.3, 1]$. Assuming a stationary covariance structure forces a trade-off in which the estimated stationary covariance reflects the average smoothness over the entire domain, but fails to reflect the true local smoothness in each region.



(a) True function

(b) Kriging prediction (stationary covariance)

Figure 3.1 Example of Kriging prediction with stationary covariance

One natural approach to solving this problem is to consider relaxing the stationary covariance assumption and allowing a non-stationary one. The idea of using non-stationary covariance in metamodeling can be found in the engineering design literature (Lin et al., 2004 and Farhang Mehr et al., 2005). However, all existing works consider the irregular performance behavior only in sampling but not in fitting metamodels. Based on the prediction error and the irregularity of a response surface, the entries of the covariance matrix are adjusted, which essentially leads to a non-stationary covariance for choosing sample sites. While samples generated by these methods tend to be non-uniform in the input space, all these existing work used ordinary stationary Kriging for building the metamodels. Moreover, they use heuristic

methods of adjusting the covariance matrix that do not guarantee that the covariance matrix is positive definite, a crucial property for the stability of a fitted Kriging model.

Non-stationary covariance Gaussian process models have been used for fitting response surface models in the fields of statistics, geostatistics and machine learning. However, this has primarily been under the scenario of physical experiments in relatively low dimensions (Santner et al., 2003). Various approaches have been proposed to formulate the non-stationary covariance structure. Sampson et al. (1992) developed a spatial deformation approach to reallocate all the points. Gibbs (1997) and MacKay et al. (1998) proposed two methods of representing the non-stationary behavior: the first is to directly formulate a non-stationary covariance function, and the second is the so-called nonlinear map approach, in which the original Euclidean space is mapped to a new one for which the covariance can be approximated as stationary. Paciorek (2003) used a process convolution approach extended from Higdon et al. (1997)'s method and Gibbs' first method. Other related works could be found in Schmidt and O'Hagan (2003), Pintore et al. (2004), and Stein (2005). Gramacy et al. (2004) presented an approach that utilizes Gaussian process trees to implement the non-stationary Gaussian process. However, discontinuity of the response across subregions cannot be avoided.

Little prior work has been conducted on non-stationary covariance modeling for complex system design based on computer experiments. This is most likely because complex design problems are often high dimensional, and non-stationary covariance functions tend to be overparameterized in high dimensions. In this work, we develop an efficient method that allows non-stationary covariance in Kriging metamodeling for high-dimensional engineering applications with computer experiments. We use a nonlinear mapping approach to represent the non-stationary covariance structure, in which a parameterized density function is used to map the

original space to one in which the covariance becomes approximately stationary. Although high-dimensionality is undoubtedly a prohibitive problem with physical experimental data, on which most of the prior work in non-stationary covariance modeling has focused, we argue that the approach can be made quite robust for high dimensional computer experimental data. This is due to two factors: First, unlike physical experiments, computer experiments are usually perfectly repeatable, which drastically reduces the amount of data required to accurately fit non-stationary covariance functions in high dimensions. Second, we propose a modified version of Gibb's nonlinear map approach (1997), with a sparse, yet flexible, parameterization that is well suited for high-dimensional computer experimental data.

The organization of this work is as follows. In Chapter 3.2, a review of Kriging modeling with a stationary covariance function is first provided; the Gibbs' nonlinear map approach is then introduced. Details of the proposed approach are provided in Chapter 3.3. Computational issues related to the optimization strategies for estimating the hyperparameters is also addressed. In Chapter 3.4, mathematical and engineering examples are used to illustrate the effectiveness of the proposed approach. We demonstrate that the proposed method not only improves the accuracy of metamodels for functions with changing irregularity, but also effectively quantifies the prediction uncertainty associated with the use of metamodels in engineering applications. Concluding remarks are given in Chapter 3.5.

3.2. Technological Base

3.2.1 Kriging metamodeling with a stationary covariance function

In the conventional Kriging model (Sacks et al., 1989), the performance $y(x)$ is modeled as

$$y(\mathbf{x}) = \boldsymbol{\beta}^T \mathbf{h}(\mathbf{x}) + Z(\mathbf{x}), \quad (3.1)$$

where $\boldsymbol{\beta}^T \mathbf{h}(\mathbf{x})$ is the regression component (e.g., a polynomial) which captures global trends; $Z(\mathbf{x})$ is assumed a Gaussian process indexed by input variables \mathbf{x} , with zero mean and stationary covariance. From a Bayesian perspective (Currin et al., 1991, Morris et al., 1993), the prior knowledge of the performance $y(\mathbf{x})$ is specified by a Gaussian process, which is characterized by the prior mean (i.e. the global trend) and prior covariance. Given the observations, the posterior process is also a Gaussian process (treating the covariance parameters as known and assuming a Gaussian prior distribution for $\boldsymbol{\beta}$). The prediction of $y(\mathbf{x})$ is usually taken to be the posterior mean, and the prediction uncertainty is quantified by the posterior covariance.

The conventional Kriging model assumes that the Gaussian process has stationary covariance, with the covariance function defined as follows:

$$C_{st}(\mathbf{x}_m, \mathbf{x}_n; \Theta) = \sigma^2 \rho_{st}(\mathbf{x}_m, \mathbf{x}_n; \boldsymbol{\theta}), \quad (3.2)$$

where ρ_{st} is the correlation function. The hyperparameter set Θ is composed of $\{\sigma^2; \boldsymbol{\theta}\}$. A frequently used Gaussian correlation function is:

$$\rho_{st}(\mathbf{x}_m, \mathbf{x}_n; \boldsymbol{\theta}) = \exp\left(-\sum_{l=1}^L \theta^{(l)} (\mathbf{x}_m^{(l)} - \mathbf{x}_n^{(l)})^2\right). \quad (3.3)$$

The variance σ^2 provides the overall vertical scale relative to the mean of Gaussian process in the output space, $\boldsymbol{\theta} = \{\theta^{(l)} (l=1, 2, \dots, L)\}$ are the correlation parameters (scaling factors) associated with each input variable $\mathbf{x}^{(l)}$, which reflects the smoothness of the true performance. The stationary covariance indicates that the correlation function $\rho_{st}(\mathbf{x}_m, \mathbf{x}_n; \boldsymbol{\theta})$ between any two

sites \mathbf{x}_m and \mathbf{x}_n depends on only the distance (scaled by θ) between \mathbf{x}_m and \mathbf{x}_n . In Eqs. (2.2) and (2.3), the subscript ‘*st*’ means ‘stationary’.

3.2.2 Representing Non-stationary Covariance: The Nonlinear Map Approach

Various approaches exist in literature to represent non-stationary covariance structures. The nonlinear map method (Gibbs, 1997) is attractive among others because it is intuitively interpretable with a notion of space mapping. A simple one-dimensional illustration of the map is provided in Figure 3.2. A mapping function $f(\mathbf{x})$ is defined by integrating a density function $g(\mathbf{x})$ (see Eq. (3.4) for details). It can be seen in the original space (Figure 3.2 (a)) that the true function, denoted as $y(\mathbf{x})$, is hard to be modeled with a stationary covariance due to abruptly changing smoothness of $y(\mathbf{x})$. However, through mapping to the new space, the new response exhibits an improved uniformity of smoothness across the whole region. Hence the stationary covariance can be employed in the new space. Following the definition of the mapping function $f(\mathbf{x})$ as the integration of $g(\mathbf{x})$, the distance between point C and D in the new space $|\tilde{\mathbf{x}}_D - \tilde{\mathbf{x}}_C|$ corresponds to the shaded area in panel (a). Obviously, the higher density function around point C accounts for the higher abruptness of the real response. In other words, the relation between the density function $g(\mathbf{x})$ and the smoothness of the real response can be established.

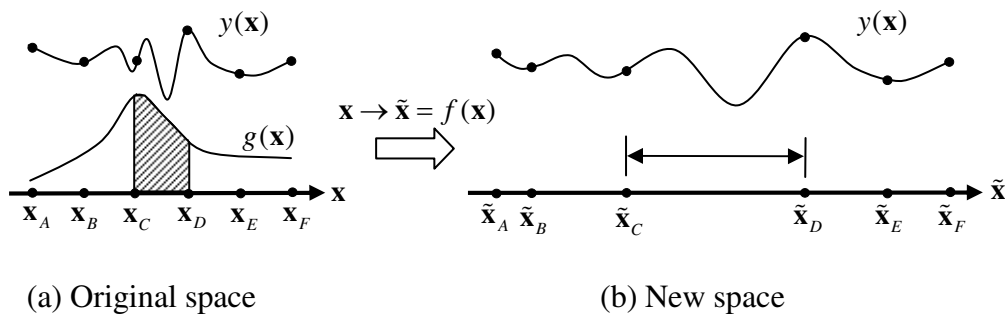


Figure 3.2 A conceptual illustration of the nonlinear map

The mapping function becomes more complicated in high-dimensional situations. It is noteworthy that as long as the density function is positive and continuous, the positive-definiteness of the resulting non-stationary covariance can be strictly guaranteed. This is one significant characteristic of the approaches based on map and space deformation. In Gibbs' approach (refer to Paciorek (2003) for further details), the multidimensional mapping functions must be one-to-one and continuous, which ensures the order of points on any non-intersecting line in original \mathbf{x} space is preserved in the new $\tilde{\mathbf{x}}$ space and the line in the $\tilde{\mathbf{x}}$ space is non-intersecting. Denote the mapping from \mathbf{x} to $\tilde{\mathbf{x}}$ as $\tilde{\mathbf{x}} = \mathbf{f}(\mathbf{x}) = (f^{(1)}(\mathbf{x}), f^{(2)}(\mathbf{x}), \dots, f^{(L)}(\mathbf{x}))$, where $f^{(l)}(\mathbf{x})$ defines the l^{th} coordinate of $\tilde{\mathbf{x}}$, i.e., $\tilde{x}^{(l)}$. To achieve the aforementioned mapping, the l^{th} mapping function $f^{(l)}(\mathbf{x})$ is defined as an integral over a density function $g^{(l)}(\mathbf{x})$.

$$f^{(l)}(\mathbf{x}) = x_0^{(l)} + \int_{x_0^{(l)}}^{x^{(l)}} \dots \int_{x_0^{(L)}}^{x^{(L)}} g^{(l)}(\mathbf{x}') dx'^{(1)} \dots dx'^{(L)}, \quad (3.4)$$

where L is the number of input variables; $\mathbf{x}_0 = (x_0^{(1)}, \dots, x_0^{(L)})$ is a reference vector, which is often chosen to be somewhere in the center of the data; The density function $g^{(l)}(\mathbf{x})$ is further defined as a weighted sum of positive radial basis functions:

$$g^{(l)}(\mathbf{x}) = \sum_{j=1}^J \omega_j^{(l)} \psi_j(\mathbf{x}), \quad (3.5)$$

where $\{\psi_j(\mathbf{x})\}$ are a set of positive basis functions, common to all density functions $g^{(l)}(\mathbf{x})$; J is the number of basis functions. To ensure positive weights, $\omega_j^{(l)}$ can be taken as $\omega_j = e^{\alpha_j^{(l)}}$. The integral in Eq. (3.4) should be easily evaluated. To this end, uncorrelated Gaussian basis is utilized to form $\psi_j(\mathbf{x})$, i.e.

$$\psi_j(\mathbf{x}) = \exp \left[-\frac{1}{2} \sum_{l=1}^L \frac{(x^{(l)} - c_j^{(l)})^2}{\sigma^{(l)2}} \right], \quad (3.6)$$

where $c_j^{(l)}$ and $\sigma^{(l)}$ quantify respectively the center and width for l^{th} dimension of the j^{th} basis function. $c_j^{(l)}$ and $\sigma^{(l)}$ are predetermined and viewed as known and fixed. Applying the mapping function Eq. (3.4) to the stationary covariance function in Eq. (3.1), the non-stationary version of the covariance/correlation function in Eq. (3.2) is obtained by

$$C_{non-st}(\mathbf{x}_m, \mathbf{x}_n; \Theta) = \sigma^2 \rho_{non-st}(\mathbf{x}_m, \mathbf{x}_n; \Theta) = \sigma^2 \exp \left(-\sum_{l=1}^L \left(f^{(l)}(\mathbf{x}_m) - f^{(l)}(\mathbf{x}_n) \right)^2 \right), \quad (3.7)$$

where the subscript ‘*non-st*’ means ‘non-stationary’. Note the original $\mathbf{x}^{(l)}$ in Eq. (3.2) is replaced by $f^{(l)}(\mathbf{x})$ and the original $\theta^{(l)}$ disappears. As a result, the hyperparameter set Θ becomes $\{\sigma^2; \alpha_j^{(l)} (j=1, 2, \dots, J; l=1, 2, \dots, L)\}$, as opposed to its stationary counterpart $\{\sigma^2; \theta^{(l)} (l=1, 2, \dots, L)\}$.

3.3. A Proposed Non-stationary Covariance Structure

Drawbacks of Gibbs’ nonlinear map method are immediately observable. From Eqs. (3.4~3.6), the mapping function $f^{(l)}(\mathbf{x})$ and the density function $g^{(l)}(\mathbf{x})$ are multivariate functions of \mathbf{x} . The unknown hyperparameters $\alpha_j^{(l)}$ in $g^{(l)}(\mathbf{x})$ for different dimensions are indeed independent. In other words, with the nonlinear map method, the non-stationary covariance structure relies on $J \times L$ unknown hyperparameters $\alpha_j^{(l)}$ s’ in total. It should be pointed out that J is the number of function basis centers, and it should be large enough so that the non-stationary structure is able to cover the design space. This formulation is affordable in low dimensional situations with small J and L , but can yield a large number of

hyperparameters $\alpha_j^{(l)}$ in high dimensional cases because J increases with L. In other words, the non-stationary covariance will be over-parameterized in high dimensional situations, which has undesirable consequences on the stability and robustness of the model fitting. It is the goal in this section to develop certain forms of density functions using as few hyperparameters as possible to address the aforementioned difficulties.

3.3.1 Proposed Density Function

The non-stationary structure is simplified by assuming that the varying smoothness behavior in any single input variable is independent with respect to the other input variables. This simplifying assumption reduces the multivariate density functions to *univariate* density functions in which $g^{(l)}(\mathbf{x})$ depends only on a particular $x^{(l)}$. By substituting $g^{(l)}(x^{(l)})$ in place of $g^{(l)}(\mathbf{x})$, the mapping function in Eq. (3.4) becomes

$$f^{(l)}(\mathbf{x}) = f^{(l)}(x^{(l)}) = x_0^{(l)} + \int_{x_0^{(l)}}^{x^{(l)}} g^{(l)}(x') dx', \quad (3.8)$$

where $x_0^{(l)}$ is the reference point. Instead of using the nonlinear form in Gibb's approach, further simplifications are made by assuming that $g^{(l)}(x^{(l)})$ is a continuous piecewise linear function in $x^{(l)}$. The continuity of $g^{(l)}(x^{(l)})$ is emphasized here because it is a critical requirement of the mapping functions as stated in section 3.2.2. For a selected number of pieces K, $g^{(l)}(x^{(l)})$ is defined as a summation of K linear components,

$$g^{(l)}(x^{(l)}) = \sum_{k=1}^K g_k^{(l)}(x^{(l)}; a_k^{(l)}, b_k^{(l)}). \quad (3.9)$$

Each component $g_k^{(l)}(x^{(l)}; a_k^{(l)}, b_k^{(l)})$ is a single linear function over its support interval, while being zero elsewhere:

$$g_k^{(l)}(x^{(l)}; a_k^{(l)}, b_k^{(l)}) = \begin{cases} a_k^{(l)} + b_k^{(l)} x^{(l)}, & x^{(l)} \in [\xi_{k-1}, \xi_k] \\ 0, & x^{(l)} \notin [\xi_{k-1}, \xi_k] \end{cases}, (k=1, 2, \dots, K), \quad (3.10)$$

where $\{a_k^{(l)}, b_k^{(l)}\}$ are the linear parameters for the k^{th} linear component; $\{\xi_0, \xi_1, \dots, \xi_K\}$ are a series of knots placed along input variable $x^{(l)}$. Imposing the continuity constraints to $g^{(l)}(x^{(l)})$, Eq. (3.10) can be reformulated using the following linear substitutions:

$$\begin{cases} a_k^{(l)} = (\xi_k \eta_{k-1}^{(l)} - \xi_{k-1} \eta_k^{(l)}) (\xi_k - \xi_{k-1})^{-1} \\ b_k^{(l)} = (\eta_k^{(l)} - \eta_{k-1}^{(l)}) (\xi_k - \xi_{k-1})^{-1} \end{cases}, (k=1, 2, \dots, K). \quad (3.11)$$

The original linear parameters $\{a_k^{(l)}, b_k^{(l)}\}$ ($k=1, 2, \dots, K$) are now replaced by $K+1$ new parameters $\{\eta_0^{(l)}, \eta_1^{(l)}, \dots, \eta_K^{(l)}\}$. It can be verified that $\{\eta_0^{(l)}, \eta_1^{(l)}, \dots, \eta_K^{(l)}\}$ are equal to the density values at each knot respectively, i.e., $g^{(l)}(\xi_k) = \eta_k^{(l)}$, ($k=0, 1, 2, \dots, K$). According to Eq. (3.8), if the reference point is placed at the knot ξ_0 , the mapping function $f^{(l)}(x^{(l)})$ can be formulated as

$$\begin{aligned} f^{(l)}(x^{(l)}) &= \xi_0 + \int_{\xi_0}^{x^{(l)}} g^{(l)}(x') dx' \\ &= \xi_0 + \int_{\xi_0}^{\xi_1} g^{(l)}(x') dx' + \dots + \int_{\xi_{M-1}}^{\xi_M} g^{(l)}(x') dx' + \int_{\xi_M}^{x^{(l)}} g^{(l)}(x') dx', \quad (3.12) \\ &= \xi_0 + \sum_{k=1}^M \int_{\xi_{k-1}}^{\xi_k} g_k^{(l)}(x'; \eta_{k-1}^{(l)}, \eta_k^{(l)}) dx' + \int_{\xi_M}^{x^{(l)}} g^{(l)}(x'; \eta_{k-1}^{(l)}, \eta_k^{(l)}) dx' \end{aligned}$$

where M ($0 \leq M < K$) is the index of the knot left-neighboring $x^{(l)}$, i.e., $\xi_M < x^{(l)} \leq \xi_{M+1}$. The number of parameters or the d.o.f. of $g^{(l)}(x^{(l)})$ is $K+1$. In particular, $K=1$ means that $g^{(l)}(x^{(l)})$ reduces to a single linear function $g^{(l)}(x^{(l)}; \eta_0^{(l)}, \eta_1^{(l)})$. Because $g^{(l)}(x^{(l)})$ is linear and univariate, all integrals in Eq. (3.12) can be easily computed in analytical way. The sum of integrals in $f^{(l)}(x^{(l)})$ over the interval $[\xi_0, x^{(l)}]$ corresponds to the shaded area in Figure 3.3.

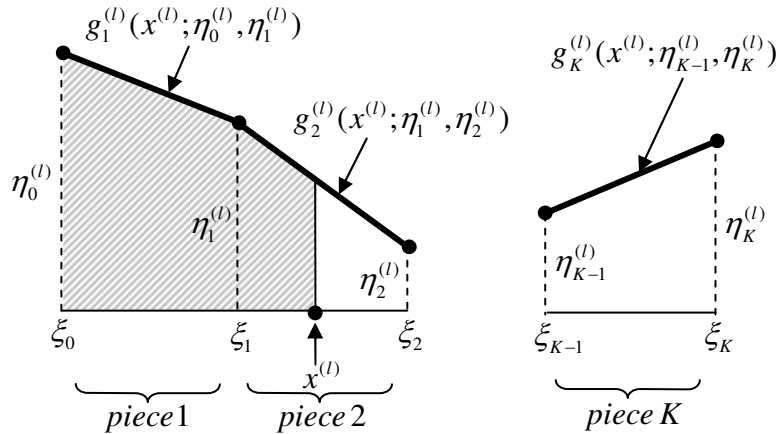


Figure 3.3 Continuous piecewise linear density function

Constraining $g^{(l)}(x^{(l)})$ is equivalent to imposing a bound to $\eta_k^{(l)}$ since $g^{(l)}(x^{(l)})$ is linear. For instance, $lb < \eta_k^{(l)} < ub$, for $k = 0, 1, \dots, K$, is equivalent to $lb < g^{(l)}(x^{(l)}) < ub$. When $\eta_0^{(l)} = \dots = \eta_{K-1}^{(l)} = \eta_K^{(l)}$, $g^{(l)}(x^{(l)})$ is essentially a constant, hence the non-stationary covariance reduces to the stationary one. The number of knots ξ_k (which is $K+1$) reflects the resolution and complexity of the density function.

3.3.2 Determining Hyperparameters

Various methods exist for estimating the Kriging hyperparameters. One way is to perform the integration over Θ using Monte Carlo methods (Handcock et al., 1993, Gibbs 1997). The method identifies the best values of the hyperparameters as the mean, median, or the mode of the posterior distribution of Θ . In an alternative approach, the most probable value of Θ is identified by maximum likelihood estimation (MLE) method (Mackay 1998, Li et al., 2003). Martin et al. (2004) compared the use of the AIC (Akaike Information Criterion) and the CV (Cross Validation) criterion. In this work, the MLE method is used to estimate the

hyperparameters for the non-stationary covariance. The Simulated Annealing method (Goffe et al., 1994) is used for optimization due to the highly nonlinear nature of the MLE function.

Compared to other non-stationary covariance structures, the proposed non-stationary covariance structure employs very few hyperparameters, even though the total number will be larger than that of the stationary Kriging model. One way to alleviate the problem is to place fewer knots along each variable in high dimensional problems or to place more knots along critical variables. The other way is to impose reasonable bounds for each $\eta_k^{(l)}$ to expedite the search. This is easy to implement through the proposed density function. For bounding $\eta_k^{(l)}$, a multiple-stage strategy is employed, in which the density function is estimated sequentially. Figure 3.4 illustrates the idea of such strategy with, for example, two stages. In the first stage, the density function is constructed with a low d.o.f., say, $K=1$ (i.e. d.o.f.=2). After $\eta_0^{(l)}$ and $\eta_1^{(l)}$ are estimated (the filled squares), the density function is determined (the dashed line). In the second stage, the complexity of the density function could be increased, say, with $\{\eta_0^{(l)}, \eta_1^{(l)}, \eta_2^{(l)}\}$. Based on the estimated density function from the first stage, reasonable bounds can be set for $\{\eta_0^{(l)}, \eta_1^{(l)}, \eta_2^{(l)}\}$. It is worth noting that imposing the bounds for $\eta_k^{(l)}$ not only facilitates the optimization, but also allows us to express the belief about the abruptness of changing smoothness. If the smoothness is not expected to change abruptly, narrower bounds closer to their neighbors are preferred.

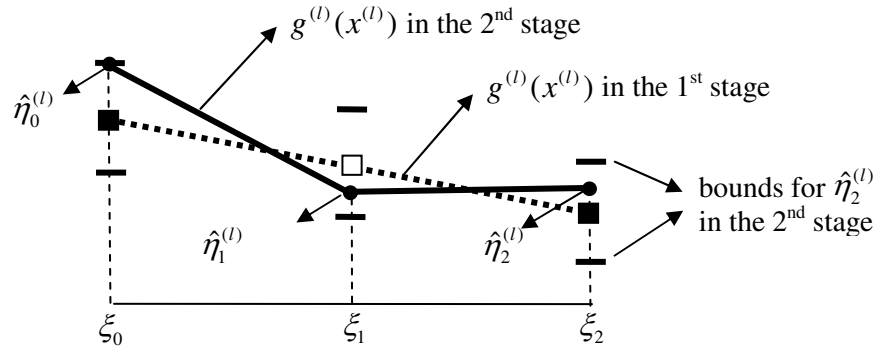


Figure 3.4 Setting bounds for the to-be-estimated $\hat{\eta}_k^{(l)}$'s

3.4 Case Study

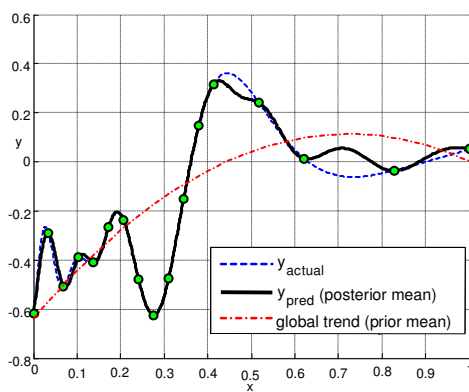
In this section, a few mathematical and engineering examples are presented to illustrate and verify the effectiveness of our proposed non-stationary covariance structure for modeling the varying smoothness of different responses. We first illustrate important characteristics of the approach with simple one- and two-dimensional examples. In Chapter 3.4, the approach for a high-dimensional vehicle crash/safety design example is demonstrated. A quadratic polynomial is used for the prior mean function in all cases. All input variables are normalized to the range $[0, 1]$. Based on the density function derived from the first stage, reasonable bounds for the Kriging model with non-stationary covariance are used in the second stage. In Chapter 3.4.2, the effectiveness of the proposed method in quantifying prediction uncertainty is illustrated.

3.4.1 Improvement of Prediction Accuracy

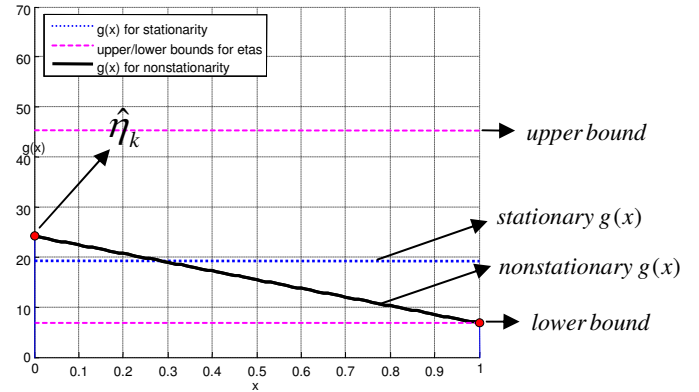
Ten mathematical examples and one engineering example are provided and discussed in that paper. For demonstrative purpose, only two 2D mathematical examples are selected and presented in this section.

(1) One-Dimensional Example

First consider the same example (Figure 3.1) used in the Introduction of this chapter, in which 17 sampling points are used to fit the Kriging model with a quadratic prior mean. The mathematical form of the true function is Function 11 (Eq. A11) in Appendix A. As observed earlier, the conventional Kriging model with stationary covariance fails to capture the varying level of smoothness of the function. Using the non-stationary Kriging method proposed in this work, two Kriging models are built by using density functions of different d.o.f. Figure 3.5 and Figure 3.6 show respectively the results of the fitted Kriging model and the density function used for both cases with our proposed method. In Figure 3.5(b) and Figure 3.6(b), the stationary density function (a horizontal straight line) used for the conventional Kriging is also provided for comparison. The difference between Figure 3.5 and Figure 3.6 is that the former has only two d.o.f. ($K=1$) for the density function, while the latter has nine d.o.f. ($K=8$). The hyperparameters $\hat{\eta}_k^{(l)}$ (hence the density functions) are estimated for each Kriging model by using the MLE approach discussed in section 3.3.



(a) Kriging prediction



(b) Estimated density function

Figure 3.5 Results of non-stationary Kriging with single linear density function ($K=1$)

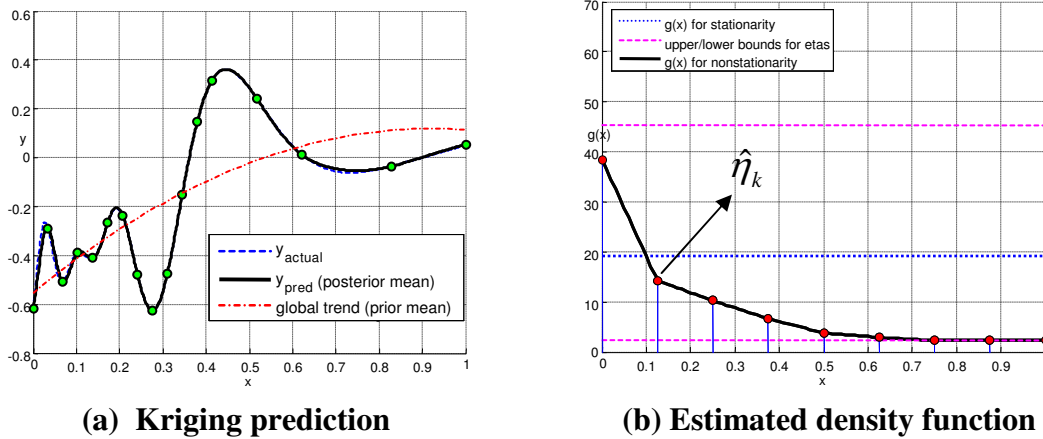


Figure 3.6 Results of non-stationary Kriging with piecewise linear density function ($K=8$)

To assess the accuracy of the fitted Kriging models, the response was predicted for 1000 evenly spaced test points generated over the interval $[0, 1]$. Table 3.1 provides the accuracy comparison of the three Kriging models. Three well-known accuracy metrics are employed, namely the R^2 (R-square), the RMSE (Rooted Mean Square Error) and the RAME (Relative Absolute Max Error). For R^2 , the larger the better; for RMSE and RAME, the smaller the better.

From Figure 3.5(b) it is noted that the single linear mapping function identified by maximizing the MLE has a negative slope, i.e., density function is smaller in the right half than in the left half. This properly reflects the fact that the left half region has higher roughness than the right part. Figure 3.5(a) indicates that prediction gaps still exist when using the single density function. The model in Figure 3.6 uses a slightly more complicated piecewise density function as well as wider bounds for $\hat{\eta}_k^{(l)}$. The density function adapts to the local behavior more closely and leads to almost perfect predictions.

Table 3.1 The accuracy comparison (* the best values)

Covariance structure	K	$d.o.f.$	R^2	$RMSE$	$RAME$
----------------------	-----	----------	-------	--------	--------

Stationary	N/A	1×1	0.9196	0.0743	0.7523
Non-stationary	1	2×1	0.9771	0.0396	0.4401
	8	9×1	0.9991*	0.0109*	0.2157*

The accuracy comparison across the above three metamodels is summarized in Table 3.1. The worst performance comes with the conventional Kriging with the stationary covariance shown in Figure 3.1, where R^2 is 0.9196, RMSE is 0.0743, and RAME is 0.7523. For the non-stationary Kriging model with the single linear density function in Figure 3.5(b), the accuracy is significantly improved. R^2 increases to 0.9771, while RMSE and RAME drop to 0.0396 and 0.4401 respectively. The best accuracy is offered by the Kriging model with the largest complexity ($K=8$), which provides enough flexibility and resolution to capture the locally changing smoothness.

(2) Two-Dimensional Example: evenly spaced sampling points

The second mathematical example (Function 1, Appendix A) is a two-dimensional problem. From the true surface in Figure 3.7 (a), it is observed that the smoothness of the real performance varies spatially. For the non-stationary Kriging, a density function with 4 d.o.f. ($K=3$) is used for each $x^{(l)}$. In this example, 18 sampling points are generated using the Optimal Latin Hypercube approach (Jin et al., 2005).

For verification, after fitting the various models based on the 18 sampling points, the response was predicted for a 300×300 grid of input values over the $[0, 1]^2$ region. The accuracy comparison between the stationary Kriging model and non-stationary Kriging models is summarized in Table 3.1. R^2 , RMSE and RAME are all significantly improved, respectively from 0.9591 to 0.9861, from 0.1238 to 0.0723, and from 1.0779 to 0.6058.

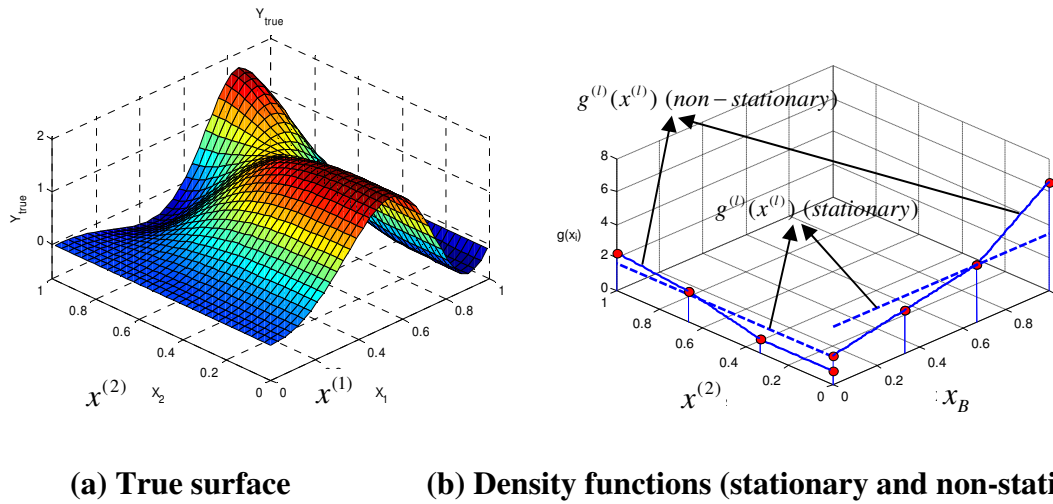


Figure 3.7 The true surface and the results of density functions (Function 1)

Table 3.1 The accuracy comparison (* the better values)

Covariance structure	K	$d.o.f.$	R^2	$RMSE$	$RAME$
Stationary	N/A	1×2	0.9591	0.1238	1.0779
Non-stationary	3	4×2	0.9861*	0.0723*	0.6058*

(3) Two-Dimensional Example: Adaptive Sampling Points

In example 1, the sampling points are evenly spaced by certain space-filling criteria. In this example, adaptive sampling points are examined (e.g. Sacks et al. 1989; Currin, et al., 1991; Lin et al., 2004; Farhang Mehr et al. 2005). With adaptive sampling, additional points are sequentially placed in regions that are identified with highly nonlinear or irregular behavior.

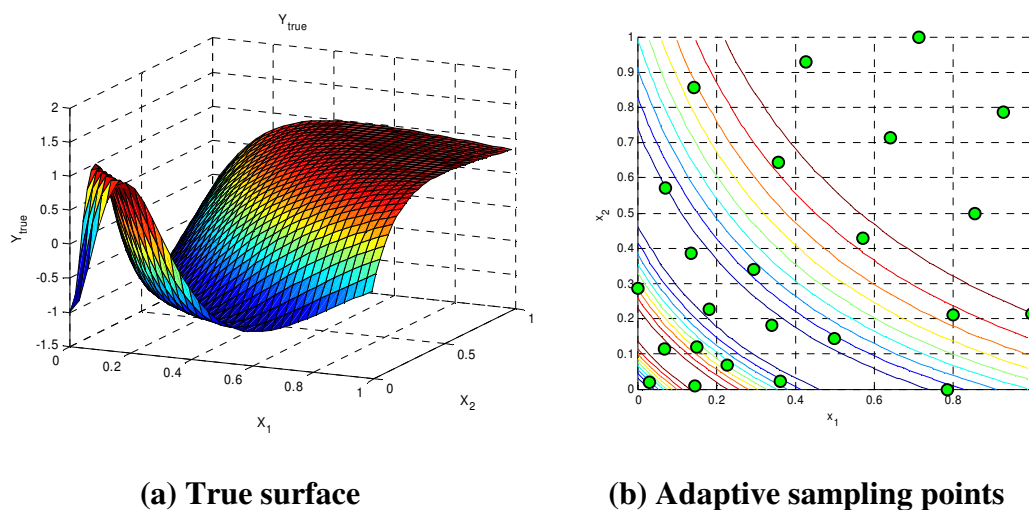


Figure 3.8 The true surface and adaptive sampling points

The assessment of the accuracy of the two Kriging models is summarized in Table 3.2. The accuracy of the non-stationary Kriging model is found to be much better than the stationary Kriging in terms of R^2 , RMSE, and RAME.

Table 3.2 The accuracy comparison (* the better values)

Covariance structure	K	d.o.f.	R^2	RMSE	RAME
Stationary	N/A	1×2	0.9346	0.1758	1.0996
Non-stationary	3	4×2	0.9777*	0.1025*	0.8610*

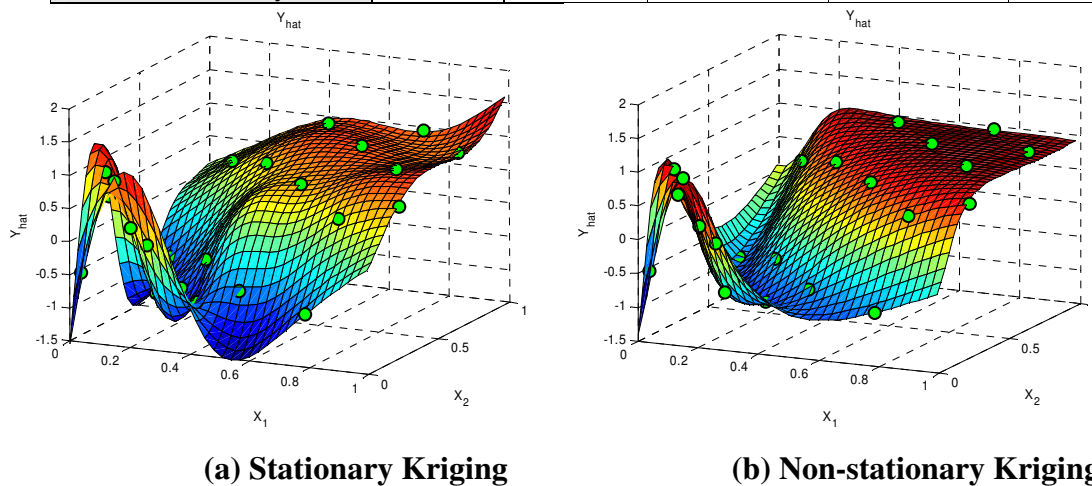


Figure 3.9 The predicted surface via the two Kriging models

The predicted surfaces via the stationary Kriging and the non-stationary Kriging are shown in Figure 3.9, indicating that the stationary Kriging model yields worse prediction in the smoother regions, in which fewer sampling points are placed. In contrast, the non-stationary Kriging shows superior capability in capturing the varying density of sampling points as well as the varying smoothness between regions.

(4) Tests via Multiple Functions and Various Sampling Sizes

Many factors contribute to the accuracy of a metamodel, e.g., the true response behavior, problem dimension, and the sampling size. It is our interest to test the robustness of the proposed method against various conditions on a set of functions (formulations and 3-D plots of ten testing functions are provided in Appendix A). We note that Functions 1-5 exhibit large changing smoothness; Functions 6-10 appear to be of less variability. We roughly categorize these into two groups, i.e., a non-stationary group and a stationary group.

To compare the robustness with respect to different sampling sizes, ten tests are conducted for each of the selected functions. In each test, the results from using stationary Kriging and non-stationary Kriging are compared. The number of pieces (i.e. K) is chosen at 3 for the non-stationary Kriging. For Functions 1-5, {30, 33, 36, 39, 42, 45, 48, 51, 55, 60} are used as the sampling size for the ten tests; for Functions 6-10, the sampling size follows {15, 17, 19, 21, 23, 25, 27, 29, 31, 33}. Note the sampling size in the latter set is smaller considering that Functions 6-10 are smoother than Functions 1-5. The Optimal Latin Hypercube is used to produce the sampling points throughout all tests; 300×300 grid points are used for accuracy

assessment. The results for the tests on Functions 1-5 and Functions 6-10 are summarized in Table 3.3.

Table 3.3 The accuracy comparison for Functions 1-10

Fun. No.	1	2	3	4	5	Total
N_{Stat}	1	3	2	2	2	10
$N_{Nonstat}$	9	7	8	8	8	40
Fun. No.	6	7	8	9	10	
N_{Stat}	3	3	3	5	4	18
$N_{Nonstat}$	7	7	7	5	6	32

In Table 3.3, N_{stat} is used to count the tests in which the stationary Kriging outperforms the non-stationary one; $N_{Nonstat}$ is used to count the tests in which the non-stationary Kriging outperforms the stationary one. For Functions 1-5, the $N_{stat} / N_{Nonstat}$ ratio is 10/40, which means that about 80% of the tests favor the non-stationary Kriging models when the function behavior is non-stationary. For Functions 6-10, the $N_{stat} / N_{Nonstat}$ ratio is 18/32, indicating that the non-stationary Kriging slightly outperforms the stationary Kriging. Results imply that using non-stationary Kriging at least will not deteriorate the prediction.

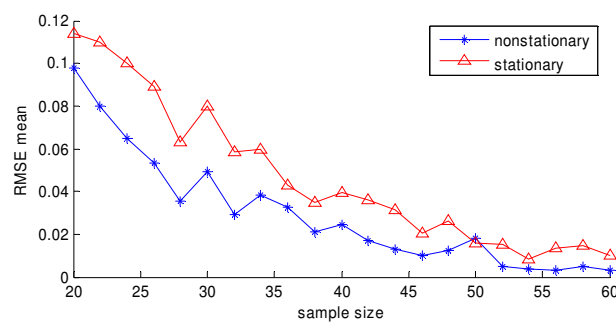


Figure 3.10 Average RMSE vs. sampling size (Function 1)

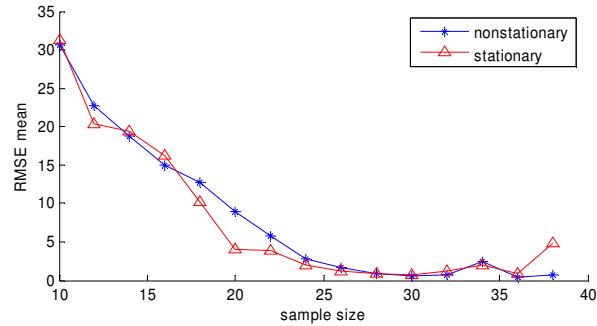


Figure 3.11 Average RMSE vs. sampling size (Function 9)

Figure 3.11 illustrates the average RMSE vs. sampling size, for Functions 1 and 9, which are selected to represent the typical non-stationary and stationary functions, respectively. Considering the random nature of Optimal Latin Hypercube, for each sampling size, ten experiment designs are conducted. From Figure 3.10, the non-stationary Kriging consistently achieves the lower average RMSE across over all the tested sampling sizes. In Figure 3.11, when the sampling size is not sufficient, the non-stationary Kriging is slightly less accurate than the stationary one; as the sampling size increases, they achieve the same level of accuracy. This indicates that when the sampling size is not sufficient, the proposed method might be misled by the sampling data.

We further test the average performance of our proposed non-stationary Kriging. In these tests, the sampling size (i.e. N_s in Table 3.4) is chosen as $N_s = 35$ for Functions 1-5 and $N_s = 25$ for Functions 6-10. Three Kriging models (one stationary Kriging model; two non-stationary Kriging models with $K=1$ and 3) are created in each test. Each test is repeated for ten times with the same sampling size (N_s) but different designs of Optimal Latin Hypercube sampling.

From Table 3.4, it is observed that most of the best and second best values of average RMSE result from the non-stationary Kriging model. When the sampling sizes are sufficient for

the respective function behaviors, the non-stationary Kriging outperforms the stationary Kriging in majority of the tested functions. It is also observed that the more complicated ($K=3$) non-stationary Kriging models are generally more accurate than the less complicated ($K=1$) counterparts.

Table 3.4 The RMSE average over ten tests for each function

(** the best values; * the second best values)

Fun. No.	N_s	average RMSE		
		Stat	Nonstat ($K=1$)	Nonstat ($K=3$)
1	35	0.0029	0.0009**	0.0012*
2	35	0.0213**	0.0263*	0.0304
3	35	0.0635	0.0592*	0.0371**
4	35	0.0001*	0.0001*	0.0001**
5	35	0.0029	0.0028*	0.0020**
6	25	0.0106*	0.0321	0.0041**
7	25	0.2553*	0.2375**	0.2782
8	25	0.2882	0.2560*	0.1606**
9	25	3.8846	2.6053*	1.8511**
10	25	1.94E9*	2.13E9	1.93E9**

3.4.2 Improvement of Uncertainty Quantification

In this work, whether the use of nonstationary covariance could improve the quantification of prediction uncertainty by Kriging model. A one-dimensional example in Figure 3.8 is used here for demonstrative purpose. To verify whether the theoretical prediction error variance provided by the Kriging modeling approach accurately quantifies the actual prediction error, plots of the actual absolute prediction error (i.e., $|e(x)|$, where $e(x) = y(x) - \hat{y}(x)$) and the theoretical prediction error standard deviation ($STD_{pred}(x)$) are provided in Figures 3.13 and 3.14, respectively for the stationary Kriging and the non-stationary Kriging. In both Figures 3.13 and 3.14, panels (b) and (c) are two zoom-in plots of panel (a) around two selected sampling

points $x_A (= 0.0690)$ and $x_B (= 0.8276)$. It is observed from panel (a) that the actual and theoretical prediction error quantification is generally in much better agreement for the non-stationary Kriging model than for the stationary Kriging model.

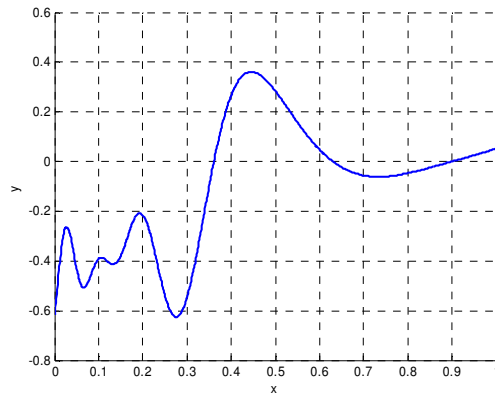


Figure 3.12 True function of the one-dimensional example

Moreover, from the zoom-in plots in panels (b) and (c) of Figure 3.13, it is found that the theoretical prediction error standard deviation from the non-stationary Kriging model has different behavior in different regions of the input space, depending on the local level of smoothness in the function. The stationary Kriging model does not possess this desirable characteristic. Specifically, Figure 3.13 (b and c) show that for the stationary covariance model, when x moves away from sampling points x_A (plot (b)) and x_B (plot (c)), the theoretical $STD_{pred}(x)$ increases at nearly identical rates (the slight slower increase of $STD_{pred}(x)$ around x_A is caused by the fact that more sampling points were placed near x_A than near x_B). This is in disagreement with the fact that the response is known to be smoother in the vicinity of x_B , and hence it is expected that the prediction uncertainty to increase at a slower rate as we move away

from x_B . In contrast, the non-stationary Kriging model is able to capture this phenomenon. Figures 3.14 (b and c) show that the theoretical prediction uncertainty for the non-stationary Kriging model increases at much higher rates in regions in which the response is rougher than in regions in which the response is smoother.

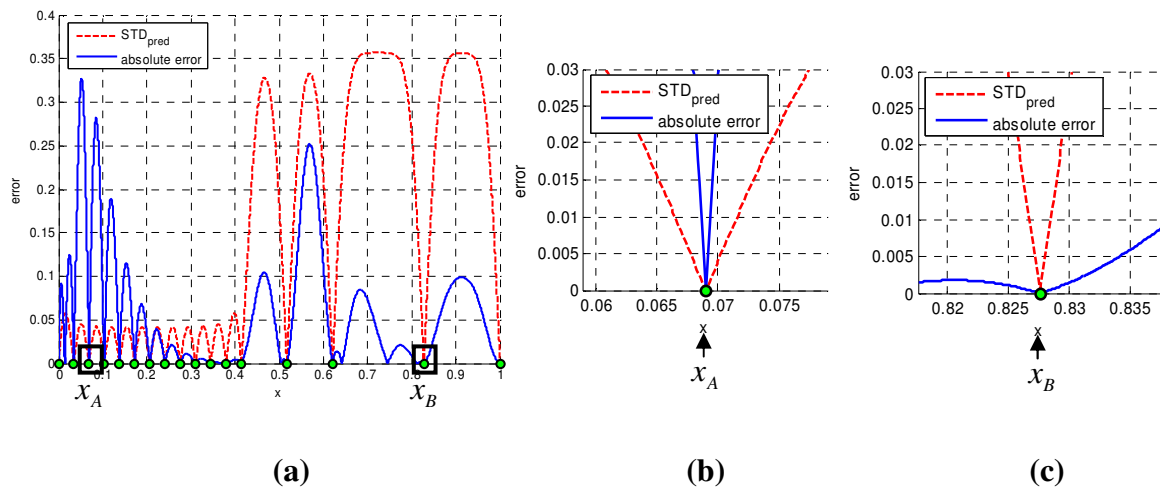


Figure 3.13 The theoretical standard deviation of prediction error vs. the actual absolute prediction error yielded by stationary Kriging.

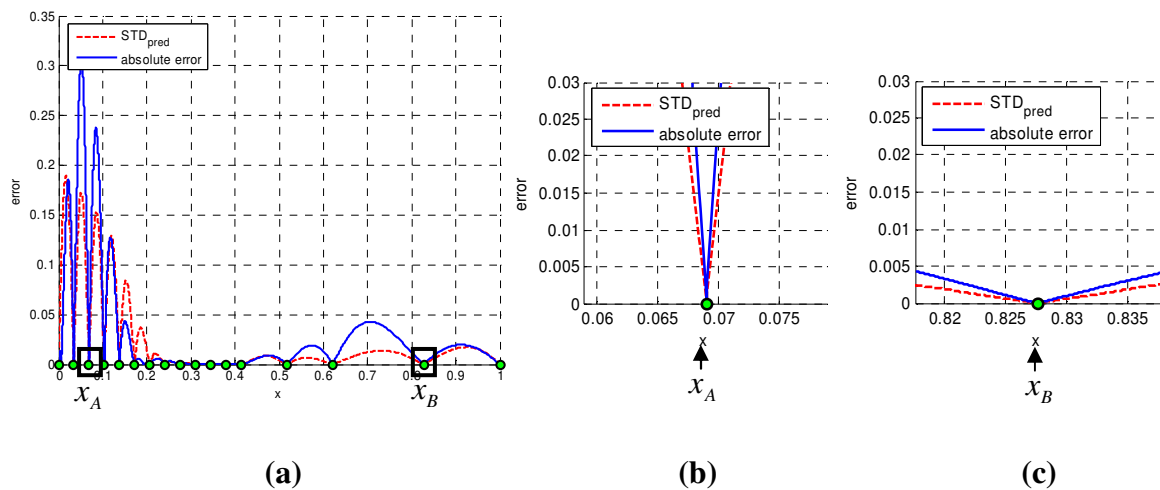


Figure 3.14 The theoretical standard deviation of prediction error vs. the actual absolute prediction error yielded by non-stationary Kriging

3.5 Summary

In this chapter, Kriging models with non-stationary covariance structure for metamodeling is investigated based on data from computer experiments. Non-stationary covariance based methods in the existing literature suffer from over-parameterization difficulties, which are compounded in high-dimensional problems typical in complex system design optimization. To this end, a modified version of Gibb's nonlinear map approach is proposed, with a sparser, yet flexible, parameterization.

Through both mathematical and engineering examples, the Kriging modeling based on the proposed non-stationary covariance representation is flexible enough to capture the changing smoothness behavior of the response. It is demonstrated that, when the response surface has non-stationary behavior, the non-stationary Kriging yields more effective quantification of the prediction uncertainty than the stationary Kriging. The robustness of the proposed non-stationary Kriging method was also demonstrated via testing multiple functions under different sampling situations. When the response performance exhibits obvious varying smoothness levels, the non-stationary Kriging model is able to effectively capture local features and significantly enhance the prediction accuracy. For functions not exhibiting strong changing smoothness behavior, the non-stationary Kriging model performs no worse than the non-stationary covariance structure. With moderately selected model complexity and sufficient sampling, the robustness of the non-stationary Kriging is reasonably assured. It is also demonstrated that the nonstationary Kriging is even more effective when the data are obtained from adaptive sequential sampling in which the density of sampling points varies over the regions with different irregularity.

Chapter 4. Model Bias-Correction with Uncertainty Quantification

Nomenclature

$Y^e(\mathbf{x})$	physical experimental observation
$\varepsilon(\mathbf{x})$	experimental error
$y^r(\mathbf{x})$	outcome true reality
$y^m(\mathbf{x})$	computer model
$y^h(\mathbf{x})$	high fidelity (HF) computer model
$y^l(\mathbf{x})$	low fidelity (LF) computer model
$y_s^l(\mathbf{x})$	scaled Low fidelity (LF) model
$\delta(\mathbf{x})$	bias function
\mathbf{x}	$\mathbf{x} = (x_1, \dots, x_p)^T$, design in a p -dimensional space
D_e	$D_e = \{\mathbf{x}_1, \dots, \mathbf{x}_{n_e}\}$, for physical experiments
D_m	$D_m = \{\mathbf{x}'_1, \dots, \mathbf{x}'_{n_m}\}$, for computer experiments
n_m, n_e	size of D_m / D_e , the number of computer / physical experiments
σ_ε^2	variance parameter of $\varepsilon(\mathbf{x})$
σ_δ^2	variance parameter of the prior Gaussian process $\delta(\mathbf{x})$
ϕ_δ	correlation parameter of the prior Gaussian process $\delta(\mathbf{x})$

τ	ratio of σ_e^2 to σ_δ^2
$n_{\delta e,m}$	degree of freedom of t distribution
$\mu_{\delta e,m}(\mathbf{x})$	noncentrality parameter of t distribution
$\sigma_{\delta e,m}^2(\mathbf{x})$	scale parameter of t distribution
$M_D(\mathbf{x}^*)$	design validation metric

4.1 Introduction

As depicted in Figure 1.1 in Chapter 1, model updating is one of the key activities involved in the framework of predictive modeling by combining the results from both computer model and physical experiments. *Bias-correction*, together with model calibration, are common strategies for model updating that improves the model accuracy through mathematical means. As introduced in Section 2.7, bias-correction is regarded complementary to model calibration, when improvement cannot be made by solely calibrating model parameters (Easterling et al., 2002).

The basic idea of bias-correction is to adjust the *original model* $y^m(\mathbf{x})$ by adding a *bias function* $\delta(\mathbf{x})$ to it. One general interpretation of bias-correction approach is that it captures the potential model or method error (e.g., due to incorrectly modeling a non-linear behavior with a linear model), which often cannot be compensated by other means. There are various formulations of bias-correction seen in literature. A general bias-correction has the form

$$y(\mathbf{x}) = y^m(\mathbf{x}) + \delta(\mathbf{x}), \quad (4.1)$$

where $y^m(\mathbf{x})$ is the original model to be bias-corrected, and $\delta(\mathbf{x})$ denotes the bias function to be estimated, and $y(\mathbf{x})$ denotes the updated model after bias-correction. There are two aspects of concerns with the use of bias-function $\delta(\mathbf{x})$, (1) how to characterize the formulation of $\delta(\mathbf{x})$ to

best correct the original model, (2) how to quantify the uncertainty of $\delta(\mathbf{x})$ to reflect the uncertainties that are involved in the bias-correction process. Here the uncertainties include the uncertainty of experiment data and the uncertainty of the bias-function itself.

In this work, bias-correction involves **two scenarios** depending on the type of experiment data that is utilized: (1) Bias-correction of computer model against physical experiment data; (2) Bias-correction of Low Fidelity (LF) model against High fidelity (HF) model simulation data. It is noted that scenario (2) can be treated as a special case of scenario (1) when the uncertainty of physical experimental data in scenario (1) degenerates to zero. Because two levels of models are involved in scenario (2), the bias-correction in scenario (2) is also referred to as *model fusion*.

The uncertainty of predictive model $y(\mathbf{x})$ in Eq. (4.1), called *model uncertainty*, plays a critical role optimization under uncertainty. Quantification of model uncertainty is critical to many activities in the process of using predictive models for engineering design, such as *design driven model validation* (see Chapter 6) and *sequential sampling (experimentation)* that is needed to update a predictive model (see Chapter 7). In this chapter, we investigate a Bayesian approach that offers a flexible mathematical framework to quantify the model uncertainty under the two **scenarios** defined in the preceding paragraph. A review of basic techniques of **Bayesian approaches** can be found in Bayarri et al. (2002). The fundamental difference between the frequentist and the Bayesian approach is that the former draws confidence intervals of prediction based on statistical data analysis, while the latter assumes that the model parameters themselves are random and follow a prior distribution. The prior distribution will be updated once experimental data is available and becomes the posterior distribution. The Bayesian approach is preferred to the classical statistical approach when it is too expensive to obtain a statistically sufficient amount of data, which is often the case in engineering design.

4.2 Bias-correction of Computer Model against Physical Experiment Data

Using \mathbf{x} to represent model input variables and y stand for model response, the relationship between the experimental observation $y^e(\mathbf{x})$ and the result generated by a computer model $y^m(x)$ is often generalized as follows:

$$y^e(\mathbf{x}) = y^m(\mathbf{x}) + \delta(\mathbf{x}) + \varepsilon(\mathbf{x}), \quad (4.2)$$

where $\varepsilon(\mathbf{x})$ is the random variable representing the experimental error (relating to both experimental setup and measurement) that may depend on \mathbf{x} , and $\delta(\mathbf{x})$ is the error of the model (Mahadevan and Rebba, 2006), or called the *prediction bias*, i.e.,

$$\delta(\mathbf{x}) = y^r(\mathbf{x}) - y^m(\mathbf{x}), \quad (4.3)$$

which captures the model inadequacy, where $y^r(\mathbf{x})$ is the true output.

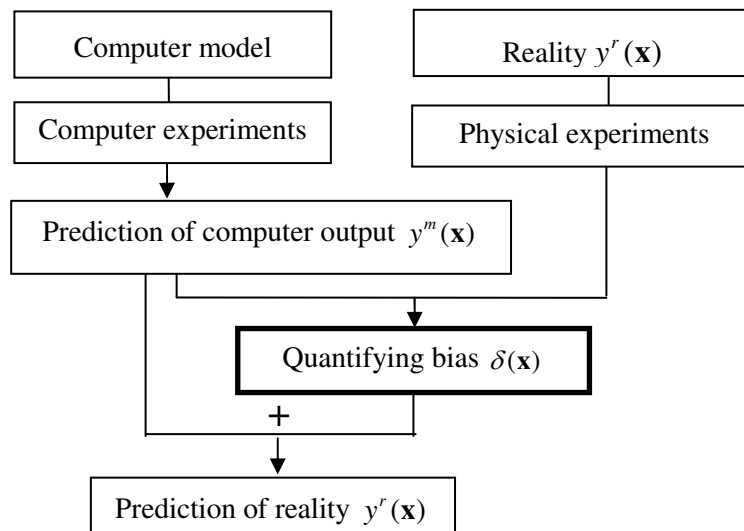


Figure 4.1 Flowchart of the Bias-correction of Computer Model against Physical Experiment Data

In the above equations, the prediction bias $\delta(\mathbf{x})$ can be directly used to assess the model accuracy, while the prediction of the true model output $y^r(\mathbf{x})$ is essential for assessing the probabilistic response. Most research in validating computer models has focused on estimating *bias*, but much less work had been done on characterizing *prediction uncertainty* and *bias* under general situations. It can be noted from Eq. (4.4) that estimating the prediction bias $\delta(\mathbf{x})$ is an intermediate step for estimating the true model output $y^r(\mathbf{x})$. Based on the experimental data, outputs of the computer model, and the experimental error $\varepsilon(\mathbf{x})$, the estimated prediction error, $\delta(\mathbf{x})$, and its probability distribution is first obtained. The estimated prediction $\hat{y}^r(\mathbf{x})$, or *Bayesian prediction model*, can then be obtained by $\hat{y}^r(\mathbf{x}) = y^m(\mathbf{x}) + \hat{\delta}(\mathbf{x})$.

Kennedy and O'Hagan (2001) developed a general Bayesian approach to calibrate computer models, while also characterizing the bias between the computer model and the physical experimental data. Their method utilizes the following mathematical relationship,

$$y^e(\mathbf{x}) = \rho \cdot y^m(\mathbf{x}, \boldsymbol{\theta}) + \delta(\mathbf{x}) + \varepsilon, \quad (4.4)$$

where ρ is an unknown regression parameter. The uncertainty of calibration parameter $\boldsymbol{\theta}$, regression parameter ρ , and the bias function $\delta(\mathbf{x})$ are quantified based on Bayesian analysis. Their work was not carried out in the context of model validation, rather centered on integrating computer outputs and physical observations into the prediction of computer models.

In the Bayesian bias-correction model proposed by Chen et al. (2007) and Wang et al. (2008), a plain additive bias-correction model is formulated as

$$y^e(\mathbf{x}) = y^m(\mathbf{x}) + \delta(\mathbf{x}) + \varepsilon, \quad (4.5)$$

where the bias function $\delta(\mathbf{x})$ is a direct measure of the difference between the computer model $y^m(\mathbf{x})$ and the physical process $y^e(\mathbf{x})$. As compared to the bias-correction model presented by Kennedy & O'Hagan (2002) in Eq. (4.4), the bias-correction in Eq. (4.5) only considers the case where all inputs (\mathbf{x}) of both the computer model ($y^m(\mathbf{x})$) and the physical process ($y^e(\mathbf{x})$) are assumed as observable and controllable. The bias function $\delta(\mathbf{x})$ is assumed to be a Gaussian Process model, the uncertainty of which reflects the uncertainty involved in a model validation process such as the experimental error, lack of data, etc. One advantage of using the above formulation is that the closed form Bayesian posterior of the Gaussian process model $\delta(\mathbf{x})$ can be derived. In Wang et al. (2008), the bias function $\delta(\mathbf{x})$ is utilized as a direct measure of the accuracy (or validity) of a computer model at an application site or over a region.

In addition to the additive bias shown in Eqs. (4.4) and (4.5), a bias correction approach may employ a combination of multiplicative bias and additive bias, as shown in,

$$y^e(\mathbf{x}) = \rho(\mathbf{x})y^m(\mathbf{x}) + \delta(\mathbf{x}) + \varepsilon, \quad (4.6)$$

where $\rho(\mathbf{x})$ is modeled as a simple linear regression model w.r.t. \mathbf{x} , ε is assumed to be a zero mean Gaussian random variable. The scaling function $\rho(\mathbf{x})$ in Eq. (4.6) brings more flexibility to the constant adjustment parameter ρ used in Kennedy and O'Hagan (2001). The maximum likelihood estimation (MLE) method is utilized in their work to estimate the regression coefficients of $\rho(\mathbf{x})$. Closed forms Bayesian posteriors of the hyperparameters in the Gaussian Process $\delta(\mathbf{x})$ are derived for given prior distributions.

In this work, a Bayesian approach is used to provide uncertainty quantification of both $\delta(\mathbf{x})$ and $y^r(\mathbf{x})$. Theoretical details of the Bayesian approach can be found in Wang et al.

(2008), while related references for Bayesian analysis could be found in Qian and Wu (2005) and Reese et al. (2004). Bayesian inferences are preferred as they require fewer assumptions and are more flexible for engineering applications where it may be too expensive to obtain experimental data (Gunawan and Papalambros, 2006). In addition, Bayesian methods may be preferable as additional information or designer's belief can be incorporated through prior distributions. Below, some details of each step in the Bayesian procedure are provided. It should be pointed out that the mathematical framework considered in this work is similar to the one in Kennedy and O'Hagan (2001), however, this work focuses on characterizing the behavior of the prediction bias $\delta(\mathbf{x})$ while the emphasis of Kennedy and O'Hagan (2002)'s work is on the *calibration* of computer models based on physical observations, with the term $y^m(\mathbf{x})$ in Eq. (4.4) replaced by $\rho y^m(\mathbf{x}, \Theta)$, where ρ is an unknown regression parameter, and Θ is the vector of calibration parameters.

The bias-correction of computer models against physical experiments proposed in this work can be outlined with the following steps.

*Step (1): Collect both **physical** and **computer** model data*

*Step (2): Determine the **priors** of Gaussian process parameters for **bias***

*Step (3): Compute the **posterior** of **bias** based on observations*

*Step (4): Compute the Bayesian **prediction model***

Each step will be elaborated as follows:

(1) Collect both physical and computer model data

Both physical observations and computer model outputs are essential to model validation.

Let $\mathbf{x} = (x_1, \dots, x_p)^T$ be a point in a p -dimensional design variable space. Let $D_e = \{\mathbf{x}_1, \dots, \mathbf{x}_{n_e}\}$ and $D_m = \{\mathbf{x}'_1, \dots, \mathbf{x}'_{n_m}\}$ be the design settings for physical experiments and computer experiments, respectively; $\mathbf{y}^e = (y^e(\mathbf{x}_1), \dots, y^e(\mathbf{x}_{n_e}))^T$ and $\mathbf{y}^m = (y^m(\mathbf{x}'_1), \dots, y^m(\mathbf{x}'_{n_m}))^T$ be the corresponding physical experimental observations and deterministic computer model outputs, respectively. Note that D_e and D_m may or may not overlap. Physical observations are desired to be as many as possible and close to the intended design region. Compared to physical observations, computer model outputs are less costly and should be simulated at design settings where the physical observations are available and close, if not within, the intended design regions.

When D_e and D_m do not overlap and computer simulations are expensive and time-consuming, a metamodel ($\hat{y}^m(\mathbf{x})$) that interpolates the computer model data may be used to replace $y^m(\mathbf{x})$. One approach to approximating $y^m(\cdot)$ is to fit a Gaussian process model based on the available computer experiments (Santner et al., 2003).

(2) Determine the priors of Gaussian process parameters for bias

One advantage of the Bayesian approach is its ability to take into account scientific knowledge and past information in the form of prior distributions for model parameters. From Eq. (4.3), the prediction bias $\delta(\mathbf{x})$ could be formulated as $\delta(\mathbf{x}) = y^e(\mathbf{x}) - y^m(\mathbf{x}) - \varepsilon(\mathbf{x})$. In this work $\delta(\mathbf{x})$ is treated as a Gaussian process, with the process parameters denoted as $\theta = (\sigma_\delta^2, \beta_\delta, \phi_\delta, \sigma_\varepsilon^2)$, which respectively represent the variance parameter (σ_δ^2), the location parameter (β_δ), the correlation parameter (ϕ_δ), and the variance parameter related to the experiment error $\varepsilon(\mathbf{x})$ (σ_ε^2). The following forms of priors for the variance parameter σ_δ^2 and

location parameter β_δ are adopted (similar treatments could be found in Reese et al., 2004, Qian and Wu, 2005):

$$\sigma_\delta^2 \square IG(\alpha_\delta, \gamma_\delta), \quad \beta_\delta | \sigma_\delta^2 \square N(\mathbf{b}_\delta, \sigma_\delta^2 \mathbf{V}_\delta),$$

where $IG(\alpha, \gamma)$ denotes the inverse gamma distribution. As will be detailed in the following description of step (3), to simplify the Bayesian analysis, no priors are specified for ϕ_δ and σ_ε^2 which are instead treated as fixed and estimated directly from data.

(3) Compute the posterior of bias function

Based on the Bayes Theory, the posterior of the bias function $\delta(\mathbf{x})$ given the physical observations \mathbf{y}^e and computer outputs \mathbf{y}^m can be obtained by integrating out θ through the following equation

$$p(\delta(\mathbf{x}) | \mathbf{y}^e, \mathbf{y}^m) = \int_\theta p(\delta(\mathbf{x}) | \mathbf{y}^e, \mathbf{y}^m, \theta) p(\theta | \mathbf{y}^e, \mathbf{y}^m) d\theta. \quad (4.6)$$

The density function $p(\delta(\mathbf{x}) | \mathbf{y}^e, \mathbf{y}^m, \theta)$ can be easily computed based on the data from both computer model and physical experiments. With some tedious mathematical derivations (refer to Appendix and Wang et al., 2008 for proof), it could be shown that the posterior of $\delta(\cdot)$ follows a t-distribution:

$$\delta(\mathbf{x}) | \mathbf{y}^e, \mathbf{y}^m, \phi_\delta, \tau \square T(n_{\delta|e,m}, \mu_{\delta|e,m}(\mathbf{x}), \sigma_{\delta|e,m}^2(\mathbf{x})), \quad (4.7)$$

with the following degree of freedom, noncentrality, and scale parameters:

$$n_{\delta|e,m} = n_e + 2\alpha_\delta, \quad (4.8)$$

$$\mu_{\delta|e,m}(\mathbf{x}) = \mathbf{f}_\delta^T(\mathbf{x}) \mathbf{A}_\delta \mathbf{v}_\delta + \mathbf{r}_\delta^T(\mathbf{x}) (\mathbf{R}_\delta + \tau \mathbf{I}_{n_e})^{-1} (\mathbf{y}^e - \mathbf{y}_{n_e}^m - \mathbf{F}_\delta \mathbf{A}_\delta \mathbf{v}_\delta), \quad (4.9)$$

$$\sigma_{\delta|e,m}^2(\mathbf{x}) = \frac{Q_\delta^2}{n_{\delta|e,m}} \cdot \left(1 - \begin{bmatrix} \mathbf{f}_\delta(\mathbf{x}) \\ \mathbf{r}_\delta(\mathbf{x}) \end{bmatrix}^T \begin{bmatrix} -\mathbf{V}_\delta^{-1} & \mathbf{F}_\delta^T \\ \mathbf{F}_\delta & \mathbf{R}_\delta + \tau \mathbf{I}_{n_e} \end{bmatrix}^{-1} \begin{bmatrix} \mathbf{f}_\delta(\mathbf{x}) \\ \mathbf{r}_\delta(\mathbf{x}) \end{bmatrix} \right), \quad (4.10)$$

where

$$Q_\delta^2 = 2\gamma_\delta + (\mathbf{y}^e - \mathbf{y}_{n_e}^m)^T (\mathbf{R}_\delta + \tau \mathbf{I}_{n_e})^{-1} (\mathbf{y}^e - \mathbf{y}_{n_e}^m) + \mathbf{b}_\delta \mathbf{V}_\delta^{-1} \mathbf{b}_\delta - \mathbf{v}_\delta^T \mathbf{A}_\delta \mathbf{v}_\delta, \quad (4.11)$$

$$\mathbf{A}_\delta^{-1} = \mathbf{F}_\delta^T (\mathbf{R}_\delta + \tau \mathbf{I}_{n_e})^{-1} \mathbf{F}_\delta + \mathbf{V}_\delta^{-1}, \quad (4.12)$$

$$\mathbf{v}_\delta = \mathbf{F}_\delta^T (\mathbf{R}_\delta + \tau \mathbf{I}_{n_e})^{-1} (\mathbf{y}^e - \mathbf{y}_{n_e}^m) + \mathbf{V}_\delta^{-1} \mathbf{b}_\delta. \quad (4.13)$$

In the above equations, $\mathbf{F}_\delta = (\mathbf{f}_\delta(\mathbf{x}_1), \dots, \mathbf{f}_\delta(\mathbf{x}_{n_e}))^T$ is the $n_e \times q_\delta$ design matrix, \mathbf{R}_δ is the $n_e \times n_e$ correlation (parameterized by ϕ_δ) matrix of δ_{n_e} , and $\mathbf{r}_m(\mathbf{x})$ is the correlation (parameterized by ϕ_δ) between $\delta(\mathbf{x})$ and δ_{n_e} . Here, $\delta_{n_e} = \mathbf{y}^e - \mathbf{y}_{n_e}^m$ could be viewed as the ‘observations’ at setting D_e , for the Gaussian process $\delta(\mathbf{x})$, and $\mathbf{y}_{n_e}^m$ is the computer model output $y^m(\cdot)$ (or the metamodel $\hat{y}^m(\cdot)$ in the case that $y^m(\cdot)$ is expensive to compute) at D_e . It naturally follows that δ_{n_e} is essentially the observed bias between physical experiments and the computer model (or metamodel) outputs.

We denote ϕ_δ as the correlation parameter underlying \mathbf{R}_δ and \mathbf{r}_δ^T ; τ as the ratio of σ_ε^2 to σ_δ^2 , i.e., $\tau = \sigma_\varepsilon^2 / \sigma_\delta^2$, where σ_δ^2 denotes the process variance of $\delta(\mathbf{x})$ while σ_ε^2 denotes the variance of $\varepsilon(\mathbf{x})$. Unlike $\delta(\mathbf{x})$ which is assumed to be the Gaussian process with spatial correlation structure, $\varepsilon(\mathbf{x})$ follows identical independent normal distribution at different design sites \mathbf{x} . To get the marginal posterior of $\delta(\mathbf{x})$, ϕ_δ and τ also need to be integrated out, which is computationally prohibitive. Alternatively, ϕ_δ and τ can be treated as their true values and estimated with methods such as the Cross Validation (CV) (Hastie et al., 2000), maximum

likelihood estimates (MLE) (Hastie et al., 2000), Markov Chain Monte Carlo (MCMC) (Geyer, 1992), and Minimum Mean Squared Error Estimates (MMSE) (Hastie et al., 2000).

(4) Compute the Bayesian prediction model

The true behavior $y^r(\mathbf{x})$ is predicted using the following equations to estimate the mean and variance,

$$\hat{y}^r(\mathbf{x}) = y^m(\mathbf{x}) + \hat{\delta}(\mathbf{x}), \quad (4.14)$$

$$\text{Var}[y^r(\mathbf{x})] = \text{Var}[\delta(\mathbf{x})] = \sigma_{\delta|e,m}^2(\mathbf{x}). \quad (4.15)$$

The covariance between $Y^r(\mathbf{x}_i)$ and $Y^r(\mathbf{x}_j)$ is given by:

$$\begin{aligned} \text{Cov}[y^r(\mathbf{x}_i), y^r(\mathbf{x}_j)] &= \text{Cov}[y^m(\mathbf{x}_i) + \delta(\mathbf{x}_i), y^m(\mathbf{x}_j) + \delta(\mathbf{x}_j)] \\ &= \text{Cov}[y^m(\mathbf{x}_i), y^m(\mathbf{x}_j)] + \text{Cov}[\delta(\mathbf{x}_i), \delta(\mathbf{x}_j)] = 0 + \sigma_{\delta|e,m}^2(\mathbf{x}_i, \mathbf{x}_j) = \sigma_{\delta|e,m}^2(\mathbf{x}_i, \mathbf{x}_j), \end{aligned} \quad (4.16)$$

where

$$\sigma_{\delta|e,m}^2(\mathbf{x}_i, \mathbf{x}_j) = \frac{Q_\delta^2}{n_{\delta|e,m}} \cdot (R_\delta(\mathbf{x}_i, \mathbf{x}_j) - \begin{bmatrix} \mathbf{f}_\delta(\mathbf{x}_i) \\ \mathbf{r}_\delta(\mathbf{x}_i) \end{bmatrix}^T \begin{bmatrix} -\mathbf{V}_\delta^{-1} & \mathbf{F}_\delta^T \\ \mathbf{F}_\delta & \mathbf{R}_\delta + \tau \mathbf{I}_{n_e} \end{bmatrix}^{-1} \begin{bmatrix} \mathbf{f}_\delta(\mathbf{x}_j) \\ \mathbf{r}_\delta(\mathbf{x}_j) \end{bmatrix}). \quad (4.17)$$

When $\mathbf{x}_i = \mathbf{x}_j = \mathbf{x}$, Eq. (4.17) reduces to Eq. (4.10) and Eq. (4.18) reduces to Eq. (4.11). The predictor of the true behavior $\hat{y}^r(\mathbf{x})$, along with its uncertainty quantification, are referred to as the *Bayesian prediction model* in this work.

In Appendix B, $\phi_{m,k}$ represents the correlation associated with the computer prediction and its uncertainty. Since computer experiments are generally less expensive, when much more data is available, the prediction uncertainty of a $\hat{y}^m(\mathbf{x})$ is usually much smaller compared with

the model uncertainty. On the other hand, $\phi_{\delta,k}$ and τ together determine the uncertainty of an estimated bias function $\hat{\delta}(\mathbf{x})$, which has a critical impact on the uncertainty quantification of the final predictive model $\hat{y}^r(\mathbf{x})$.

4.3 Bias-Correction of Low Fidelity (LF) Computer Model against High Fidelity (HF) Computer Model

In Scenario 2, the observed data is obtained from experiments of a High Fidelity (HF) computer model, while the model to be bias-corrected is a separate Low Fidelity (LF) computer model. Similar to Eq. (4.2), the mathematical relationship between the HF model $y^h(\mathbf{x})$ and the LF model $y^l(\mathbf{x})$ is represented as

$$y^h(\mathbf{x}) = y^l(\mathbf{x}) + \delta(\mathbf{x}). \quad (4.18)$$

The flowchart of the bias-correction of LF model against HF model experiment data is described in Figure 4.2.

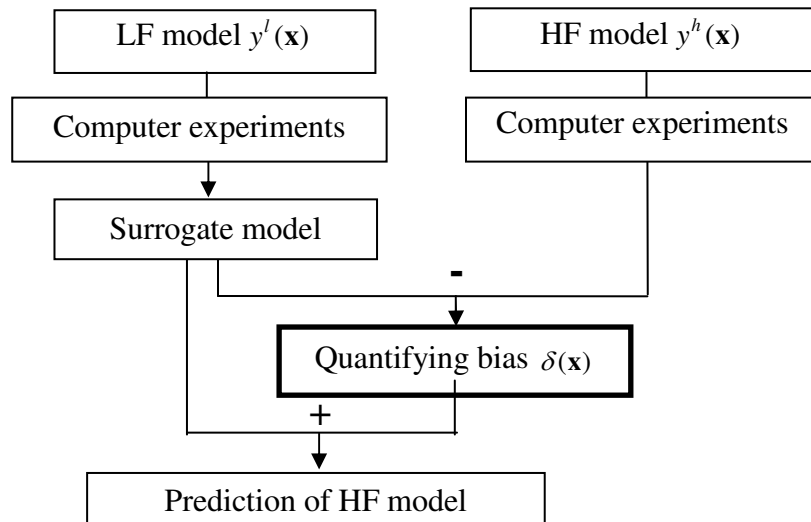


Figure 4.2 Flowchart of the Bias-correction of LF model against HF model Simulation data

Because two computer models are involved, the procedure of updating a LF model using HF simulations through bias-correction is also named as *model fusion*, which is to integrate the LF and HF models to yield an improved predictive model. Here, the modeling error of a HF model is ignored. The yielded predictive model obtained from model fusion is essentially a surrogate mode of the HF model, and should pass through (or interpolate) all HF simulation points. The interpolation uncertainty of the predictive model is quantified based on the bias function in a similar way shown for scenario 1 in Section 4.2.

Existing model fusion techniques include the difference or scaling approach (Gano et al. 2004), the Taylor-series approach (Gano et al. 2006), the space mapping approach (Bandler et al. 2004), and the multiple fidelity Kriging approach (Huang et al. 2006) etc. Due to the lack of HF simulation data in most practical problems, a **Bayesian approach** to model fusion and quantification of interpolation uncertainty is considered in this work. The model fusion approach described below follows the similar mathematical framework as combining computer and physical experiments in Chen et al. (2006).

The mathematical relationship between the HF model $y^h(\mathbf{x})$ and the LF model $y^l(\mathbf{x})$ is represented as

$$y^h(\mathbf{x}) = y_s^l(\mathbf{x}) + \delta(\mathbf{x}) = [\rho_0 + \rho_1 y^l(\mathbf{x})] + \delta(\mathbf{x}), \quad (4.19)$$

where ρ_0 and ρ_1 are two scaling parameters that define the ‘scaled’ LF model

$$y_s^l(\mathbf{x}) = \rho_0 + \rho_1 y^l(\mathbf{x}), \quad (4.20)$$

$\delta(\mathbf{x})$ is a bias function accounting for the discrepancy between the ‘scaled’ LF model $y'_s(\mathbf{x})$ and the HF model $y^h(\mathbf{x})$. $y^l(\mathbf{x})$ represents either the original LF model or its surrogate model $\hat{y}^l(\mathbf{x})$ when necessary.

The scaling parameters ρ_0 and ρ_1 help bring (or ‘scale’) the LF model as close as possible to the HF model. The application of similar linear scaling approach could be found in previous works, e.g., Gano et al. (2004) and Qian et al. (2006), even though the details of Bayesian modeling and its complexity vary. For determining the Bayesian modeling parameters, different approaches (e.g., Maximum Likelihood Estimation (Qian et al. 2006), Cross Validation (Hastie et al. 2001)) could be employed. In this work, $\hat{\rho}_0$ and $\hat{\rho}_1$ are identified by the least square (LS) method, together with bounds constraining both $\hat{\rho}_0$ and $\hat{\rho}_1$ as follows.

$$\begin{aligned} \min L(\rho_0, \rho_1) &= \sum_{i=1}^N [\rho_0 + \rho_1 y^l(\mathbf{x}_i) - y^h(\mathbf{x}_i)]^2, \\ \text{st. } l_0 < \rho_0 < u_0; l_1 < \rho_1 < u_1 \end{aligned} \quad (4.21)$$

where $L(\rho_0, \rho_1)$ stands for the loss function in a square sense; $\mathbf{x}_i(i=1 \dots N)$ are the sampling points of HF model. The bounds (l_0, u_0) and (l_1, u_1) posed on parameter ρ_0 and ρ_1 reflect, respectively, the prior belief of the global constant bias and the multiplicative scaling between HF and LF models. As an example, we may specify (l_1, u_1) to be $(0.8, 1.2)$, (l_0, u_0) to be $(-0.1 \Delta y', 0.1 \Delta y')$, where $\Delta y'$ is the range of $y^l(\mathbf{x})$, i.e., the difference of max and min values of $y^l(\mathbf{x})$ in the design range of \mathbf{x} . Using bounds mitigates the overfitting issue with a regular linear regression problem when data is insufficient, by imposing reasonable ranges of ρ_0 and ρ_1 . Due to the use of bounds, we call the proposed method the constrained linear scaling (CLS) approach.

To simplify the Bayesian modeling procedure, the scaling parameters ρ_0 and ρ_1 are assumed to be unknown but fixed in this work. This treatment is different from that in Qian et al.

(2006), where a linear function $\rho(\mathbf{x})$ is used for scaling instead of two constant parameters ρ_0 and ρ_1 used in our work. It is our belief that using ρ_1 will help better preserve the ‘profile’ of a LF model and the term ρ_0 will help satisfy the assumption of ‘zero-mean’ priors associated with the bias function $\delta(\mathbf{x})$, especially if a global bias exists between LF and HF models.

The bias function $\delta(\mathbf{x})$ accounts for the remaining discrepancy between the HF simulation data and the scaled LF model. For modeling the bias function, it is assumed that $\delta(\mathbf{x})$ follows a Gaussian process (GP) with mean function $\boldsymbol{\beta}^T \mathbf{F}(\mathbf{x})$ and a covariance function $C(\sigma^2, \boldsymbol{\theta})$, where $\boldsymbol{\beta}$ is the vector of regression coefficients $[\beta_0, \dots, \beta_p]$, $\mathbf{F}(\mathbf{x})$ is the vector of polynomial items $[f_0(\mathbf{x}), \dots, f_p(\mathbf{x})]$, σ^2 is the variance, $\boldsymbol{\theta}$ is the correlation parameters. The sampling points $\delta(\mathbf{x}_i)$ ($i=1, \dots, N^h$) for bias function $\delta(\mathbf{x})$ are available by calculating the difference between the HF simulation data $y^h(\mathbf{x}_i)$ and the scaled LF model $\hat{y}_s^l(\mathbf{x}) = \hat{\rho}_0 + \hat{\rho} y^l(\mathbf{x}_i)$, i.e.,

$$\delta(\mathbf{x}_i) = y^h(\mathbf{x}_i) - \hat{y}_s^l(\mathbf{x}) = y^h(\mathbf{x}_i) - [\hat{\rho}_0 + \hat{\rho} y^l(\mathbf{x}_i)]. \quad (4.22)$$

Given samples, a typical Kriging model (or a Gaussian process model) can be used to construct a surrogate model with uncertainty quantification for predicting $\delta(\mathbf{x})$ at site \mathbf{x} where no HF simulation is available. Details of Kriging model or a Gaussian process could be found in many references, e.g. Martin et al. (2002). It is widely agreed that when sampling data are far from sufficient to explore the behavior of the true HF model performance, Kriging approach would typically underestimate the true interpolation uncertainty (Jones 2001, Stein 1999), because all Gaussian process parameters ($\boldsymbol{\beta}$, σ^2 , $\boldsymbol{\theta}$) are treated as unknown but fixed and are determined through methods like the maximum likelihood estimation (MLE) (Qian et al. 2006) and the cross validation (CV) (Huang et al., 2006).

In this work, we investigate the Bayesian approach under the same framework described in Section 4.2, with some modification. The bias-correction of a computer model against high fidelity (HF) model proposed in this work is summarized with the following procedure.

*Step (1): Collect both **LF computer** and **HF computer** data*

*Step (2): **Scale** the **LF computer** model*

*Step (3): Determine the **priors** of Gaussian process parameters for **bias***

*Step (4): Compute the **posterior** of **bias***

*Step (5): Compute the Bayesian **prediction model***

With the Bayesian approach, the prior knowledge of the unknown bias function $\delta(\mathbf{x})$ can be expressed through the prior distribution of $(\boldsymbol{\beta}, \sigma^2, \boldsymbol{\theta})$. Recall that parameter τ was denoted as the ratio of σ_ε^2 to σ_δ^2 when describing the Bayesian bias-correction approach for scenario (1) in Section 4.2. For scenario (2), because there is no uncertainty of HF model experiments, it follows that $\sigma_\varepsilon^2 = 0$ and thus $\tau = 0$. Similar to scenario (1), the following distribution can be used to specify the prior distributions of σ^2 and $\boldsymbol{\beta}$ in the forms as

$$\sigma^2 \square IG(\alpha, \gamma), \quad \boldsymbol{\beta} | \sigma^2 \square N(\mathbf{b}, \sigma^2 \mathbf{I}), \quad (4.23)$$

where $IG(\cdot, \cdot)$ is the inverse Gamma distribution, $N(\cdot)$ is the normal distribution. The Bayesian approach is implemented while treating the correlation parameters $\boldsymbol{\theta}$ unknown but fixed, which can be estimated by the Cross Validation (CV) approach. Recall again that $\tau = 0$. Because the scaled LF model $y_s^l(\mathbf{x})$ has been pulled as close as possible to the HF simulation data, it is reasonable to assume the prior mean for $\delta(\mathbf{x})$ as a zero (i.e., $\boldsymbol{\beta}^T \mathbf{F}(\mathbf{x}) = 0$), thus $\mathbf{b} = \mathbf{0}$ in Eq. (4.19). If

no previous knowledge is available, the recommended ‘vague’ priors, i.e., $\sigma^2 \square IG(2,1)$ and $\boldsymbol{\beta} | \sigma^2 \square N(\mathbf{0}, \sigma^2 \mathbf{I})$, are also used throughout the three examples in this chapter. With the forms of priors of σ^2 and $\boldsymbol{\beta}$ in Eq. (4.23), closed forms of the posteriors of the Gaussian process model of $\delta(\mathbf{x})$ can be derived.

Since no uncertainty is posed on $\hat{\rho}_0$ and $\hat{\rho}$, the resulted scaled LF model $\hat{\rho}_0 + \hat{\rho} y^l(\mathbf{x})$ is viewed as deterministic. As a result, the surrogate model $\hat{y}^s(\cdot)$ could be represented as the predictor or the (posterior) mean

$$\hat{y}^s(\mathbf{x}) = [\hat{\rho}_0 + \hat{\rho} y^l(\mathbf{x})] + \hat{\delta}(\mathbf{x}). \quad (4.24)$$

The interpolation uncertainty of the surrogate model $\hat{y}^s(\mathbf{x})$ is only contributed by the interpolation uncertainty of the bias function $\delta(\mathbf{x})$, i.e.,

$$Var[y^s(\mathbf{x})] = Var[\delta(\mathbf{x})], \quad (4.25)$$

$$Cov[y^s(\mathbf{x}), y^s(\mathbf{x}')] = Cov[\delta(\mathbf{x}), \delta(\mathbf{x}')], \quad (4.26)$$

where $Var(\cdot)$ and $Cov(\cdot, \cdot)$ denote the variance and covariance, respectively.

4.4 Case Studies

4.4.1 Combining Variable Fidelity Computer Models: A Single Dimensional Problem

A single dimensional problem is first studied, with HF and LF models being artificially created for the illustrative purpose (see Appendix for the mathematical equations). At the initial stage (Stage 0), 3 uniform HF sampling points in region [0 1] are generated. Figure 4.2 shows the plots of the true HF model, the LF model, the scaled LF model, and the 3 HF sampling points (dark solid circles). Note there are two local minima of the HF model, and the LF model only

roughly captures the general trend of the HF model but provides a poor approximation. It is noted that the optimal design ($\mathbf{x}^*_{LF} = 0.9150$, marked with *) obtained from the LF model is a sub-optimal solution, located in an area that is quite far from the true optimum ($\mathbf{x}^*_{HF} = 0.2307$, marked with star) obtained from the HF model. After scaling, the scaled LF model are pulled close to the 3 HF data points, with the scaling parameters estimated as $[\hat{\rho}_0 \hat{\rho}_1] = [0.1844 \ 0.5371]$ based on Eq. (4.2). It should be noted that the values of $[\hat{\rho}_0 \hat{\rho}_1]$ change over different stages after more samples are added.

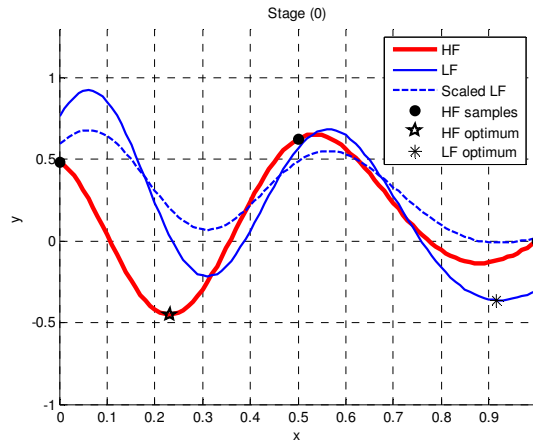


Figure 4.2 The HF model and LF model, with 3 initial HF samples (Example 1)

Different from using a single fidelity model, in variable fidelity optimization, very few data from HF simulations are available, thus LF model may be used to capture the global trend of a HF model. We note in Figure 4.2 that the scaled LF model is fairly close to the HF model. The trend information provided by the scaled LF model is integrated into the Bayesian surrogate model to enhance the accuracy of prediction.

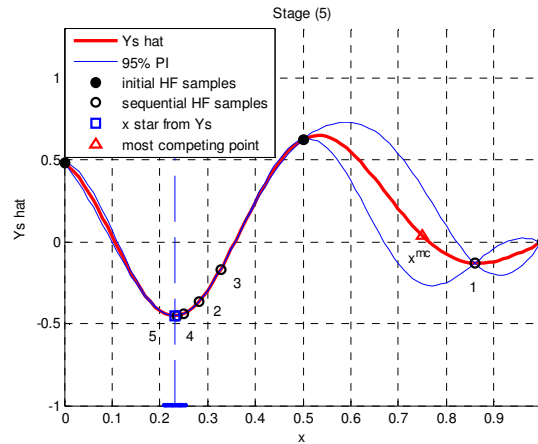


Figure 4.3 The plots of $\hat{y}^s(x)$ with uncertainty quantification (95% PI) when 5 more sampling points are added

Figure 4.3 shows the updated model with five (5) more sampling points collected. The 95% prediction interval (PI) shows the uncertainty quantification of the updated model. As expected, the amount of model uncertainty is reduced when more sample points are added.

4.4.2 Computer Model vs. Physical Experiment: Engine Piston Problem

In this section, an Engine Piston Design problem (see Appendix and Jin et al. 2005 for more details) is studied to demonstrate the bias-correction of the computer model against physical experiment. The Noise, Vibration and Harshness (NVH) characteristic of the vehicle engine is one of the critical elements of customer dissatisfaction (Jin et al. 2005). The goal of the design is to optimize the geometry of the engine piston to obtain the minimal piston slap noise.

To graphically illustrate the results and better explain the concepts of the proposed method, only one design variable is considered. The same approach can be applied to high-dimensional problems. Previous results show that the **skirt profile** (SP) strongly affects the

response (**slap noise**), therefore SP is considered the design variable. Skirt profile is represented by characteristic ratios of the shape of an engine piston, ranging continuously from 1 to 3. Piston slap noise is the engine noise resulting from piston secondary motion, which can be simulated using ADAMS/Flex, a finite element based multi-body dynamics code. All these data are provided in Tables 4.4 and 4.5, respectively. Note the design variable $\mathbf{x} = \text{SP}$ has been normalized to the unit interval $[0, 1]$.

For simplicity, only one design variable (also assumed as a noise variable) is considered. Thirty-four (34) hypothetical physical experiments are considered. Ten (10) computer experiments are conducted using the finite element model (Figure 4.3). It should be pointed out that ten computer experiments are sufficient for this one-dimensional case, although typically computer outputs are expected to be more than physical observations. Based on the available data, the Bayesian approach described is implemented.

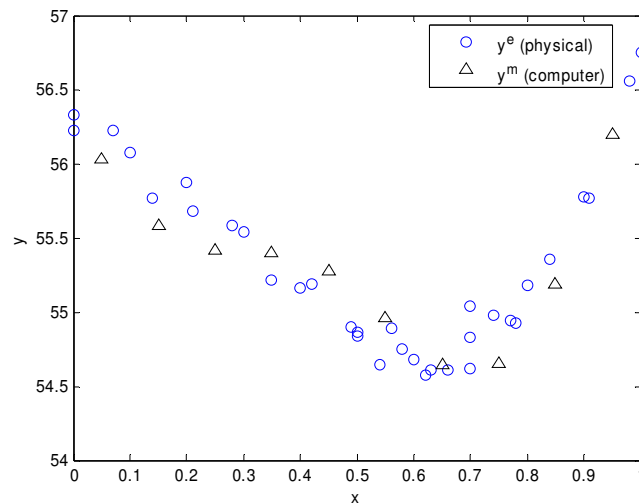


Figure 4.3 Physical and computer experiment data (circles: physical experiments; triangles: computer experiments)

Table 4.4 Thirty-four (34) physical experiments

i	1	2	3	4	5	6	7	8	9	10
$\mathbf{x}_i \in D_e$	0.000	0.100	0.200	0.300	0.400	0.500	0.600	0.700	0.800	0.900
$y^e(\mathbf{x}_i)$	56.332	56.077	55.875	55.542	55.159	54.840	54.682	55.039	55.183	55.774
i	11	12	13	14	15	16	17	18	19	20
$\mathbf{x}_i \in D_e$	1.000	0.500	0.540	0.580	0.620	0.660	0.700	0.740	0.780	0.000
$y^e(\mathbf{x}_i)$	56.749	54.867	54.646	54.748	54.576	54.614	54.623	54.978	54.923	56.224
i	21	22	23	24	25	26	27	28	29	30
$\mathbf{x}_i \in D_e$	0.070	0.140	0.210	0.280	0.350	0.420	0.490	0.560	0.630	0.700
$y^e(\mathbf{x}_i)$	56.228	55.767	55.676	55.583	55.214	55.185	54.902	54.894	54.611	54.831
i	31	32	33	34						
$\mathbf{x}_i \in D_e$	0.770	0.840	0.910	0.980						
$y^e(\mathbf{x}_i)$	54.947	55.352	55.765	56.560						

Table 4.5 Ten (10) computer experiments

i	1	2	3	4	5	6	7	8	9	10
$\mathbf{x}_i \in D_m$	0.050	0.150	0.250	0.350	0.450	0.550	0.650	0.750	0.850	0.950
$y^m(\mathbf{x}_i)$	56.033	55.584	55.417	55.402	55.278	54.957	54.641	54.656	55.191	56.193

Prediction and uncertainty quantification of $\hat{y}^m(\mathbf{x})$

From the data shown in Tables 4.4 and 4.5, there is no overlap between D_e and D_m , indicating the need to first calculate the posterior of computer model $\hat{y}^m(\mathbf{x})$. The Kriging metamodeling approach is used to predict the mean, variance and covariance of the posterior Gaussian process of $\hat{y}^m(\mathbf{x})$. The plot of the final prediction and 95% prediction interval of $\hat{y}^m(\mathbf{x})$ are shown in Figure 4.4. It is noted that $\hat{y}^m(\mathbf{x})$ passes all ten computer experiment points and there is no prediction uncertainty at each sampling site. Furthermore, owing to the smooth behavior of the computer model, ten sampling points are sufficient; hence the uncertainty due to the use of Gaussian process model replacing the computer model is small across the design range.

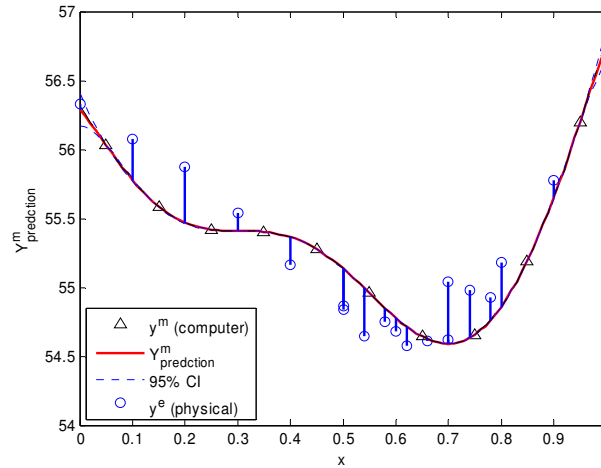


Figure 4.4 Prediction of $\hat{y}^m(\mathbf{x})$ and 95% confidence interval

Prediction and uncertainty quantification of $\hat{\delta}(\mathbf{x})$

From Eq. (4.7), the prediction of $\hat{\delta}(\mathbf{x})$ and the associated uncertainty are characterized by the posterior of $\delta(\mathbf{x})$, if given ϕ_δ and τ . Ten-fold cross validation is employed and the results show the optimal setting at $\tau=2$, $\phi_\delta=22$. Figure 4.5 displays the prediction of $\hat{\delta}(\mathbf{x})$ and the 95% confidence interval. Note the sampling points illustrated in Figure 4.5 represent the discrepancy between the physical experiment points $y^e(\mathbf{x})$ and the prediction of $\hat{y}^m(\mathbf{x})$, which correspond to the vertical line segments shown in Figure 4.4. $\hat{\delta}(\mathbf{x})$ has a relatively small variance in the region of $\mathbf{x} \in [0.6, 0.8]$ compared to $\mathbf{x} \notin [0.6, 0.8]$, which can be explained by the fact that more physical observations are available for $\mathbf{x} \in [0.6, 0.8]$.

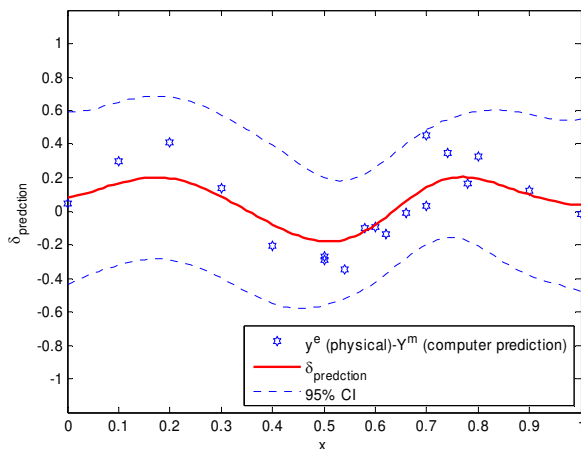


Figure 4.5 Prediction and 95% prediction interval (PI) of $\hat{\delta}(\mathbf{x})$

Prediction and uncertainty quantification of $\hat{y}^r(\mathbf{x})$

Having $\hat{y}^m(\mathbf{x})$ and $\hat{\delta}(\mathbf{x})$, the prediction of $\hat{y}^r(\mathbf{x})$ could be obtained by Eqs. (4.14~4.15). The prediction and 95% confidence interval is illustrated in Figure 4.6. In the region of $\mathbf{x} \notin [0.6, 0.8]$, where less sampling points are available for both physical and computer experiments, the uncertainty of $\hat{y}^r(\mathbf{x})$ is higher consequently.

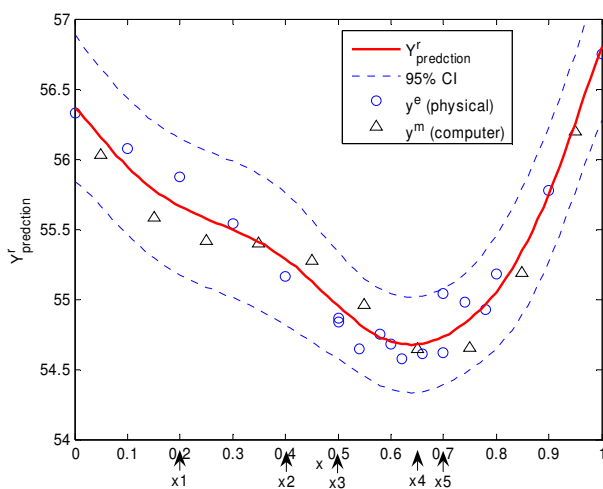


Figure 4.6 Prediction and 95% prediction interval (PI) of $\hat{y}^r(\mathbf{x})$

4.4.3 Accuracy Comparison of Different Model Fusion Approaches

In our proposed model fusion approach as described in Section 4.3, the constrained linear scaling (CLS) method is applied first to correct (or scale) the LF model, before using a bias function that accounts for the remaining discrepancy based on Bayesian modeling. To show the effectiveness of the CLS method, comparative study of different approaches over several examples is conducted. In addition to the two examples (Sections 4.4.1 and 4.4.2) we used in this chapter, another example (a Modified Branin function, see details in Chapter 7) will be included. The comparative results are shown in Table 4.1. The Root Mean Square Error (**RMSE**, see Chapter 2 for definition) is utilized as the accuracy metric: the smaller RMSE the higher accuracy. Note that all the sampling points are created with a one-shot space-filling criterion (OLH), rather than using the sequential sampling. For the same problem with the same settings of sampling sizes, the RMSE values from three modeling approaches, namely, the ‘non-fusion’ approach, the ‘non-scaled’ approach, and the proposed CLS approach are compared. By ‘non-fusion’, we mean that the information from the LF model is not considered at all for constructing the surrogate model. The only difference between the ‘non-scaled’ approach and the ‘CLS’ approach is that the former does not scale the LF model in model fusion.

Table 4.1 The accuracy (RMSE) comparison in three examples

Example 1 (1-D)					
Sampling size	5	6	7	8	10
non-fusion	0.326	0.297	0.313	0.336	0.338
non-scaled	0.221	0.114	0.060	0.044	0.003
CLS	0.286	0.112	0.052	0.036	0.003
Example 2 (Modified Branin function, 2-D)					
Sampling size	7	8	9	10	15
non-fusion	85.450	92.829	79.249	91.675	82.18
non-scaled	12.673	8.775	8.787	7.555	6.544
CLS	8.939	7.074	9.186	7.358	2.350
Example 3 (Engine Piston problem, 4-D)					
Sampling size	10	15	20	30	50
non-fusion	55.475	55.365	55.406	55.409	55.415
non-scaled	0.026	0.022	0.023	0.014	0.011
CLS	0.024	0.036	0.022	0.020	0.011

In Table 4.1, the best RMSE values are marked in bold. We note that the ‘non-fusion’ approach always ranks the worst among the three with remarkably large RMSE values, which implies that a surrogate model based on the fusion of LF and HF models is much superior over a surrogate model based on only HF model. Compared with the ‘non-scaled’ approaches, the CLS approach we propose yields higher accuracy in most of comparisons.

4.5 Summary

In this chapter, we investigated a predictive modeling approach based on bias-correction, which compensating the original computer model with a quantified bias function. This approach is applicable to two scenarios (1) when experimental data are composed of computer

experimental data of high fidelity and low fidelity, and (2) when experimental data are physical experiment data versus computer experimental data.

In all bias correction approaches, it is critical to sufficiently quantify the uncertainty of bias function. In the proposed approaches, we employ Bayesian approach to determine the model parameters based on Gaussian process model. Such Bayesian inference approach offers much flexibility as additional design knowledge and information can be easily incorporated through prior distributions, and also possesses advantages in engineering applications where it is too expensive to obtain experimental data. It also offers rigorous methods for quantifying the model uncertainty in an intended design domain that may interpolate as well as extrapolate from a tested domain. With the Bayesian approach, uncertainty in prediction related to the lack of experiment data can be captured by the magnitude of uncertainty of the bias function. Since the analytical derivation is obtained for Bayesian model parameters, the approach is expected to be more accurate and economically sound compared to the conventional numerical approach to Bayesian analysis.

The bias-correction based predictive modeling approach proposed in this chapter provides an effective means to capture systematic modeling error, as well as to capture uncertainties that impact the final predictive model as a result of bias-correction. Such a predictive modeling approach provides a mathematical foundation for the sequential chapters, in which the uncertainty quantification of prediction model will play an important role in aiding the design decision making and guiding the sequential experimentation.

Chapter 5. Better understanding of Model Updating Strategies in Validating Engineering Model

Nomenclature

$\mathbf{x} = \{x_1, x_2, \dots, x_n\}$	n observable input variables
$\boldsymbol{\theta} = \{\theta_1, \theta_2, \dots, \theta_m\}$	m uncontrollable input variables
$y^e(\mathbf{x})$	Physical experiments
$y^m(\mathbf{x})$ or $y^m(\mathbf{x}, \boldsymbol{\theta})$	Computer model
$\delta(\mathbf{x})$	Bias function
ε	Experimental error
$y^{m'}(\mathbf{x}, \Theta)$	Updated model
$y^{pred}(\mathbf{x})$	Predictive model
Θ	Model updating parameters
$L(\Theta)$	Likelihood function
$F_{x_i^e}(y_i^e)$	Cumulative distribution function (CDF) at y_i^e

5.1 Introduction

As presented in Chapter 1, an important component of the proposed predictive modeling framework is the step of model improvement that continues to improve the predictive capability of a model. Strategies for model improvement roughly fall into two categories: model refinement and model updating. *Model refinement* involves changing the physical principles in modeling or

using other means to build a more sophisticated model that better represents the physics of the problem by, for example, using a non-linear finite element method to replace a linear method, correcting and refining boundary conditions, or introducing microscale modeling in addition to macroscale modeling, etc. *Model updating*, on the other hand, utilizes mathematical means (e.g., calibrating model parameters and bias-correction) to match model predictions with the physical observations. While model refinement is desirable for fundamentally improving the predictive capability, the practical feasibility of refinement is often restricted by available knowledge and computing resources. In contrast, model updating is a cheaper means that can be practical and useful if done correctly. Here, predictive capability refers to the capability of making accurate predictions in domains (or locations) where no physical data are available.

While various model updating strategies (formulations and solution methods) exist, there is a lack of understanding of the effectiveness and efficiency of these methods. It is our interest in this work to examine various model updating strategies to achieve a better understanding of their merits. We are particularly interested in the role that model updating plays in the process of model validation. A detailed review is provided in Section 5.3. In summary, conventional calibration approaches (Leoni and Amon, 2000) assume calibration parameters are fixed and estimated, typically using least squares to match the model with the physical observations. This type of approach for model updating is inconsistent with the primary concerns of model validation in which various uncertainties should be accounted for either explicitly or implicitly. Examples of such uncertainties include experimental error, lack of data, uncertainty of the parameters (e.g. caused by the uncontrollable inputs), and model uncertainty (systematic model inadequacy). The more recent Bayesian style calibration, also named calibration under uncertainty (CUU) or stochastic calibration, treats calibration parameters as unknown entities

that are fixed over the course of the physical experiment. Initial lack of knowledge of the parameters is represented by assigning prior distributions to them, and, given the experimental data, this lack of knowledge is revised by updating their distributions (from priors to posteriors) based on the observed data through Bayesian analysis (Kennedy and O'Hagan, 2001). However, as we discuss in a more thorough examination in Section 5.3, several limitations of applying the Bayesian calibration approaches are identified.

One limitation of the aforementioned calibration approaches is that the calibration parameters are assumed to remain fixed over the entire course of the physical experiment and beyond. In contrast, it is frequently the case that some parameters vary randomly over the physical experiment, perhaps due to manufacturing variation, variation in raw materials, variation in environmental or usage conditions, etc. This violates the assumptions under which the Bayesian or regression-based calibration analyses are derived. In this situation, rather than assuming fixed parameters and updating their posterior distributions to represent our lack of knowledge of them, it is more reasonable to treat them as randomly varying and estimate their distributional properties by integrating the physical data with the model. In essence, the distributional properties (e.g., the mean and variance of the randomly varying parameters) become the calibration parameters for the model, and the objective is to identify values for them that provide the best agreement with the observed distributional properties (e.g., the dispersion, see Romero 2007) of the physical experimental data. In this paper, we present a maximum likelihood estimation (MLE) (Tamhane et al., 2000) approach for accomplishing this. The MLE method is used to estimate a set of unknown parameters (heretofore called model updating parameters) associated with several modeling updating formulations, which include the distributional properties of parameters that vary randomly over the experiment, as well as well as

more traditional fixed calibration parameters and quantities associated with bias correction and random experimental error.

The remainder of the chapter is organized as follows. In Section 5.2, we discuss the role that model updating plays versus model validation and prediction. In Section 5.3, the existing model updating formulations under two categories, namely, model bias-correction and calibration are examined. The Bayesian approach, a popular solution method is described and its limitations are highlighted. In Section 5.4, the proposed MLE based model updating approach. In Section 5.5 we will discuss the prediction model based on the updated model. In Section 5.6, a benchmark thermal challenge problem adopted by the Sandia Validation workshop^{7, 8} is used as an example to illustrate the proposed approach, draw important conclusions, and portray these conclusions in relation to conclusions from prior studies. Section 5.7 is the closure with a summary of the features of the proposed method, the relative merits of different approaches, the insights gained, and the future research direction.

5.2 Role of Model Updating in a Validation Procedure

In this work, model updating is viewed as a process that continuously improves a computer through mathematical means based on the results from newly added physical experiments, until the updated model satisfies the validation requirement or the resource is exhausted. Therefore, even though model updating is interrelated with model validation, it is viewed as a separate activity that occurs before “validation”. As shown in Figure 5.1, the model updating procedure integrates the computer simulation model y^m with the physical experiment data y^e to yield an updated model $y^{m'}(\cdot)$. This updated model is then subject to a validation procedure that utilizes additional physical experiments y^e in the intended region of interest for

validation. As noted from this diagram, unlike many contemporary model validation works, model validation in this work is used to evaluate an evolved, updated model $y^{m'}(\cdot)$, rather than the original computer model $y^m(\cdot)$. Besides, the updated model $y^{m'}(\cdot)$ is the one used for making future prediction $y^{pred}(\cdot)$ with the consideration of various sources of uncertainties. For implementing model updating and validation in a computationally efficient manner, it is indicated in Figure 5.1 that a metamodel (surrounded by a dashed box) may be used to substitute the original computer model if it is expensive to compute.

As more details are provided in the remaining sections, *model updating* utilizes mathematical means (e.g., calibrating model parameters, bias-correction) to match model predictions with the physical observations. Model updating provides not only the formulation of an *updated model*, but also the characterization of model updating parameters Θ , together with the associated assumptions. As noted, the model updating procedure, during which $y^m(\cdot)$ is treated as a black-box, is largely driven by the observed experimental data. It is our interest in this work to examine whether such a data-driven approach can improve the predictive capability of a computer model. As argued by Ferson et al. (2008), the extrapolation capability in using a model to make prediction should be carefully validated.

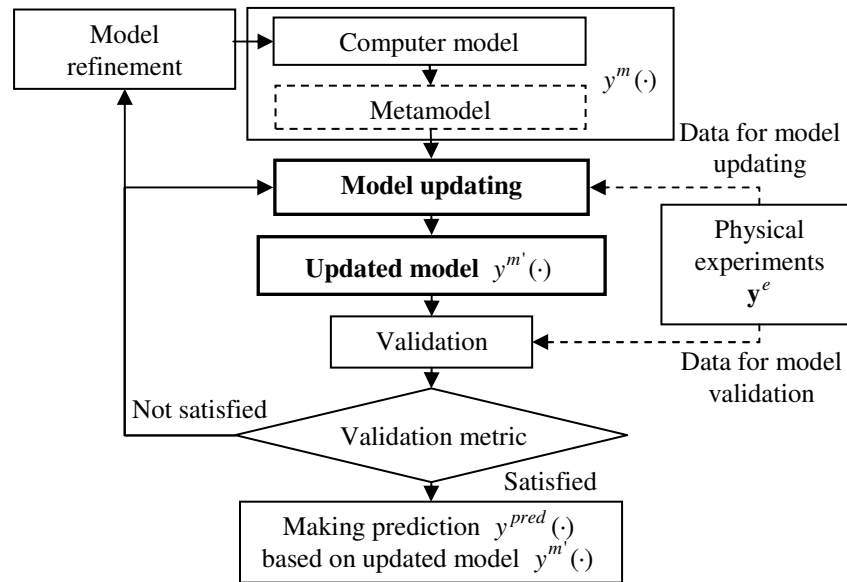


Figure 5.1 Relationship of model updating, model refinement, and model validation

5.3 Examination of Existing Model Updating Methods

The existing model updating strategies differ in their formulations, the solution method used, and the physical interpretations. In the following overview, two categories of formulations, namely, bias-correction and calibration will be first reviewed. We then discuss the limitations of using the Bayesian approach as the solution method. The physical interpretations are provided throughout the review and will be further expanded in Section 5.4.

5.3.1 Model bias-correction approaches

Bias-correction is useful when accuracy improvement cannot be accomplished by calibrating model parameters (Easterling and Berger 2002, Hasselman et al. 2005). One widely accepted interpretation of the bias-correction approach (Kennedy and O'Hagan 2001) is that it captures the potential model or method error due to the use of incorrect modeling method (e.g., modeling a non-linear behavior with a linear model), which often cannot be compensated by

other means. There are various formulations of bias-correction seen in literature. In the Bayesian bias-correction model proposed by Chen et al. (2006) and Wang et al. (2008), a plain additive bias-correction model is formulated as

$$y^e(\mathbf{x}) = y^m(\mathbf{x}) + \delta(\mathbf{x}) + \varepsilon, \quad (5.1)$$

where the bias function $\delta(\mathbf{x})$ is a direct measure of the difference between the computer model $y^m(\mathbf{x})$ and the physical process $y^e(\mathbf{x})$. The bias function $\delta(\mathbf{x})$ is assumed to be a Gaussian Process model, the uncertainty of which reflects the uncertainty involved in a model updating process such as the experimental error, lack of data, etc. One advantage of using the above formulation is that the closed form Bayesian posterior of the Gaussian process model $\delta(\mathbf{x})$ can be derived. In addition, the bias function $\delta(\mathbf{x})$ provides a direct measure of the assessed accuracy (or validity) of a computer model within a particular design region or at an application site (Wang et al., 2008).

In addition to using the additive bias shown in Eq. (5.1), a bias correction approach may employ a combination of multiplicative bias and additive bias, as shown in the following formulation (Qian and Wu, 2005),

$$y^e(\mathbf{x}) = \rho(\mathbf{x})y^m(\mathbf{x}) + \delta(\mathbf{x}) + \varepsilon, \quad (5.2)$$

where $\rho(\mathbf{x})$ is modeled as a simple linear regression model w.r.t. \mathbf{x} , ε is assumed to be a zero mean Gaussian random variable. The scaling function $\rho(\mathbf{x})$ in Eq. (5.2) brings more flexibility to the constant adjustment parameter ρ used in Kennedy and O'Hagan (2001). The maximum likelihood estimation (MLE) method is utilized in their work to estimate the regression

coefficients of $\rho(\mathbf{x})$, while the closed forms Bayesian posteriors of the hyperparameters in the Gaussian Process $\delta(\mathbf{x})$ are derived for given prior distributions.

One inherent limitation of the bias-correction method is that it assumes all inputs (\mathbf{x}) of both the computer model ($y^m(\mathbf{x})$) and the physical process ($y^e(\mathbf{x})$) are observable and controllable. In practice, it often occurs that some of the model input parameters cannot be directly observed and measured in the physical experiments. This limitation can be addressed using the model calibration approach introduced next.

5.3.2 Model calibration approaches

With a typical model calibration approach, the inputs of a computer model and the physical process are divided into controllable inputs (\mathbf{x}), and unobservable/uncontrollable parameters ($\boldsymbol{\theta}$) that are assumed to be fixed over the experiment. Note that it is $\boldsymbol{\theta}$ that are to be calibrated or tuned. A computer model for the given input vector ($\mathbf{x}, \boldsymbol{\theta}$) is denoted as $y^m(\mathbf{x}, \boldsymbol{\theta})$, while the physical process is denoted to be $y^e(\mathbf{x})$ as a function of controllable inputs \mathbf{x} only.

Deterministic calibration approach

A conventional way to carry out a deterministic parameter calibration is to formulate the problem in a fashion similar to that of the nonlinear regression analysis (Romero 2007, Bates et al. 1988, Trucano et al. 2006) through the following equation.

$$y^e(\mathbf{x}) = y^m(\mathbf{x}, \boldsymbol{\theta}) + e, \quad (5.3)$$

where e is the residual between the prediction from the calibrated computer model $y^m(\mathbf{x}, \boldsymbol{\theta})$ and the experimental observation $y^e(\mathbf{x})$. The optimal values of the calibration parameters $\boldsymbol{\theta}$ are

found by minimizing the (weighted) sum of the squared error (SSE) between the model predictions and the physical experiments (Lindgren et al., 2003), i.e.,

$$\text{Find } \boldsymbol{\theta} \text{ minimizing } \text{SSE} = \sum_{i=1}^N w_i e_i^2 = \sum_{i=1}^N w_i [y^m(\mathbf{x}_i, \boldsymbol{\theta}) - y^e(\mathbf{x}_i)]^2, \quad (5.4)$$

where $\mathbf{x}_i = [x_{i1}, x_{i2}, \dots, x_{ik}]^T$ ($i=1,2,\dots,N$) are sample points, w_i ($i=1,2,\dots,N$) are the weights for different experimental observations reflecting the quality of experimental data, $\boldsymbol{\theta} = [\theta_1, \theta_2, \dots, \theta_m]^T$ are unknown physical constants, and k is the number of input variables. Although deterministic calibration approaches are generally plausible and easy to apply, the limitation is that they cannot account for uncertainties in both computer simulation and physical experimentation.

Non-deterministic Bayesian calibration approach

Non-deterministic parameter calibration is also called calibration under uncertainty (CUU) (Bates and Watts, 1998). Kennedy and O'Hagan (2001) first developed a Bayesian approach to simultaneously calibrate the computer model and characterize the potential bias (discrepancy) between the model output and the physical experiments. Their method is based on the following relation,

$$y^e(\mathbf{x}) = \rho \cdot y^m(\mathbf{x}, \boldsymbol{\theta}) + \delta(\mathbf{x}) + \varepsilon, \quad (5.5)$$

where ρ is an unknown regression parameter (an adjustment parameter), $\delta(\mathbf{x})$ is a bias (discrepancy) function assumed to be the realization of a Gaussian Process, ε is the experimental error assumed to be a zero-mean Gaussian random variable. In essence, the formulation shown in Eq. (5.5) is a combination of both parameter calibration and bias

correction. In Kennedy and O’Hagan’s work, the Bayesian analysis is performed to update the prior distributions of the calibration parameters $\boldsymbol{\theta}$ and the hyperparameters underlying two separate Gaussian Process models: one for the bias function $\delta(\mathbf{x})$, and the other for replacing the original expensive computer model $y^m(\mathbf{x}, \boldsymbol{\theta})$. In implementation, to manage the computational complexity, priors are often only specified for a very few calibration parameters $\boldsymbol{\theta}$ and a small set of Gaussian Process model parameters, while the rest of Gaussian Process model parameters are assumed unknown but fixed.

Several variants and applications of the Bayesian calibration approach of Kennedy and O’Hagan (2001) exist in literature. In the Simulator Assessment and Validation Engine (SAVE) framework developed by Bayarri et al. (2002), followed by Higdon et al. (2004), and Liu et al. (2008), a formulation that is similar to the one used by Kennedy and O’Hagan is shown as follows with the regression parameter ρ omitted.

$$y^e(\mathbf{x}) = y^m(\mathbf{x}, \boldsymbol{\theta}) + \delta(\mathbf{x}) + \varepsilon. \quad (5.6)$$

In Liu et al. (2008), only one GP model is used to represent the bias function $\delta(\mathbf{x})$, while no GP model is used to replace the computational model $y^m(\mathbf{x}, \boldsymbol{\theta})$ assuming it is computationally cheap to run.

It is worth noting that McFarland et al. (2007) developed a simplified Bayesian calibration approach in the form of

$$y^e(\mathbf{x}^*) = y^m(\mathbf{x}^*, \boldsymbol{\theta}) + \varepsilon. \quad (5.7)$$

Their method does not consider the bias-correction, and poses the prior belief of the calibration parameters $\boldsymbol{\theta}$ as uniformly distributed. Unlike others, their calibration is only performed at one

particular site \mathbf{x}^* , based on the assumption that the results of calibration are identical at different input sites. However, such an assumption is questionable if the computer model is so wrong that the calibration at one single site could be heavily biased and is hard to be extrapolated to other sites.

5.3.3 Limitations of Bayesian approaches

While the Bayesian approach is useful when the limited data are available, there are several common issues with the Bayesian approaches to both calibration and bias correction. First, as indicated in Trucano et al. (2006), the prior distributions of calibration parameters are often difficult to specify due to the lack of prior knowledge. Subjectively assigned prior distributions of calibration parameters may yield instable posterior distributions (Liu et al., 2008), which undermines the advantage of Bayesian updating. Second, the Markov Chain Monte Carlo (MCMC) method used in most Bayesian calibration practices for obtaining the posterior distributions requires a significant amount of iterations, while the decision criterion for ceasing the Markov Chain growth is not established (Trucano et al. 2006).

Loeppky et al. (2006) examined a non-Bayesian version of the approach from Kennedy and O'Hagan (2001), but using the MLE to estimate the calibration parameters which are assumed deterministic. The issue of identifiability of model bias was addressed by examining the likelihood ratio of two model versions: one with the bias term, the other without. It was demonstrated that the MLE estimates of calibration parameters will asymptotically attain an unbiased computer model if such a model exists. However, their method provides deterministic MLE estimates without acknowledging the uncertainty of model input.

5.4 A Maximum Likelihood Estimation (MLE) Based Model Updating Methodology

We present an alternative model updating approach that differs from the existing Bayesian approach in both uncertainty treatment and computing model updating parameters, while using the similar model updating formulations reviewed in Section 5.3. The basic principle of this proposed approach is to determine the model updating parameters with the MLE, so that the best agreement between the distribution of model outputs and the dispersion of the observed physical observations \mathbf{y}^e can be achieved, while the experiment-to-experiment variation of calibration parameters is captured by the distribution of parameter distributions.

5.4.1 Model updating formulations and parameters

As reviewed in Section 5.3, various formulations are available for constructing an updated model based on the original computer model $y^m(\mathbf{x}, \boldsymbol{\theta})$. In our view, the choice of the updated formulation (denoted as $y^{m'}(\mathbf{x}, \Theta)$) and the model updating parameters Θ are problem dependent and will require insight into the error sources. In Section 5.6, we will investigate four possible model updating formulations for the specific thermal challenge problem. One typical formulation that combines both bias correction and parameter calibration is illustrated here in Eq. (5.8).

$$y^{m'}(\mathbf{x}, \Theta) = y^m(\mathbf{x}, \boldsymbol{\theta}) + \delta(\mathbf{x}) + \varepsilon. \quad (5.8)$$

In Eq. (5.8), $\mathbf{x} = \{x_1, x_2, \dots, x_n\}$ are n observable/controllable input variables, which are always deterministic. $\boldsymbol{\theta} = \{\theta_1, \theta_2, \dots, \theta_m\}$ are m unobservable/uncontrollable input variables, assumed random to capture the experimental uncertainty associated with model input. The uncertainties of

θ are parameterized by distribution parameters $\{\mu_{\theta_1}, \sigma_{\theta_1}, \dots, \mu_{\theta_m}, \sigma_{\theta_m}\}$, independent from model input \mathbf{x} . ε is an unobservable/uncontrollable output variable, also assumed random, to capture the experimental uncertainty associated with a model output. Similar to θ , the distribution of ε is parameterized by $\{\mu_\varepsilon, \sigma_\varepsilon\}$. The bias function $\delta(\mathbf{x})$ is used to capture the model systematic bias, but not intended to account for the experimental uncertainty. $\delta(\mathbf{x})$ could be parameterized in various ways, for example, a regression model $\delta(\mathbf{x}) = \beta_{\delta_0} + \beta_{\delta_1}x_1 + \dots + \beta_{\delta_n}x_n$ parameterized by $\{\beta_{\delta_0}, \beta_{\delta_1}, \dots, \beta_{\delta_n}\}$. Here the bias function $\delta(\mathbf{x})$ is treated to be a deterministic function that does not contribute to the model output uncertainty. Other possible choices could be using a constant δ , which is less flexible, or a more complicated Gaussian Process (GP) model, that provides more flexibility. Collectively, the model updating parameters for the above formulation are denoted as $\Theta = \{\mu_{\theta_1}, \sigma_{\theta_1}, \dots, \mu_{\theta_m}, \sigma_{\theta_m}; \beta_{\delta_0}, \beta_{\delta_1}, \dots, \beta_{\delta_n}; \mu_\varepsilon, \sigma_\varepsilon\}$. Notice that in contrast to traditional calibration approaches, our model updating parameters Θ do not directly include the parameters θ , because they are not assumed to be fixed. Rather, Θ includes the means and variances of the parameters θ . Figure 5.2 shows the collection of model updating parameters in a formulation with two calibration parameters and two model inputs, i.e., $\mathbf{x} = \{x_1, x_2\}$ and $\theta = \{\theta_1, \theta_2\}$. Note that in the right hand side of Eq. (8), only θ and ε are random quantities, as illustrated by the shaded vertical PDF profiles in Figure 2. Also note that we assume θ and ε follow normal distribution, thus only two parameters are needed to determine the distribution of each calibration parameter. With the statistical moments defined for the calibration parameters, the various sources of uncertainties in a model updating process can be propagated to form the uncertainty of the updated model $y^{m'}(\mathbf{x}, \Theta)$, as illustrated by the shaded horizontal PDF profile in Figure 5.2.

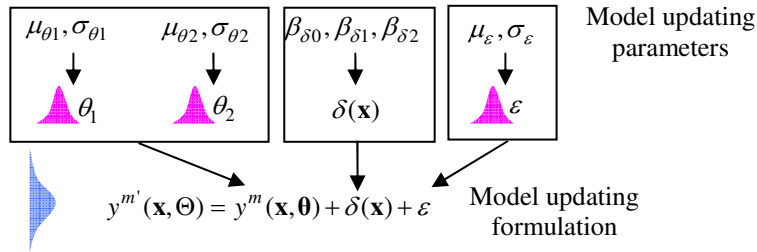


Figure 5.2 Model updating parameters Θ in formulation $y^{m'}(\mathbf{x}, \Theta)$

5.4.2 Determining model updating parameters via MLE

To determine the deterministic values of all model updating parameters, the maximum likelihood estimation (MLE) method is adopted towards matching the output distribution of the updated model $y^{m'}(\mathbf{x}, \Theta)$ with the dispersion observed in physical experiments $y^e(\mathbf{x})$.

To construct a likelihood function, the following equation relating data $y^e(\mathbf{x})$ with the probabilistic output from $y^{m'}(\mathbf{x}, \Theta)$ is established,

$$y^e(\mathbf{x}) = y^{m'}(\mathbf{x}, \Theta), \quad (5.9)$$

based on the assumption that the experimental data $y^e(\mathbf{x})$ can be hypothetically regenerated through the updated model $y^{m'}(\mathbf{x}, \Theta)$. Therefore, the likelihood $L(\Theta | \mathbf{y}^e)$ as a function of Θ conditioned on all observations \mathbf{y}^e is equal to the joint PDF of a N^e dimensional multivariate distribution of $y^{m'}(\mathbf{x}, \Theta)$ evaluated at \mathbf{y}^e . In this work, the N^e observations are assumed independent, then the likelihood function is the multiplication of N^e separate PDF functions, i.e.,

$$L(\Theta) = L(\Theta | \mathbf{y}^e) = p(\mathbf{y}^e | \Theta) = \prod_{i=1}^{N^e} p(y_i^e | \Theta), \quad (5.10)$$

where Θ are all model updating parameters to be estimated, $p(y_i^e | \Theta)$ is the value of PDF yielded from $y^{m'}(\mathbf{x}, \Theta)$ at (x_i^e, y_i^e) . Figure 5.3 depicts the plots of output distributions (the PDF of which are represented by shaded PDF profiles) of two $y^{m'}(\mathbf{x}, \Theta)$ models. With the same experimental data (empty circles), the model of the left side figure, which corresponds to a larger likelihood function value, shows a better match between the two distributions.

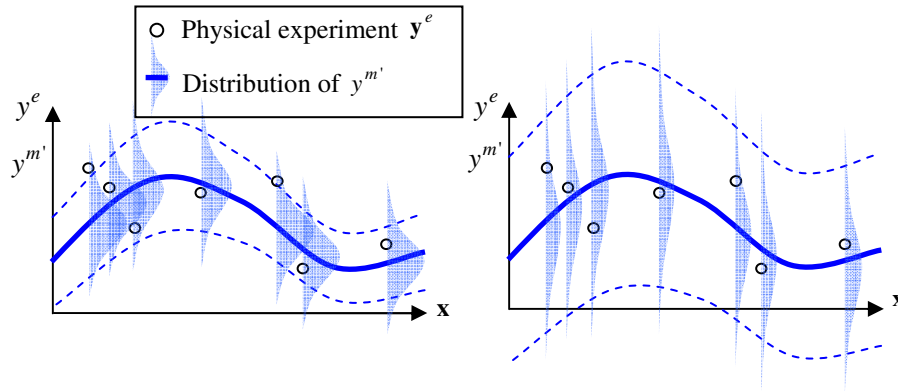


Figure 5.3. Likelihood value indicates the agreement between the output distribution of the updated model and the dispersion of physical experiments

To alleviate the computational burden associated with evaluating the PDF function in MLE, in our implementation, the output distribution of $y^{m'}(\mathbf{x}, \Theta)$ is approximated with a Gaussian distribution by only characterizing its first two moments. As the result, the PDF function $p(y_i^e | \Theta)$ in Eq. (5.10) for experiment y_i^e can be expressed through the Gaussian distribution,

$$y_i^e | \Theta \square N\left(E_{\Theta}\{y^{m'}(\mathbf{x}_i, \Theta)\}, \text{Var}_{\Theta}\{y^{m'}(\mathbf{x}_i, \Theta)\}\right). \quad (5.11)$$

To efficiently compute the mean $E_{\Theta}\{y^m(\mathbf{x}_i, \Theta)\}$ and the variance $Var_{\Theta}\{y^m(\mathbf{x}_i, \Theta)\}$ in the above equation, the numerical integration approach based on the tensor-product quadrature rule (Abramowitz and Stegun, 1972, Lee et al., 2007) is adopted in this work.

5.4.3 Comparison of the MLE based model updating with traditional Bayesian approach

To better reveal the features of the proposed MLE based model updating approach, several remarkable differences between this approach and the traditional Bayesian approach are highlighted.

With a traditional Bayesian calibration approach (Higdon et al., 2004), for the model updating formulation shown in Eq. (5.6), the likelihood function $L(\sigma_m, \mathbf{r}_m, \mu_m; \sigma_{\delta}, \mathbf{r}_{\delta}; \sigma_{\varepsilon}; \boldsymbol{\theta} | \mathbf{y}^{em})$ can be obtained from the PDF function of a multivariate Gaussian distribution as follows²³

$$\mathbf{y}^{em} | \sigma_m, \mathbf{r}_m, \mu_m; \sigma_{\delta}, \mathbf{r}_{\delta}; \sigma_{\varepsilon}; \boldsymbol{\theta} \square N(\mathbf{y}^{em} - \mu_m \mathbf{1}, \Sigma_{em}), \quad (5.12)$$

with covariance matrix Σ_{em} expressed by

$$\Sigma_{em} = \sigma_m^2 \mathbf{R}_m + \begin{pmatrix} 0 & 0 \\ 0 & \sigma_{\delta}^2 \mathbf{R}_{\delta} + \sigma_{\varepsilon}^2 \mathbf{I} \end{pmatrix}, \quad (5.13)$$

where \mathbf{y}^{em} denotes the joint data $(\mathbf{y}^e, \mathbf{y}^m)$ of computer and physical experiments, $\sigma_m, \mathbf{r}_m, \mu_m$ are the parameters of the GP model that replaces the expensive computer model $y^m(\mathbf{x}, \boldsymbol{\theta})$ with \mathbf{R}_m being the correlation matrix; $\sigma_{\delta}, \mathbf{r}_{\delta}$ are the parameters of the GP model for $\delta(\mathbf{x})$ with \mathbf{R}_{δ} being the correlation matrix; σ_{ε} is the standard deviation of the experimental error ε ; and \mathbf{I} is the identity matrix of the same size of \mathbf{R}_{δ} . It is noted from Eqs. (5.12) and (5.13) that the observed experimental uncertainty of $y^e(\mathbf{x})$ using the Bayesian approach is essentially attributed to three

sources, namely, random variable ε , GP model of $\delta(\mathbf{x})$, and GP model of $y^m(\mathbf{x}, \boldsymbol{\theta})$. The calibration parameters $\boldsymbol{\theta}$ are assumed to be fixed but unknown and do not contribute to the experimental uncertainty at all. Although the final inference of $\boldsymbol{\theta}$ through Bayesian posterior has randomness, such randomness only reflects the lack of knowledge, but not the experimental uncertainty that might be contributed by the variability of parameters $\boldsymbol{\theta}$ in experiment setup.

Based on the above introduction of Bayesian approach, we generalize several major differences between the Bayesian approach and the MLE based model updating approach. First, different types of experimental uncertainty are accounted for in different approaches. With the MLE based model updating approach, the experimental uncertainty is explicitly accounted for by both the random parameters $\boldsymbol{\theta}$ (for experiment-to-experiment variation) and the error term ε . In Bayesian approach, $\boldsymbol{\theta}$ is assumed fixed but unknown due to the lack of knowledge, while only one random parameter ε accounts for the experimental uncertainty, which is caused by random measurement error.

The second difference is associated with the handling of the expensive original computer model. In the traditional Bayesian calibration approaches, if an original computer model is expensive, a Gaussian Process model is used to replace it and the GP parameters are estimated using the Bayesian analysis together with other unknown model updating parameters. This adds much computational complexity to the Bayesian approach. With the MLE based model updating approach, a metamodel is first constructed to replace the expensive computer model even before the model updating procedure is initiated. It is then the metamodel, but not the original computer model, that is updated and used for prediction.

5.5 Prediction Using the Updated Model

Once an updated model $y^{m'}(\mathbf{x}, \Theta)$ is determined, it is used to form a predictive model $y^{pred}(\mathbf{x})$ for prediction. In this research, we consider prediction uncertainty of the predictive model $y^{pred}(\mathbf{x})$ to be characterized by propagating the uncertainties defined by the *model updating parameters* Θ through the updated model $y^{m'}(\mathbf{x}, \Theta)$, which by itself has a deterministic form. The form of the $y^{pred}(\mathbf{x})$ for prediction, i.e.,

$$y^{pred}(\mathbf{x}) = y^{m'}(\mathbf{x}, \Theta). \quad (5.14)$$

Since the original expensive computer model $y^m(\mathbf{x}, \theta)$ will be replaced by a metamodel using our approach, uncertainty propagation can be done in a rather efficient manner using a combination of Monte Carlo simulations and numerical methods, given the mean and standard deviation of θ . As a result, the prediction incorporates the uncertainties involved in a model updating and validation process.

5.6 Case Study: Comparative Studies Using the Thermal Challenge Problem

5.6.1 Problem description

The thermal challenge problem was developed by the Sandia National Laboratory (<http://www.esc.sandia.gov/VCWwebsite/vcwhome.html>) as a testbed for demonstrating various methods of prediction and validation (Dowding et al. 2008, Hills et al. 2008). The same problem is adopted as a numerical example in this work to demonstrate the features of our proposed model updating approach.

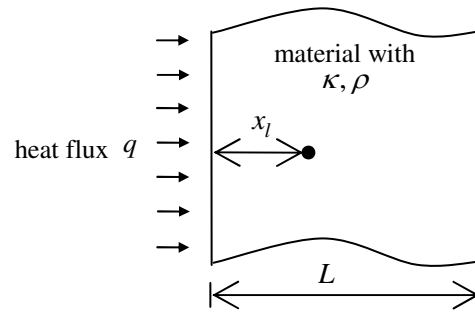


Figure 5.4 Schematic of thermal challenge problem

A schematic Figure of the thermal challenge problem is provided in Figure 4, in which the device is a material layer that is exposed to a constant heat flux. To predict the temperature T^m of a spot in the device at a specific location and time, an analytical computer model $y^m(\mathbf{x}, \boldsymbol{\theta})$ given in Eq. (5.15) was used as the original model.

$$y^m(\mathbf{x}, \boldsymbol{\theta}) = T^m(q, L, x_l, t, \kappa, \rho) = T_0 + \frac{qL}{k} \left[\frac{(k/\rho)t}{L^2} + \frac{1}{3} - \frac{x_l}{L} + \frac{1}{2} \left(\frac{x_l}{L} \right)^2 - \frac{2}{\pi^2} \sum_{n=1}^6 \frac{1}{n^2} e^{-n^2 \pi^2 \frac{(k/\rho)t}{L^2}} \cos(n\pi \frac{x_l}{L}) \right], \quad (5.15)$$

where $\mathbf{x}=(q, L, x_l, t)$ are controllable input variables, and $\boldsymbol{\theta}=(\kappa, \rho)$ are uncontrollable input parameters for calibration. Among the controllable input variables, x_l is the distance from the surface to the point being measured, q is the applied heat flux, L is the thickness, T_0 is the initial temperature of the device at time zero, and t is time. Since T_0 is fixed at 25 °C for all data and analyses, it is considered as a static model parameter instead of an input variable. Among the uncontrollable input parameters, κ and ρ stand for the thermal conductivity and the volumetric heat capacity, respectively; both κ and ρ are material properties vary from unit to unit due to manufacturing processes. The goal of this challenge problem is to assess if a regulatory

requirement is satisfied for a specified setting of model input, i.e., at an application site $\mathbf{x}^* = (q^*, L^*, x_l^*, t^*)$. To satisfy the regulatory requirement, the probability that the predicted temperature at a particular time not exceeding a threshold value 900°C , should be less than the target probability limit (0.01), that is,

$$P\{T^{pred}(q^* = 3500, L^* = 0.019, x_l^* = 0, t^* = 1000) > 900\} < 0.01. \quad (5.16)$$

As described in the original problem statement, the prior knowledge about κ, ρ are given in the form of material property characterization (MPC) data, which is listed in Tables C.1 and C.2 in the Appendix. Note that the measurements are collected under different temperatures T at the material subcomponent level rather than at the device level. Therefore the information of MPC cannot be directly used for device level prediction. The first two moments of the distribution of the above two parameters are evaluated based on the MPC data are summarized in Table 5.1. An obvious linear dependency of κ versus the temperature T can be observed (Figure 5.5). Since temperature T is also an output response of the device-level model (Eq. (5.16)), this creates a closed-loop situation where T is both an input and output of the model.

Table 5.1 Statistics of the given material characterization (MPC) data

κ		ρ	
μ_κ	σ_κ	μ_ρ	σ_ρ
0.0628	0.0099	393900	36252

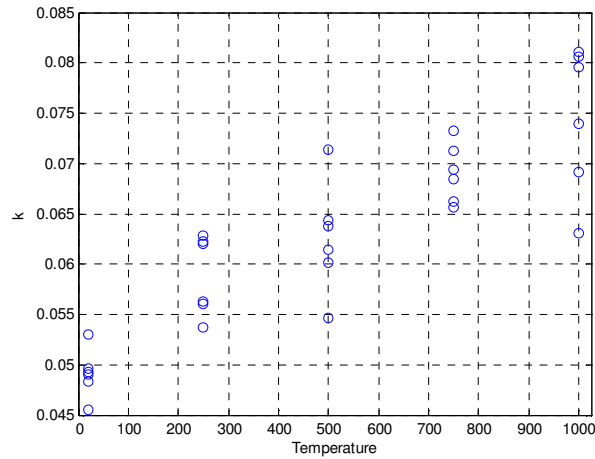


Figure 5.5 The dependency of thermal conductivity κ to temperature T

The full set of physical experiments consist of a subset of ‘ensemble’ (EN) data of 176, and a subset of ‘accreditation’ (AC) data of 126. The primary difference between the EN data and the AC data is that the former is gathered at model input sites far from the application site, while the latter is closer. Both EN and AC data are collected at several configurations (different settings of \mathbf{x}), and each configuration is a combination of model inputs (q, L, x_l) , while t varies at discrete time interval spot (11 spots for EN, 21 spots for AC) within the range 0~1000. For each configuration, data is collected respectively for 1~4 times. Table 5.2 lists the values of these configurations. The EN data and the AC data are selectively used at three levels of data sufficiency, namely, low, medium, and high. The sizes of EN data and AC data are considered at three different levels of sufficiency: 44+63 for low level, 88+63 for medium level, and 176+126 for high level. In this work, EN and AC data are used at the high levels of sufficiency by default.

Table 5.2 Statistics of the given characterization data

Data set	Config #	(q, L, x_l)	
EN	Config 1	$x_l=0$	$q=1000, L=1.27$
	Config 2		$q=1000, L=2.54$
	Config 3		$q=2000, L=1.27$
	Config 4		$q=2000, L=2.54$
AC	Config 5.1	$x_l=0$	$q=3000, L=1.9$
	Config 5.2	$x_l=L/2$	
	Config 5.3	$x_l=L$	

5.6.2 Bayesian approaches to the thermal challenge problem

Several different approaches have been developed and presented in literature for the thermal challenge problem as the result of the Sandia Validation workshop (<http://www.esc.sandia.gov/VCWwebsite/vcwhome.html>). We find these methods differ in how they utilize three different data sources (MPC, EN and AC data), the model updating formulations (e.g., including bias or not), and the solution method (e.g., Bayesian or non-Bayesian). Additionally, some of these works focus on prediction (whether the regulatory requirement will be met), while some others also study the model validity (accuracy). The readers should refer to Hills et al. (2008) for a complete summary of the existing approaches.

In terms of the solution method, the Bayesian calibration methodology of Kennedy and O'Hagan (2001) was followed by Higdon et al. (2008), Liu et al. (2008), McFarland and Mahadevan (2008) to calibrate κ and ρ with the bias function included. In Liu et al.(2008) and Higdon et al. (2008), no formal model validation is considered, while in McFarland and Mahadevan (2008), model validation metrics based on the significance test are employed. These works use different prior specifications of Gaussian Process hyperparameters and assume different prior distributions for calibration parameters κ and ρ . The works of Liu et al.(2008) and Higdon et al. (2008) assign prior distributions for parameters κ and ρ based on either full or

partial MPC data. The work of McFarland and Mahadevan (2008) specifies vague priors for κ and ρ without using any MPC data. By utilizing both the EN and AC data, the predicted failure probabilities are determined to be 0.03 for using all levels of data sufficiency in Higdon et al. (2008), and are determined to be 0.02 and 0.04 respectively for using the medium and high levels of data sufficiency in Liu et al. (2008). In McFarland and Mahadevan (2008), the failure probability is computed as 0.166 using the high level of data sufficiency. All studies indicate that the thermal device cannot meet the regulatory requirement (<0.01) as specified in Eq. (16).

5.6.3 Three model updating formulations used for testing the MLE method

In this study, the proposed MLE based model updating approach is tested with three different model updating formulations. The formulations of the updated model $y^{m'}(\mathbf{x}, \Theta)$ and the corresponding model updating parameters Θ adopted for the thermal challenge problem are listed in Table 5.3.

Table 5.3. Model updating formulations and model updating parameters

Model form. #	$y^{m'}(\mathbf{x}, \Theta)$	Model updating parameters Θ		
		for θ (i.e., κ and ρ)	for ε	for $\delta(\mathbf{x})$
(1)	$y^m(\mathbf{x}, \theta) + \varepsilon$	$\mu_\kappa, \sigma_\kappa, \mu_\rho, \sigma_\rho$;	$\mu_\varepsilon (= 0), \sigma_\varepsilon$	
(2)	$y^m(\mathbf{x}, \theta) + \delta(\mathbf{x}) + \varepsilon$	$\mu_\kappa, \sigma_\kappa, \mu_\rho, \sigma_\rho$	$\mu_\varepsilon (= 0), \sigma_\varepsilon$	$\beta_{\delta 0}, \beta_{\delta 1}, \dots, \beta_{\delta 4}$
(3)	$y^m(\mathbf{x}, \theta(\mathbf{x})) + \delta(\mathbf{x}) + \varepsilon$	$\beta_{\kappa 0}, \beta_{\kappa 1}, \sigma_\kappa, \mu_\rho, \sigma_\rho$	$\mu_\varepsilon (= 0), \sigma_\varepsilon$	$\beta_{\delta 0}, \beta_{\delta 1}, \dots, \beta_{\delta 4}$

In all formulations, we assume that the uncontrollable output variable ε is a zero-mean random variable ($\mu_\varepsilon = 0$). Formulation (2) is exactly the one used in Eq. (5.8) to explain the MLE method in Section 5.4. While Formulation (1) is the simplest updating formulation, the

bias function $\delta(\mathbf{x})$ is introduced in both Formulations (2) and (3), where a first order polynomial regression model, governed by parameters $\beta_{\delta_0}, \beta_{\delta_1}, \dots, \beta_{\delta_4}$, is used to represent $\delta(\mathbf{x})$. To capture the linear dependency of κ versus the temperature T observed from the MPC data (Figure 5.5), in Formulation (3), it is assumed that θ is a function of \mathbf{x} , i.e., $\theta = \theta(\mathbf{x})$. Given that the temperature field of the thermal device is primarily influenced by distance (x_l) from the surface to the measured point, the function of $\theta(\mathbf{x})$ is further simplified, by modeling the mean of κ , namely μ_κ , as linearly dependent on x_l (rather than all \mathbf{x}) through a linear model $\mu_\kappa = \beta_0 + \beta_1 x_l$.

5.6.4 Results of model updating parameters of different formulations

Using the MLE method described in Section 5.4, the model updating parameters for each formulation are obtained based on the selected data from the given data set EN and AC. To study the extrapolation capability of the updated model, three scenarios are considered, each of which corresponds to a specific combination of EN and AC, as shown in Table 5.4. In searching for model updating parameters Θ via MLE optimization, the mean and variance values from the MPC information in Table 1 are utilized to provide search bounds. In this example, we use a relatively loose bounds by multiplying a factor 0.1 ~ 10. For example, based on $\mu_\kappa = 0.0628$ and $\sigma_\kappa = 0.0099$ in Table 1, the bounds applied in MLE optimization are 0.00628 ~ 0.628 for μ_κ and 0.00099 ~ 0.099 for σ_κ .

Table 5.4. Scenarios of using validation data (EN and AC) as model updating data

	Data for model updating
Scenario 1	EN
Scenario 2	AC
Scenario 3	EN + AC

For the purpose of demonstration, we provide in Table 5.5 only the results of the model updating parameters under Scenario 1 with high level data sufficiency. These results provide statistical representations of model updating parameters, which will be used further to characterize the uncertainty of model response in both prediction and validation.

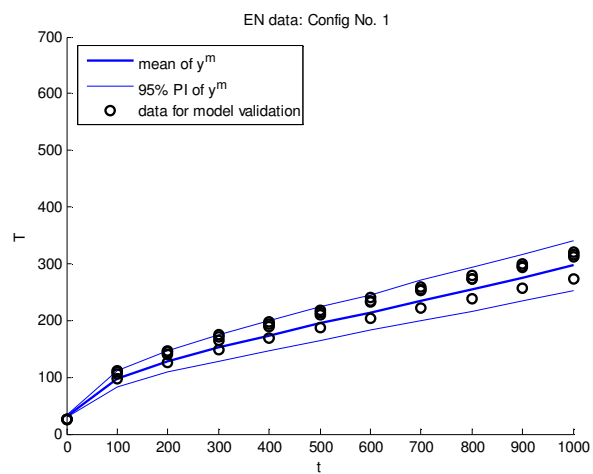
Table 5.5. Estimated model updating parameters (Scenario 1)

Model #	κ		ρ		ε	$\delta(\mathbf{x})$	
	μ_{κ}	σ_{κ}	μ_{ρ}	σ_{ρ}	σ_{ε}	$\beta_{\delta 0}, \beta_{\delta 1}, \dots, \beta_{\delta 4}$	
(1)	0.0579	0.00099	387026	12266	9.8001	N/A	
(2)	0.0493	0.00099	399822	22210	5.2399	14.751, 118.593, -0.010, -663.605, 0	
	$\beta_{\kappa 0}$	$\beta_{\kappa 1}$					
(3)	0.0508	0.025850	0.00110	391171	20549	5.4833	14.293, 176.377, -0.010, -606.117, 0

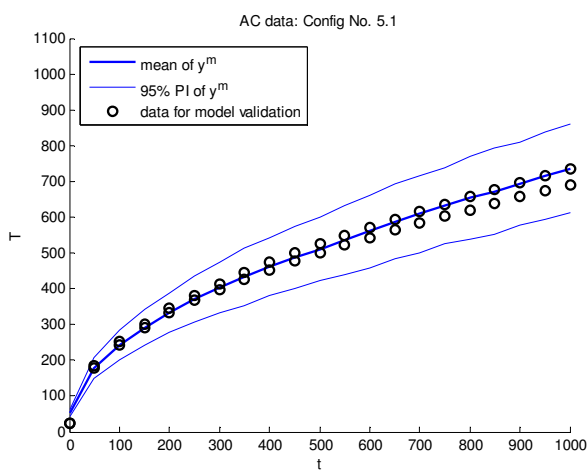
5.6.5 Studying of the predictive capability of the updated models

We use the results from Formulation (2) as an example to demonstrate how the predictive capability of an updated model can be studied. As a reference, the results from the ‘Original’ model without model updating (Eq. 5.16) are first shown, but with the consideration of uncertainty of model parameters κ and ρ as observed from the MPC data. Figure 5.7 shows the predicted response with uncertainty yielded by the ‘Original’ model at two selected configuration sites: Config 1 and Config 5.1 (Table 5.2). Uncertainty of the prediction is represented by the 95% prediction intervals (PIs). Also plotted in the Figures are the validation data collected (EN data for Config 1 in (a); AC data for Config 5.1 in (b)). It is observed that for this particular problem, even without model updating, uncertainty predictions based on the MPC

data encompass the physical observations quite well. However, the magnitude of the prediction uncertainty at Config 5.1 (the accreditation site) appears to be much larger than the true dispersion observed from data.



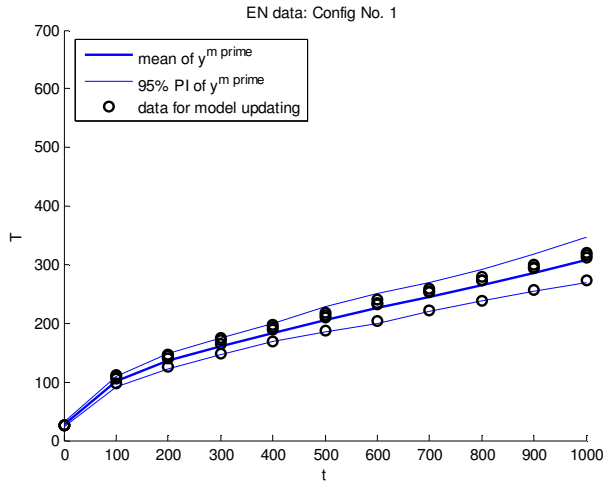
(a) Config 1



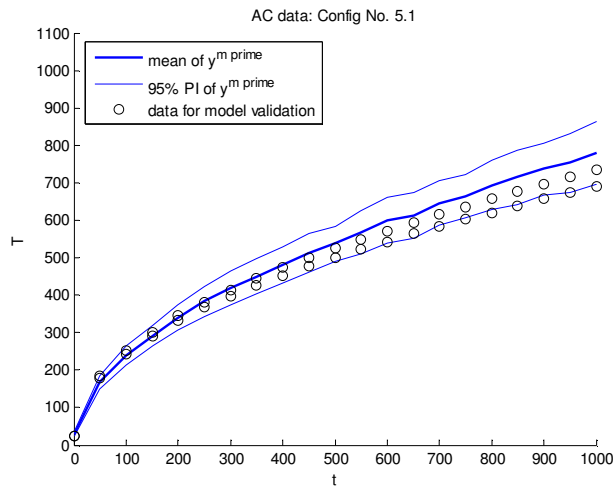
(b) Config 5.1

Figure 5.5 Prediction through the ‘Original’ model at Config 1 and Config 5.1

Figures 5.5 and 5.6 show the predictions using the updated model based on Formulation (2) under data Scenario 1 and Scenario 2, respectively. Only data at Config 1 and Config 5.1 are shown. In Figure 5.6, the EN data is used for model updating while EN data ('in-sample' test) and AC data ('out-sample' test) are used separately to validate the updated model (Scenario 1).



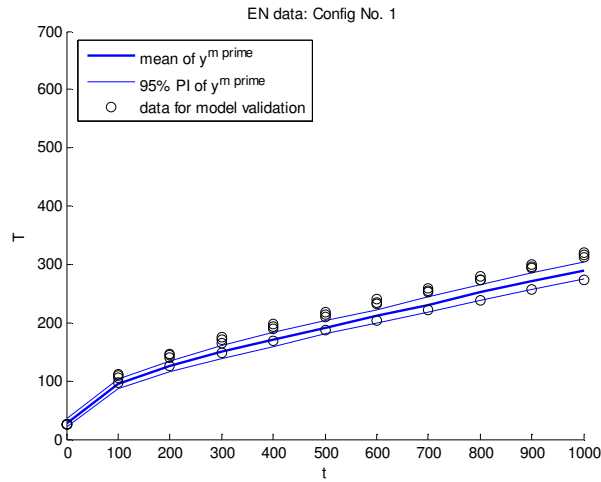
(a) in-sample test



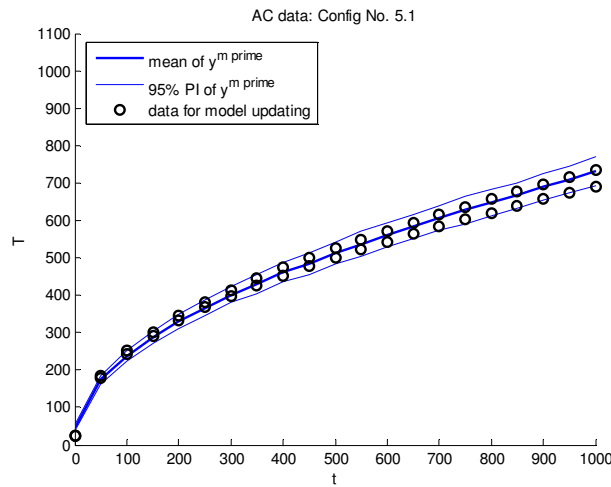
(b) out-sample test

Figure 5.6 Prediction through Formulation (2) (Scenario 1)

In Figure 5.7, the AC data is used for model updating while EN (‘out-sample’ test) and AC (‘in-sample’ test) are used separately as validation data (Scenario 2).



(a) out-sample test



(b) in-sample test

Figure 5.7 Prediction through Formulation (2) (Scenario 2)

In comparing Figure 5.6 (a) with Figure 5.5(a), and then Figure 5.7(b) with Figure 5.5(b), it is observed that after using our proposed MLE method for model updating, the predictions

with uncertainty quantification match much better with what observed in the physical data, i.e., the uncertainty bandwidth is significantly reduced to match with the dispersion of physical data. Such an improvement is accredited to using MLE as the optimization criterion for determining the model updating parameters. Figure 5.6(b) and Figure 5.7(a) (both for out-sample test) show the predictive capability of the updated models. It is found that the prediction in the out-sample tests is not as good as those in the in-sample tests, and somewhat worse than the prediction made by the ‘Original’ model (Figure 5.5).

5.6.6 Model validation metrics

For comparing the validity (accuracy) and predictive capability of four different model updating formulations, the model validation results under three different scenarios outlined in Table 5.4 are provide in Tables 5.6~5.8, all with high data sufficiency level.

The ‘u-pooling’ metric (Chapter 2.6) is used for assessing the relative accuracy of multiple model updating formulations. In addition, we also employ the Rooted Mean Square Error (RMSE) (Chapter 2.6), a traditional accuracy metric, to assess the goodness-of-fit in terms of the mean prediction. In calculating the RMSE, the residual error e_i is the difference between y_i^e and the mean of the updated model $y^{m'}(\mathbf{x}, \Theta)$ at \mathbf{x}_i^e , i.e., $e_i = y_i^e - E_{\Theta} y^{m'}(\mathbf{x}_i^e, \Theta)$.

Under Scenario 1 (Table 5.6) and Scenario 2 (Table 5.7), one set of data (either EN or AC) is used for model updating, called in-sample test; while the other set is used for verifying the predictive capability, called out-sample test. Under Scenario 3 (Table 5.8), both EN and AC data are used in model updating. Validation is performed over the joint data set, which is essentially an ‘in-sample’ test. For comparison, the metrics are evaluated for the original model, with the uncertainty of parameters κ and ρ characterized directly from the material property

characterization (MPC) data without updating the model itself. The results are summarized in the row marked with ‘Original’.

In Tables 5.6 and 5.7, the best and the second best ‘u-pooling’ or RMSE values in any single column across different model formulations are marked out with ‘***’ and ‘*’ respectively. In Table 5.6, when the EN data is used for model updating, Formulation (2) is found to be the best in the in-sample test in terms of both ‘u-pooling’ and RMSE values. In the out-sample test, Formulation (2) ranks the second best under ‘u-pooling’ and the best under RMSE. This indicates that when the EN data is used for model updating, Formulation (2), which uses constant calibration parameter θ and bias function $\delta(\mathbf{x})$, can best adapt to the data with acceptable extrapolation capability. In Table 5.7, when the AC data is used for model updating, Formulation (2) again wins over others in the in-sample test. However, in the out-sample test, no model updating formulation is superior to the ‘Original’ model, which indicates that, although an updated model favors the data it used, the extrapolation should be treated with caution. In Table 5.8, where EN data and AC data are both incorporated in model updating, Formulation (2) is the best over other formulations and the ‘Original’ model. Overall, Formulation (2) achieves the best performance over other formulations and the ‘Original’ model. One common observation in Tables 5.6~5.8 is that all four model updating formulations are better than the ‘Original’ in all in-sample test columns. It is interesting to note that Formulation (3), in which one of the calibration parameters θ is considered as a function of model input x_i , do not bring a significant benefit as is expected based on the physical principle.

Table 5.6 Summary of model validation metrics (Scenario 1)

Model #	Validation data: EN (in-sample test)		Validation data: AC (out-sample test)	
	u-pooling	RMSE	u-pooling	RMSE
Original	0.634	16.96	0.830**	29.13
(1)	0.566	15.12*	1.138	33.36
(2)	0.521**	15.07**	0.901*	19.43**
(3)	0.579	15.16	1.041	31.39

Table 5.7 Summary of model validation metrics (Scenario 2)

Model #	Validation data: EN (out-sample test)		Validation data: AC (in-sample test)	
	u-pooling	RMSE	u-pooling	RMSE
Original	0.634**	16.96**	0.830	29.13
(1)	0.891	17.87*	0.540	11.27*
(2)	0.813*	18.14	0.471*	11.24**
(3)	1.002	19.53	0.463**	11.40

Table 5.8 Summary of model validation metrics (Scenario 3)

Model #	Validation data: EN + AC (in-sample test)	
	u-pooling	RMSE
Original	0.456	22.84
(1)	0.420*	14.98
(2)	0.388**	14.29**
(3)	0.429	14.60*

5.6.7 Comparison of regulatory test results

Based on the study of the predictive capability in previous sections and the fact that the application site \mathbf{x}^* is close to the domain of AC data, it is determined that both the EN and AC data sets should be used for updating the model (i.e., Scenario 3), which will be further used to

make the final prediction at \mathbf{x}^* in the regulatory test. All data in EN and AC (i.e., high level data sufficiency) is considered. The method introduced in Chapter 5.5 is used for predicting the regulatory requirement stated in Eq. (5.17). To assess the failure probability, 1000 Monte Carlo simulations are used for propagating the parameter uncertainty determined by the model updating parameters which are identified using the MLE approach. Table 5.9 shows the estimated failure probabilities using different model updating formulations including the ‘Original’ model. The specified threshold value (0.01) is exceeded in all cases.

Table 5.9 Summary of predicted failure probability (Scenario 3)

	Original	Model #			
		(1)	(2)	(3)	(4)
$P\{T^{pred}(\mathbf{x}^*) > 900\}$	0.26	0.060	0.028	0.088	0.092

It is found that our estimations of failure probabilities are consistent with the results reported in the other works (Liu et al. 2008, and Higdon et al. 2008) on the thermal challenge problem. Considering that Formulation (2) achieves the best overall accuracy over others, our best estimation of failure probability is 0.028.

5.7 Summary

In this chapter, we examine various strategies for model updating and study its relationship with model validation activities. The maximum likelihood estimation (MLE) method is introduced as an alternative approach to the traditional Bayesian method to estimate the model updating parameters, so that it seeks optimal distribution parameters underlying model updating

parameters through MLE. Unlike the traditional Bayesian approach which treats calibration parameters as fixed but unknown due to lack of knowledge, the MLE based approach treats calibration parameters as intrinsic random to account for the uncertainty due to experiment-to-experiment variability. Other differences of the two methods are summarized in Section 4.3 and will not be repeated here.

Through the thermal challenge example, it is demonstrated that model updating can be treated as an integral part of a model validation process which improves a model based on the physical observations gathered. We illustrate that without running into numerical complexity, the model updating method proposed in this work is easier to implement and interpret compared to the existing Bayesian methods. Using the newly developed u-pooling method by Ferson et al (2008), it is shown that the metric can be applied to both the original and the updated models to assess the accuracy and predictive capability of different model updating formulations. Through in-sample and out-sample tests based on different data sets, it is observed that the proposed model updating approach improves the agreement between the model and the physical experiment data. However, when applying the updated model at a region that is far from the domain of data used for model updating, the extrapolation capability of the updated model is not guaranteed. By comparing our approach to the existing works on the thermal challenge problem, the differences of various methods in utilizing available data, the model updating formulations adopted, and the solution method employed, are pointed out. Even though our method is different, it is found the conclusion reached on device failure probability is identical to other methods in literature. As for which model updating formulation is the most appropriate, unless it can be specified based on the pre-existing knowledge, we think it is problem dependent and should be selected by exercising the model validation metrics as demonstrated. While model

updating is shown to be useful for improving the accuracy of a model, as the process is fully data-driven, we believe the method should be used with caution when used for extrapolation.

Chapter 6. Design Driven Model Validation Metrics and Procedure

Nomenclature

$y^e(\mathbf{x})$	physical experimental observation
$\varepsilon(\mathbf{x})$	experimental error
$y^r(\mathbf{x})$	true response outcome
$y^m(\mathbf{x})$	outcome of computer model
$\delta(\mathbf{x})$	the bias (or error) of computer model
$f(\mathbf{x})$	design objective function
$U(\mathbf{x})$	design utility function
$Z(\mathbf{x})$	difference function
\mathbf{x}	$\mathbf{x} = (x_1, \dots, x_p)^T$, design in a p -dimensional space
D_e	$D_e = \{\mathbf{x}_1, \dots, \mathbf{x}_{n_e}\}$, for physical experiments
D_m	$D_m = \{\mathbf{x}'_1, \dots, \mathbf{x}'_{n_m}\}$, for computer experiments
n_m, n_e	size of D_m / D_e , the number of computer / physical experiments
σ_ε^2	variance parameter of $\varepsilon(\mathbf{x})$
σ_δ^2	variance parameter of the prior Gaussian process $\delta(\mathbf{x})$

ϕ_δ	correlation parameter of the prior Gaussian process $\delta(\mathbf{x})$
τ	ratio of σ_ε^2 to σ_δ^2
$n_{\delta e,m}$	degree of freedom of t distribution
$\mu_{\delta e,m}(\mathbf{x})$	noncentrality parameter of t distribution
$\sigma_{\delta e,m}^2(\mathbf{x})$	scale parameter of t distribution
$M_D(\mathbf{x}^*)$	design validation metric
H	design tolerance
X^0	indifferentiable region
Ω_d	set of feasible design alternatives
K	number of design candidates or competing designs

6.1 Introduction

It was brought up in Chapter 1 that in the existing work on model validation, most approaches are primarily carried out from the perspective of *model builders* (or analysts) but not from that of *designers* (model users). On the other hand, most of the existing validation metrics are based on limited test points without considering the predictive capability at *untested* but potential design space and the various sources of uncertainties. Therefore, it is argued that the existing approaches for validating analysis models are not directly applicable for assessing the confidence of using predictive models in engineering design.

In the engineering design research community, special attentions have been given to how models and information are used in design decision making (McAdams and Dym, 2004).

Preliminary efforts have been made on characterizing and assessing the validity of behavior models and their predictions in design (Malak and Paredis, 2004). Hazelrigg (2003) brought up the notion that validation of a predictive model can be accomplished only in the context of a specific decision, and only in the context of subjective input from a decision maker, including preferences. From model users' (designers') perspective, a good model should be considered as the one that can provide the discrimination (good resolution) between design candidates. As noted by Hazelrigg (2003), rather than the *accuracy* of a model, designers care more about the ability of models to discriminate between alternatives, namely the *resolution* of the model, for the decisions we have made. This concept could be illustrated by Figure 6.1, where two designs alternatives \mathbf{x}_A and \mathbf{x}_B are to be differentiated by a model $f(\mathbf{x})$. When the model $f(\mathbf{x})$ has model uncertainty, it is important to assess the probability of design x_A to produce an outcome that is preferred to or indifferent to another alternative x_B , i.e., $P_{AB} = P(f(\mathbf{x}_A) < (\mathbf{x}_B))$, assuming the smaller-the-better scenario. In Figure 6.1 (b), since the predictive model has a better capability of differentiating designs x_A and x_B than in (a), the resolution of (b) is higher than that of (a).

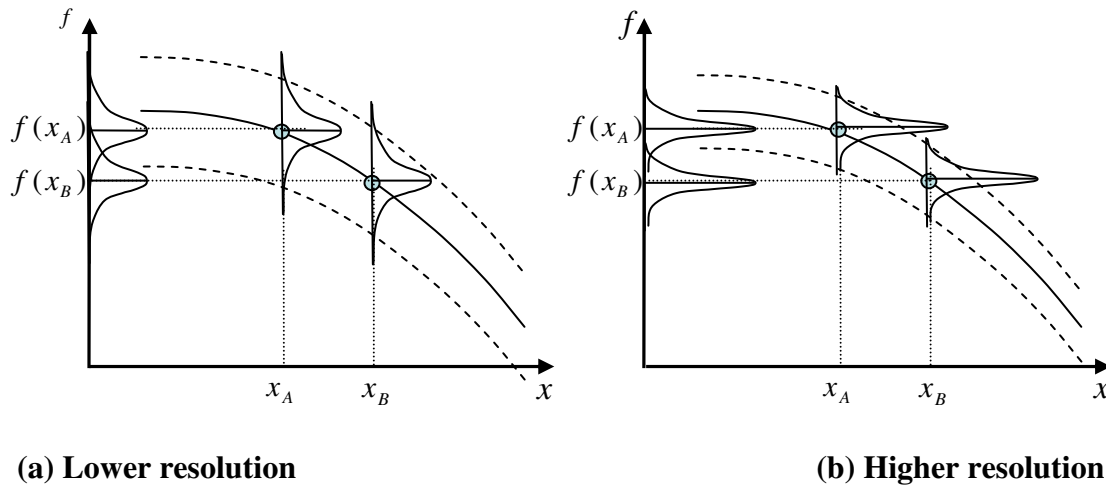


Figure 6.1 Comparing two designs under model uncertainty: the concept of model ‘resolution’

Although the need for validating models from the perspective of engineering design has been brought up (Malak and Paredis, 2004; Hazelrigg 2003), few have developed quantitative means to define and to assess model validity under model uncertainty, and many of them cannot provide stochastic measurements with regard to the confidence in using a model. Chen et al. (2004) and Buranathiti et al. (2004) developed an approach was developed to provide stochastic assessment of the validity of a model. However, the approach is more useful for rejecting (invalidating) a model rather than accepting (validating) a model. In the recent work of Mahadevan and Rebba (2005), a Bayes network approach is proposed for validating the reliability assessment made by computational models. In their work, validation was treated as a hypothesis testing problem. However, the emphasis was on validating the modeling accuracy at tested design points, but not in the context of a new design.

In most of the existing work, model validation is viewed as verifying the accuracy of a computer model, measured by the agreement between computational and experimental results.

One major limitation with this approach is that, practically speaking, physical data can be only collected at limited sites across a design space, often at locations far from the final design solution. For this reason, none of the validation metrics that are based on accuracy measures from limited sample points provides a true representation of model validity at untested design points.

In this work, we are motivated to investigate a new *design oriented* validation approach along with suitable validation metrics. The proposed validation procedure is aimed for yielding a predictive model that aids design decision making under *model uncertainty*. The proposed validation metric will be used to provide model users with confidence measures that a design being better than other design choices.

In Chapter 4, we described a bias-correction based predictive modeling approach, which captures systematic modeling error as well as uncertainties that impact the final predictive model. With the quantified uncertainty of Bayesian predictive models, we further develop some decision validation metrics to provide confidence measures of using Bayesian prediction in making a specific design choice for a given design objective. The implications of using such metrics are examined and the computational requirements are discussed for cases with either discrete or continuous design alternatives.

6.2 A Proposed Design-Driven Model Validation Procedure

Different from the current point of view in literature where model validation is viewed as the means to assess the accuracy of a computer model, model validation is viewed in this work as a process to provide designers with support on a set of decisions made using the improved

predictive model resulted from the validation process. The goal of model validation is not limited to validating (accepting) or invalidating (rejecting) the computer model, but to enhance the predicative capability of the predictive model $\hat{y}(x)$ with uncertainty quantification for design decision making. The general framework of the proposed design-driven model validation process is depicted in Figure 6.4. Figures 6.3 and 6.4 provide a comparison between the traditional model validation and the proposed model validation procedures.

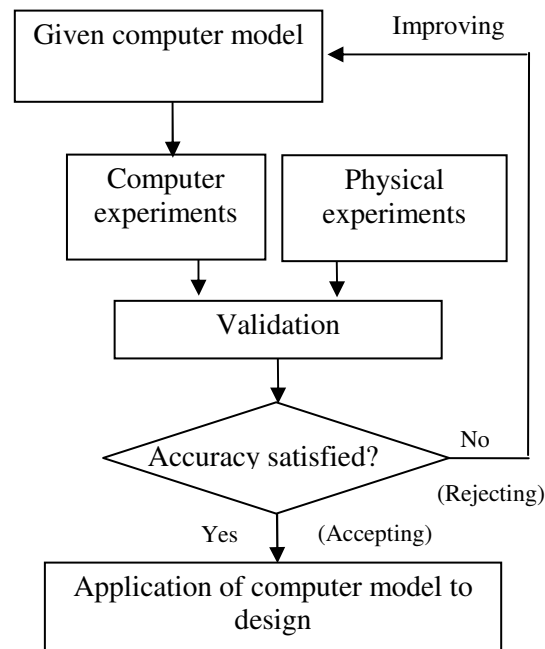


Figure 6.3. Traditional Validation Approaches

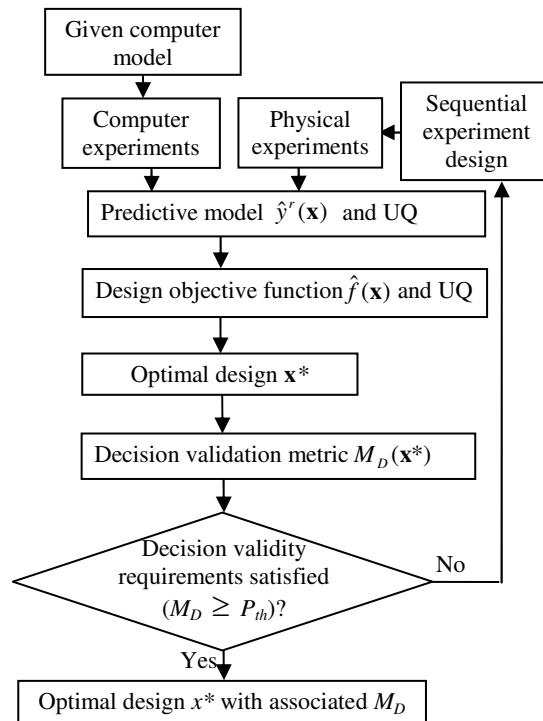


Figure 6.4 Proposed Validation Approaches

The proposed validation process starts with a given computer model, which is assumed to have passed the model verification test. By combining the results from computer experiments and physical experiments, a *predictive model* [represented by $y(\mathbf{x})$] with uncertainty quantification is obtained. It is noted that the predictive model here does not refer to the original computer model, rather, it is viewed as a corrected computer model by characterizing the bias between the computer model and the reality. The uncertainty of the predictive model is quantified by considering both the interpolation uncertainty due to the use of metamodel replacing the computer model and the random error of physical experiments.

To rank-order different design alternatives, they are compared against each other based on a *model of design utility* [represented by $U(y(\mathbf{x}))$ or simply $U(\mathbf{x})$], which is a function of single or multiple responses $y(\mathbf{x})$, and might have various forms from one design problem to the

other. When uncertainty of design variables/parameters (named as “other sources of uncertainty”) is considered, for example, in a typical robust design (Chen et al. 1996) problem, we view the utility function U , a function of both the mean μ_y and the standard deviation σ_y of performance, a complex design objective. The value of utility needs to be predicted by propagating other sources of uncertainty related to \mathbf{x} through the predictive model $y(x)$. To quantify the uncertainty of $U(\mathbf{x})$, statistical inference techniques must be developed to first quantify the uncertainty associated with the prediction of the response $y(\mathbf{x})$ based on the results from both models and physical experiments.

Based on the predicted utility model $\hat{U}(\mathbf{x})$, an optimal design (denoted as \mathbf{x}^*) could be identified by maximizing the mean of $\hat{U}(\mathbf{x})$ w.r.t \mathbf{x} . Two types of design scenarios are considered in this work, namely,

- 1) discrete design space, in which a set (denoted as X) of finite design alternatives are considered, and
- 2) continuous design space, in which an intended design region (denoted as Ω_d) is specified by the designer.

Once the optimal design \mathbf{x}^* is chosen, design *validation metrics* are used to assess the validity of using the predictive model for making this specific design choice. Corresponding to the above two design scenarios, different validation metrics are proposed, denoted respectively as $M_D(\hat{U}, \mathbf{x}^*, X)$ and $M_D(\hat{U}, \mathbf{x}^*, \Omega_t)$, where Ω_t represents the *tolerance zone* specified by designer when a continuous design space is considered.

As will be detailed in the later sections, the two proposed validation metrics essentially represent certain confidence levels of accepting a specific design \mathbf{x}^* as an optimal solution. A

pre-specified confidence level (or a threshold, denoted as P_{th} , such as 95%, 99%) should be assigned. If $M_D \geq P_{th}$, the optimal design \mathbf{x}^* is concluded with the confidence level as high as M_D . If $M_D < P_{th}$, it means that the utility model $\hat{U}(x)$ can not provide sufficient *resolution* to support the design decision \mathbf{x}^* made, and more information needs be gathered through additional physical experiments to reduce the uncertainty of $\hat{U}(\mathbf{x})$, therefore, to improve the confidence level of accepting a design solution.

To best exploit the information from physical experiments, *sequential experiment design* has to be carefully carried out. Where to put the next physical experiment considering the experiment restrictions is the question to be addressed in this work. With the added experiments, the same model validation process is repeated until the validity requirement is satisfied. However, as will be disclosed in the later sections, with the accumulation of experiments, there may not be sufficient gain from collecting more physical experiments. Therefore, associated with the experiment design is the issue of resource analysis. In the case that the validity requirement continues to be unsatisfied, the resource analysis is essentially to decide at what point the whole validation process should be terminated when further expense of experiment is predicted not to bring enough information.

6.3 Design-Driven Model Validation Metrics

Different from the existing validation metrics that assess the predictive capability (accuracy) of a model, some design validation metrics (denoted as M_D in general) are proposed, which provide a probabilistic measure of whether the real outcome of one candidate design is better than other design choices. Instead of the predictive model $\hat{y}^r(\mathbf{x})$ of performance, the

design objective function $\hat{f}(\mathbf{x})$ [or, more generally, the design *utility* function $\hat{U}(\mathbf{x})$] is used to determine the optimal design. In design under uncertainty, the design utility function could be a complex design objective, such as the robust design objective which is a function of both the mean μ_y and the standard deviation σ_y of performance. However, due to the uncertainty of $\hat{y}^r(\mathbf{x})$, $\hat{U}(\mathbf{x})$ is associated with uncertainty. Essentially, it is the uncertainty in design utility function $\hat{U}(\mathbf{x})$ that influences the confidence in making design decisions. The uncertainty of $\hat{y}^r(\mathbf{x})$ is reducible with more experiment data added; if uncertainty of $\hat{y}^r(\mathbf{x})$ is completely eliminated, $\hat{U}(\mathbf{x})$ reduces to a deterministic model. Complicated by the model uncertainty of $\hat{y}^r(\mathbf{x})$, the uncertainty in design utility $\hat{U}(\mathbf{x})$ is difficult to be quantified. Apley et al. (2005) addressed the similar issue and developed an analytical approach to formulate the effect caused by the uncertainty of $\hat{y}^r(\mathbf{x})$ (termed as the ‘interpolation uncertainty’ in their work) on a robust design objective.

For defining the validation metrics, two scenarios are considered separately, namely, 1) *finite design candidates* and 2) *continuous design space*. While both are possible scenarios in design practice, validation evaluation of the later scenario is more complicated than the former case. Even though the forms of these two types of validation metrics are slightly different, both types of M_D are interpreted as essentially the *confidence* of the chosen optimal design x^* being truly the optimal among a set of candidates or within a given design region. If large uncertainty remains in predicting a design outcome, e.g., because the design sites are far from the tested region of physical experiments, the achieved M_D may be too low to meet the design validity

requirements, forcing designers to add new experiment(s) to reduce model uncertainty or to lower the validity requirement.

(1) Validation toward Finite Design Candidates

Based on the predictive model $\hat{y}^r(\mathbf{x})$, when design parameter uncertainty is present, design alternatives are compared against the utility $\hat{U}(\mathbf{x}_i)$ (assuming larger utility is preferred). With the consideration of model uncertainty, differentiating the predicted performance at \mathbf{x}_i and \mathbf{x}_j is essentially to examine the probability of one design is better than the other. This is mathematically evaluated by the *Probability Based Pair-wise Comparison* between two random variables $\hat{U}(\mathbf{x}_i)$ and $\hat{U}(\mathbf{x}_j)$, i.e.,

$$P(\mathbf{x}_i, \mathbf{x}_j) \square P\{\hat{U}(\mathbf{x}_i) > \hat{U}(\mathbf{x}_j)\}. \quad (6.1)$$

The larger the probability $P(\mathbf{x}_i, \mathbf{x}_j)$, the higher capability of utility model $\hat{U}(\mathbf{x}_i)$ in differentiating designs \mathbf{x}_i and \mathbf{x}_j . The Monte Carlo simulation method may be used to sample a relatively large number (e.g., $N_s=1000$) of two-dimensional points. The probability of $P(\mathbf{x}_i, \mathbf{x}_j)$ is calculated as

$$P(\mathbf{x}_i, \mathbf{x}_j) = N\{\hat{U}_n(\mathbf{x}_i) > \hat{U}_n(\mathbf{x}_j)\} / N_s, \quad (6.2)$$

where $N\{\hat{U}_n(\mathbf{x}_i) > \hat{U}_n(\mathbf{x}_j)\}$ represents the number of two-dimensional sampling points at which $\hat{U}_n(\mathbf{x}_i)$ is larger than $\hat{U}_n(\mathbf{x}_j)$.

Before introducing the design-driven validation metrics, three forms of *point-wise metrics*, namely, the Multiplicative Metric, the Average (Additive) Metric, and the Worst-Case Metric are defined as:

$$M^{Multip}(\mathbf{x}_i, X) \square \left[\prod_{j=1, j \neq i}^K P\{\hat{U}(\mathbf{x}_i) > \hat{U}(\mathbf{x}_j)\} \right]^{1/(K-1)}, \quad (6.3)$$

$$M^{Average}(\mathbf{x}_i, X) \square \frac{1}{K-1} \sum_{j=1, j \neq i}^K P\{\hat{U}(\mathbf{x}_i) > \hat{U}(\mathbf{x}_j)\}, \quad (6.4)$$

$$M^{Worstcase}(\mathbf{x}_i, X) \square \min_{j=1, \dots, K, j \neq i} P\{\hat{U}(\mathbf{x}_i) > \hat{U}(\mathbf{x}_j)\}, \quad (6.5)$$

where $\hat{U}(\mathbf{x}_i)$ stands for the prediction of the utility function estimated at \mathbf{x}_i . $M(\mathbf{x}_i, X)$ metrics in Eqs. (6.3) and (6.4) provide an averaged measure of the probability that the real outcome of \mathbf{x}_i is better than or indifferent from other design choices, representing the confidence of using a predictive model to select \mathbf{x}_i as the optimal design choice. If $M(\mathbf{x}_i, X)=1$, it indicates that a designer should have full confidence in accepting \mathbf{x}_i as the optimal design. The $M(\mathbf{x}_i, X)$ metric in Eq. (6.5) stands for the worst case instead of the average.

For a set of given design alternatives $X = \{\mathbf{x}_i | i=1, \dots, K\}$, the *Validation Metric* over the set X is defined as

$$M_D(\hat{U}, \mathbf{x}^*, X) = M(\mathbf{x}^*, X), \quad (6.6)$$

where \mathbf{x}^* is the optimal design among the design candidates identified from the utility model $\hat{U}(\mathbf{x}_i)$.

(2) Validation within Continuous Design Space

For a given continuous design region, what is more relevant to designers is the confidence of an identified optimal design \mathbf{x}^* being truly the optimal one among other design points in the region. Distinguishing neighboring designs in a continuous design space with the consideration of model uncertainty is more challenging than separating discrete and distinctive design choices, because two designs might be hard to be differentiated if they are sufficiently close to each other. Hence, differentiating two closely adjacent designs is less meaningful because they can be viewed indifferent to each other.

The basic idea of formulating the validation metric M_D for a continuous case is to examine the neighboring points outside a small tolerance zone (denoted as Ω_t) from the chosen optimal point \mathbf{x}^* : the higher the probability of \mathbf{x}^* being better than the other points outside the tolerance zone, the better resolution of the model. Ω_t is the tolerable neighboring region around \mathbf{x}^* so that even if the chosen optimal design \mathbf{x}^* is not the “true” optimal, it is still tolerable because \mathbf{x}^* is indifferentiable from the true optimal design in this neighborhood. To perform the point-wise comparison between \mathbf{x}^* and all the points outside the tolerance zone is not feasible. Instead it is assumed, the points sitting on the boundary of the tolerance zone are the worst-case points. Average is taken over the boundary. Accordingly, the validation metric is defined as

$$M_D(\hat{U}, \mathbf{x}^*, \Omega_t) \square \underset{\mathbf{x}_i \in X_c}{\text{average}}\{P(\mathbf{x}^*, \mathbf{x}_i)\}, \quad (6.7)$$

where X_c is a set of points on the boundary of the tolerance zone Ω_t centered on \mathbf{x}^* . Averaging over a set of points allows us to relate the validation metric for the continuous case to that of the discrete case. Eq. (3.32) could be written as

$$M_D(\hat{U}, \mathbf{x}^*, \Omega_t) = M_D\{\hat{U}, \mathbf{x}^*, X\}, \quad (6.8)$$

where $X = \{\mathbf{x}^*\} \cap X_c$.

6.4 Case Study: Engine Piston Design

In this section, we continue with the Engine Piston Design problem used in Chapter 4 (Jin et al. 2005) to demonstrate the proposed validation framework with proposed model validation metrics. For the purpose of comparison, the predictive models are built in *two stages*. In the *first stage*, the first 19 points out of 34 physical experiment points in Table 6.1 are used. The remaining 15 points are added in the *second stage*.

Table 6.1 First Stage (19) physical experiments

i	1	2	3	4	5	6	7	8	9	10
$\mathbf{x}_i \in D_e$	0.000	0.100	0.200	0.300	0.400	0.500	0.600	0.700	0.800	0.900
$y^e(\mathbf{x}_i)$	56.332	56.077	55.875	55.542	55.159	54.840	54.682	55.039	55.183	55.774
i	11	12	13	14	15	16	17	18	19	
$\mathbf{x}_i \in D_e$	1.000	0.500	0.540	0.580	0.620	0.660	0.700	0.740	0.780	
$y^e(\mathbf{x}_i)$	56.749	54.867	54.646	54.748	54.576	54.614	54.623	54.978	54.923	

Table 6.2 Second stage (15) physical experiments

i	20	21	22	23	24	25	26	27	28	29
$\mathbf{x}_i \in D_e$	0.000	0.070	0.140	0.210	0.280	0.350	0.420	0.490	0.560	0.630
$y^e(\mathbf{x}_i)$	56.224	56.228	55.767	55.676	55.583	55.214	55.185	54.902	54.894	54.611
i	30	31	32	33	34					
$\mathbf{x}_i \in D_e$	0.700	0.770	0.840	0.910	0.980					
$y^e(\mathbf{x}_i)$	54.831	54.947	55.352	55.765	56.560					

Prediction and uncertainty quantification of $f(\mathbf{x})$

A robust design objective $f(\mathbf{x})$ is considered, i.e., $f(\mathbf{x}) = w_1 \cdot \mu_y + w_2 \cdot \sigma_y$ where μ_y and σ_y are the mean and standard deviation of y (engine slap noise), and the weights w_1 and w_2 are set at $w_1=1$ and $w_2=3$. The robust design objective is utilized to reduce the impact of the uncertainty associated with the randomness of \mathbf{x} . Note that $f(\mathbf{x})$ is under the ‘smaller-is-better’ scenario.

Although approximation of the mean and variance of $f(\mathbf{x})$ analytically is proposed by Apley et al. (2005), Monte Carlo simulation is employed in this work for simplicity. Based on the mean, variance and covariance of $y^r(\mathbf{x})$ by Eqs. (6.24)~(6.26), one can simulate a large amount (e.g., 100) of realizations of the random process $\hat{y}^r(\mathbf{x})$. For simplicity, only three of such realizations are selected and shown in Figures 6.5 and 6.6. Each single realization of $\hat{y}^r(\mathbf{x})$ determines the corresponding realization of $f(\mathbf{x})$ subject to the randomness of \mathbf{x} . As a result, the prediction of $f(\mathbf{x})$ and its uncertainty is quantified, as shown in the bold lines in Figures 6.5 and 6.6. Figures 6.5 and 6.6 show the results in the first stage and the second stage, respectively. With more physical experiment data, $f(\mathbf{x})$ in (b) has a narrower 95% prediction interval, which indicates a more accurate model.

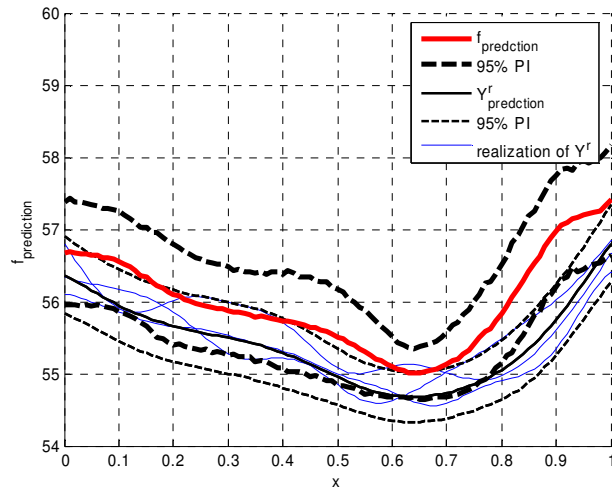


Figure 6.5 Prediction of $f(x)$ and 95% prediction interval in stage 1 (19 physical experiments)

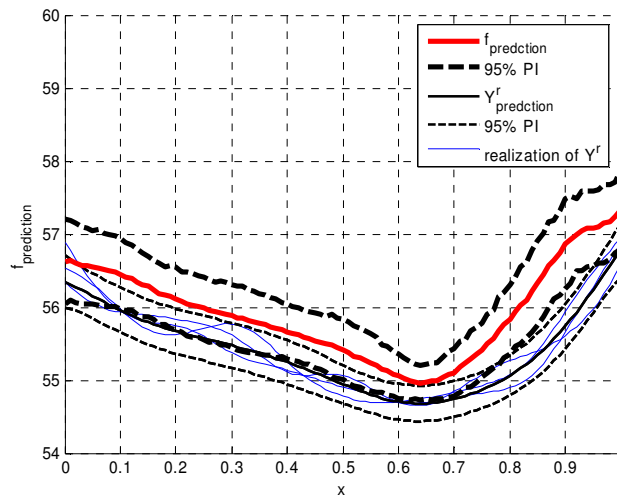


Figure 6.6 Prediction of $f(x)$ and 95% prediction interval in stage 2 (19+15 physical experiments)

Application of Design Validation Metrics

Considering a *discrete design scenario*, the design validation metrics $M_D(\hat{U}, \mathbf{x}^*, X)$ proposed in Eq. (6.31) will be applied to $\hat{f}(\mathbf{x})$ with five design candidates that have been

identified as $X=\{0.2, 0.4, 0.5, 0.65, 0.7\}$. The points generated by Monte Carlo simulation of

$\hat{f}(\mathbf{x})$ are illustrated in Figure 6.7.

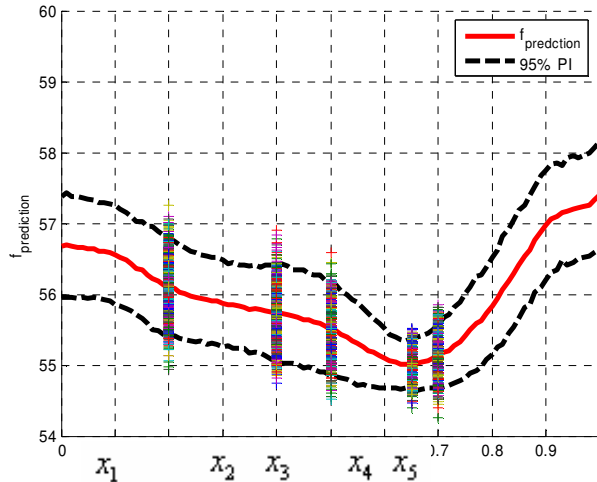


Figure 6.7 Comparison between five design alternatives ($\hat{f}(\mathbf{x})$ is built with 19 physical experiments)

Table 6.3 Three types of $M(x_i, X)$ and validation metric M_D (with 19 physical experiments)

	i	1	2	3	4	5
Type 1	$M^{Multip}(x_i, X)$	0.0000	0.1057	0.3379	0.8870 = M_D	0.6938
Type 2	$M^{Average}(x_i, X)$	0.0842	0.2715	0.4830	0.8957 = M_D	0.7655
Type 3	$M^{Worstcase}(x_i, X)$	0.0000	0.0150	0.1010	0.6990 = M_D	0.3010

Table 6.4 Three types of $M(x_i, X)$ and validation metric M_D (with 19+15=34 physical experiments)

	i	1	2	3	4	5
Type 1	$M^{Multip}(x_i, X)$	0.0000	0.0000	0.2137	0.9101 = M_D	0.7170
Type 2	$M^{Average}(x_i, X)$	0.0160	0.2850	0.4807	0.9192 = M_D	0.7990
Type 3	$M^{Worstcase}(x_i, X)$	0.0000	0.0000	0.0310	0.7080 = M_D	0.2920

In both the first stage and the second stage, x_4 achieves the best value of the mean of $\hat{f}(\mathbf{x})$, thus is chosen as the optimal design among the five candidates. Tables 6.3 and 6.4 provide the calculated values of three types of $M(\mathbf{x}_i, X)$ by Eqs. (6.28~6.30) for each \mathbf{x}_i in the two stages. The value of validation metric $M_D(\hat{U}, \mathbf{x}^*, X)$, which is equal to $M(\mathbf{x}_4, X)$, is also marked in the column of x_4 . It is noted that the values of all three types of $M_D(\hat{U}, \mathbf{x}^*, X)$ in stage one are larger in stage two, indicating larger confidence in differentiating design alternatives.

6.5 Summary

In this chapter, a design-driven validation approach is proposed, built upon the Bayesian prediction procedure presented in Chapter 4 that provides quantitative assessments of model uncertainty. Some decision validation metrics are proposed to provide probabilistic assessments of designer's confidence in making a specific design choice. Unlike most of the existing model validation works that focus on the assessment of model accuracy, model validation is viewed in this work as a process to improve designer's confidence in making a design choice using the improved predictive model, which is an augmented model based on the original computer model as well as the estimated bias function.

This work offers a new and improved way of viewing model validation by relating its definition to a specific design choice with a particular design objective. By providing direct estimations of the global impact of uncertainty sources on the confidence in a design decision, the approach overcomes the limitations of many existing model validation approaches. Our proposed decision validity metrics are generally applicable for both cases with either a discrete

or continuous set of design candidates, with the worst-case metric demonstrated to be the most appropriate. As has been illustrated, besides the model itself, the validation result highly depends on subjective inputs from designers, such as the construction of the design objective function, and the specification of tolerance and confidence level in identifying the indiffereniable region.

In this work, we treat model uncertainty separately from design variable/parameter uncertainty. The consideration of parameter uncertainty is embedded into the design objective formulation, such as the robust design objective as shown in one of the case studies, while the prediction uncertainty of a design objective is quantified with respect to only the model uncertainty. The way we separate model uncertainty from design variable/parameter uncertainty facilitates sampling in sequential experimentation, as its goal is to reduce model uncertainty. The topic of sequential experimentation will be further explored in Chapter 7.

Even though the proposed approach is demonstrated for a simplified one dimensional engineering design problem for ease of visualization, the same approach can be applied to problems with multidimensional design inputs and the interest is always to provide the probabilistic assessment on whether the design objective value of one particular design is better than others. Since the analytical derivation has been obtained for implementing the Bayesian approach, the proposed method can be easily extended to multidimensional problems.

Chapter 7. Objective Oriented Sequential Experimentation

Nomenclature

SLB	Statistical Lower Bounding
PSC	periodical switching criteria
DC	Design confidence
X^0	indifferentiable region
H	design tolerance
C_{X^0}	confidence level
\mathbf{x}^{mc}	most competing (MC) design
LF	Low Fidelity
HF	High Fidelity
Ω_d	intended design region
Ω_n	forbidden region

7.1 Introduction

Sequential experimentation is an important research issue in predictive modeling in engineering design because it aims for obtaining the most amount of information out of a limited number of simulations sampled sequentially, especially when simulations are computationally

expensive or physical experiments are resource taking. In Chapter 2, a broad review on sequential sampling strategies for computer experiments was made, together with a summary of advantages of sequential sampling strategies in various aspects of engineering design. Among the two categories of sequential sampling, the category of objective-oriented sequential sampling approaches shows advantages over the category of space-filling based sequential approaches for global metamodeling, because they are driven by the intended optimization objective in engineering design, and therefore are able to narrow the sampling space to the most promising design region in a more effective manner.

In this chapter, we present a new objective oriented sequential sampling approach (Section 7.2) for computer experiments, with a proposed periodical switching criterion which is shown to be effective in guiding the sequential sampling towards improving a design objective as well as reducing the interpolation uncertainty. A design confidence (DC) metric is proposed (Section 7.3) as the stopping criterion to facilitate design decision making against the interpolation uncertainty. In Section 7.4, we apply the proposed objective oriented sequential sampling approach to the *variable fidelity optimization* where both high-fidelity and low-fidelity simulations are integrated.

In Section 7.5, we study two examples of variable fidelity optimization problems to demonstrate the effectiveness of the proposed sequential sampling approach.

It should be noted that sequential sampling approaches used in computer simulation can be extended to sequential physical experiment designs. In Section 7.6 we describe a general framework that guides objective oriented sequential physical experimentation, considering the uncertainty of physical experimentation and restrictions on experimentation location.

Conclusion of this chapter will be made in Section 7.7.

7.2 A New Objective Oriented Sequential Sampling Approach

In this work, we examine the use of the Statistical Lower Bounding (SLB) criterion for choosing the new sample in each stage of a sequential sampling process by considering the “interpolation uncertainty” of a surrogate model (Jones 2001, Cox et al. 1997). The SBL criterion has the following form:

$$\text{Minimize } SLB(\mathbf{x}_{N+1}) \equiv \mu_{y^s}(\mathbf{x}_{N+1}) - k\sigma_{y^s}(\mathbf{x}_{N+1}), \quad (7.1)$$

where $\mu_{y^s}(\mathbf{x}_{N+1}) = \hat{y}^s(\mathbf{x}_{N+1})$, $\sigma_{y^s}(\mathbf{x}_{N+1}) = Var^{1/2}[y^s(\mathbf{x}_{N+1})]$, and k is a user-defined parameter. A larger k value implies the emphasis on reducing interpolation uncertainty or the need for global search. The SLB criterion is easier to control and interpret than the EI criterion. By assigning $k = 0$ and $k = +\infty$, respectively, we get two extreme values of the SLB criterion:

$$\text{Maximize } Var(\mathbf{x}_{N+1}) \equiv \sigma_{y^s}^2(\mathbf{x}_{N+1}) \text{ ('Max Var')}, \quad (7.2)$$

$$\text{Minimize } Mean(\mathbf{x}_{N+1}) \equiv \mu_{y^s}(\mathbf{x}_{N+1}) \text{ ('Min Mean')}. \quad (7.3)$$

‘Max Var’ focuses on the aspect of exploring regions with large interpolation uncertainty; ‘Min Mean’ focuses on the aspect of locating local optima. In the work of Sasena (2002), it was proposed to alternate the two criteria under a subjective guideline. In the method described by Sekishiro et al. (2006), two sampling points, one based on ‘Max Var’ and the other on ‘Min Mean’, are used at each stage. One possible drawback common to these strategies is that consecutive sampling points may pile up at extremes, causing ill-conditioning when calculating the inverse of the covariance matrix used in Gaussian process modeling.

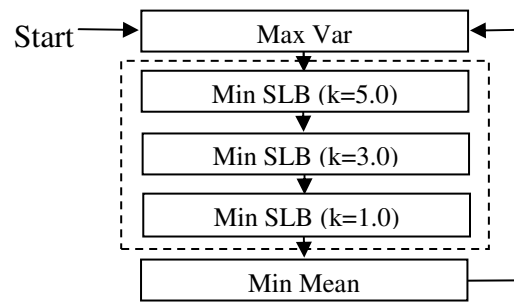


Figure 7.1 The proposed periodical switching criteria (PSC) strategy

To overcome these difficulties, we propose a *periodical switching criteria* (PSC) strategy as depicted in Figure 7.1. The sequence of the periodical alternation of criteria begins with an extreme global search ‘Max Var’, and ends up with an extreme local search ‘Min Mean’, while using in-between several compromising searches with different k values. By applying the compromise strategy with ‘Min SLB’ in the middle, sampling points are far less likely to cluster around the local minimum. Due to such cyclic pattern, the algorithm will always give the algorithm a chance to explore those less explored regions, even when a local minimum seems to have been settled on. This strategy is applied repeatedly throughout the whole sequential sampling procedure until certain stopping criterion (introduced in next section) is satisfied. Based on the research of Cox and John (1997), although an empirical selection of k value as 2 was used, it was acknowledged that the best k value is problem dependent. According to the tests, we found that three compromising searches with k values 5.0, 3.0, and 1.0 (as displayed in the dashed box in Figure 7.1) work quite well in the tested examples in this work. A more adaptive criterion is worthy of investigating in the future.

7.3 Stopping Criteria for Sequential Sampling

The *Design confidence* (DC), described in Chapter 5 is defined as a probabilistic measure (Hazelrigg 2003) of a chosen optimal design being better than other design choices with the consideration of model uncertainty. In the proposed sequential sampling approach, design confidence $DC(\mathbf{x}^*)$ is defined as the probability of whether an optimal design \mathbf{x}^* is the true optimum, in comparison with all designs outside the indiffereniable region X^0 , considering the interpolation uncertainty of using a surrogate model $y^s(\mathbf{x})$, i.e.,

$$DC(\mathbf{x}^*) = \min_{\mathbf{x} \in X^0} \{P[y^s(\mathbf{x}^*) < y^s(\mathbf{x})]\} = \min_{\mathbf{x} \in X^0} \{P[Z_{\mathbf{x}^*}(\mathbf{x}) > 0]\}, \quad (7.4)$$

where \mathbf{x}^* is identified by optimizing the predictor or the mean of $y^s(\mathbf{x})$, i.e.,

$$\mathbf{x}^* = \arg \min_{\mathbf{x}} \{\hat{y}^s(\mathbf{x})\}. \quad (7.5)$$

$Z_{\mathbf{x}^*}(\mathbf{x}) = y^s(\mathbf{x}) - y^s(\mathbf{x}^*)$ is assumed to follow the Gaussian distribution with mean

$$\mu_{Z_{\mathbf{x}^*}}(\mathbf{x}) = \hat{y}^s(\mathbf{x}) - \hat{y}^s(\mathbf{x}^*), \quad (7.6)$$

and variance

$$\sigma_{Z_{\mathbf{x}^*}}^2(\mathbf{x}) = \text{Var}[y^s(\mathbf{x})] + \text{Var}[y^s(\mathbf{x}^*)] - \text{Cov}[y^s(\mathbf{x}), y^s(\mathbf{x}^*)]. \quad (7.7)$$

Figure 3 shows an illustrative example of the uncertainty of $y^s(\mathbf{x})$ at three design points, namely, \mathbf{x}^* , \mathbf{x}_a , and \mathbf{x}_b , where \mathbf{x}^* is identified as the optimum based on the mean of prediction. Correspondingly, the mean and variance of $Z_{\mathbf{x}^*}(\mathbf{x})$ at the same three points are illustrated in Figure 4, where the probabilistic distribution of $Z_{\mathbf{x}^*}(\mathbf{x}_i)$ ($\mathbf{x}_i = \mathbf{x}^*$, \mathbf{x}_a , and \mathbf{x}_b) is calculated from Eqs. (14) and (15). Note that $Z_{\mathbf{x}^*}(\mathbf{x})$ has zero mean and zero variance at \mathbf{x}^* .

The assessment of DC in Eq. (12) involves the evaluation of probability that \mathbf{x}^* is better than the most competing design \mathbf{x} outside the indiffereniable region X^0 . The concept of indiffereniable region X^0 is introduced because, with model uncertainty, designs with performance values close to \mathbf{x}^* should be considered as equally good. More strictly, X^0 is defined as a region within which the design points are claimed indifferent to \mathbf{x}^* for a given design tolerance H with a confidence level $C_{x^0} = 1 - \alpha$ (e.g. $\alpha = 0.05$ or 0.10), as follows,

$$X^0 \equiv \left\{ \mathbf{x} \mid P[|Z_{\mathbf{x}^*}(\mathbf{x})| < H] > C_{x^0} \right\}. \tag{7.8}$$

It is worth emphasizing that the values of design tolerance H and confidence level C_{x^0} are specified based on designer's preference. Choosing a tolerance H expresses how close two design objective values can be deemed the same or indiffereniable.

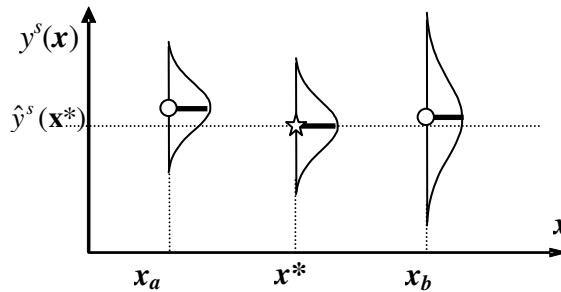


Figure 7.2 The uncertainty of $y^s(x)$ at x^* , x_a , and x_b

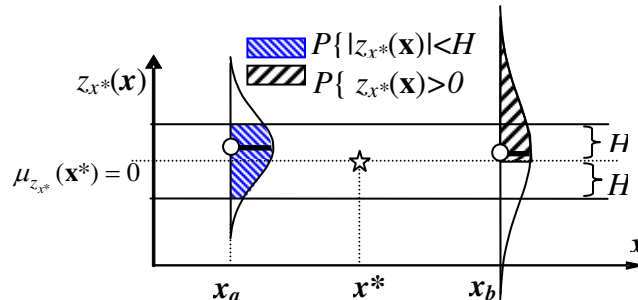


Figure 7.3 The uncertainty of $z_{\mathbf{x}^*}(\mathbf{x})$ at \mathbf{x}^* , \mathbf{x}_a , and \mathbf{x}_b

Note that X^0 may include not only the close neighborhood of \mathbf{x}^* , but also regions not adjacent to \mathbf{x}^* . The evaluation of Eq. (12) requires the search of the *most competing* (MC) design \mathbf{x}^{mc} w.r.t. the optimal design \mathbf{x}^* , though minimizing the probability P outside the indifferentiable region X^0 . The obtained \mathbf{x}^{mc} is then used to calculate the design confidence of \mathbf{x}^* through

$$DC(\mathbf{x}^*) = P[Z_{\mathbf{x}^*}(\mathbf{x}^{mc}) > 0]. \quad (7.9)$$

In the existing literature of global optimization, the commonly used stopping criteria are based on the convergence behavior in either design space of \mathbf{x} , or performance space of y (Gano et al. 2004, Sekishiro et al. 2006). Although generally applicable, none of them provide probabilistic measure regarding the validity of an optimal design considering model uncertainty. In this work, we view the sequential sampling as a process of reducing the interpolation uncertainty of surrogate models, as well as improving the confidence in accepting a design solution. We propose a stopping criterion based on the design confidence values of any two consecutive stages. If any two consecutive design confidences $DC(\mathbf{x}^*)$ meet (higher than) a desired confidence level (e.g., 90%, 95%) prescribed by designers, the sequential sampling process can then be terminated. Often times, due to the limited resources (time and cost, etc), designers have to determine whether the current best design is acceptable or not without additional simulation. The information of design confidence provides a base for designers to make such decisions.

7.4 Application of the Proposed Sequential Sampling Approach in Variable Fidelity

Optimization

7.4.1 Background of variable-fidelity optimization

Computational models of varying fidelity have been widely applied in various engineering communities. In a broad sense, variable-fidelity models can be represented by data-fitting approximations, variable-resolution models, variable-convergence models, or variable physical fidelity models (Alexandrov, et al. 2000). Descriptions of variable fidelity and other model management methods can be found in a number of publications (Alexandrov et al. 1999; Gano et al., 2004; Marduel et al., 2004; Rodriguez, et al., 2001). As shown in Figure 7.4, with the classical variable fidelity optimization strategy, both LF and HF models are used directly in optimization for response evaluations. Existing approaches tend to maximize the use of LF, cheaper models in iterative procedures to provide a descent direction through gradient evaluations with occasional, but systematic recourse to HF, more expensive models. Different forms of scaling functions have been proposed to approximate the HF model using LF analyses, e.g., the first-order multiplicative and additive corrections (Alexandrov, et al. 1999) and the Kriging based scaling function (Gano et al. 2004).

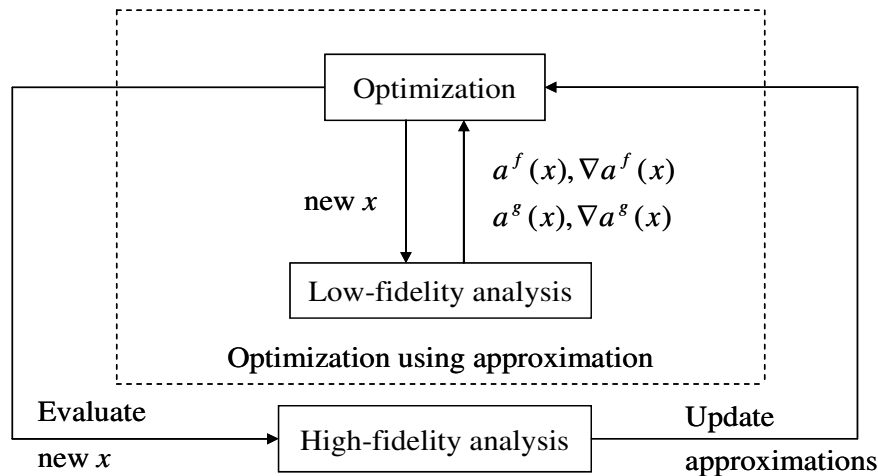


Figure 7.4 Classical Variable Fidelity Optimization (Alexandrov, et al. 1999)

Classical variable fidelity optimization emphasizes on convergence to a stationary point of the HF model, hence, the use of HF simulations is often excessive and even unaffordable. The trust-region approach (Gano et al., 2004; Rodriguez et al. 2001) has been used to expedite the convergence, however, the algorithm has the tendency to converge to local optima, while possibly overlooking the global optimum. Furthermore, one major limitation of the classical variable fidelity optimization methods is that they are not applicable for optimization under uncertainty, because it is not affordable to use directly the HF model for assessing the probabilistic behavior of a response.

7.4.2 Sequential sampling based variable-fidelity optimization approach

Based on the proposed objective oriented sequential sampling proposed in this work, a new variable-fidelity optimization framework can be depicted in Figure 7.5.

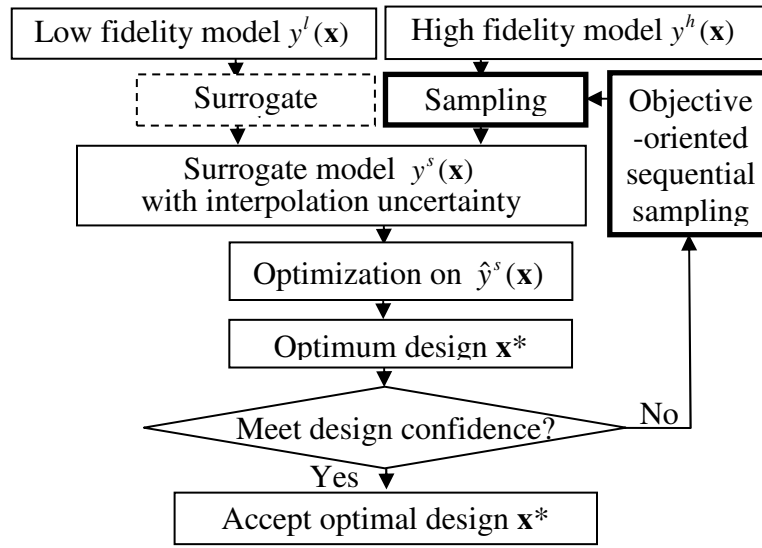


Figure 7.5 Objective Oriented Sequential Sampling Applied in Variable Fidelity

Optimization

As opposed to the classical variable fidelity optimization strategy shown in Figure 7.5, *none of the LF and HF models is directly invoked during optimization*. Instead, a *model fusion* technique is applied to combine information from both LF model $y^l(\mathbf{x})$ and HF simulations $y^h(\mathbf{x}_i)$ ($i=1, \dots, N^h$) to yield a surrogate model $y^s(\mathbf{x})$ (as a substitute for HF $y^h(\mathbf{x})$), over which optimization is performed. Details of constructing the surrogate model $y^s(\mathbf{x})$ with the proposed model fusion technique are elaborated in Chapter 4. The proposed model fusion approach follows a Bayesian modeling framework, in which the surrogate model is a combination of an augmented LF model with linear scaling plus a bias function that characterizes the remaining difference with the HF model. With the Bayesian approach, the uncertainty of $y^s(\mathbf{x})$ in predicting HF models can be quantified. As previously stated, such type of uncertainty is called the ‘interpolation uncertainty’ due to the lack of sufficient HF simulations. When a LF simulation is expensive, the surrogate of LF model (dashed line box in Figure 7.5) could be used to replace the

original LF model. Design optimization is performed using the predictor (or posterior mean) of the Bayesian surrogate model $y^s(\mathbf{x})$ obtained from model fusion. The design confidence (DC) of the newly identified optimum \mathbf{x}^* will then be assessed considering the interpolation uncertainty associated with $y^s(\mathbf{x})$. If the design confidence meets a satisfactory level, or when the computing resource has been exhausted, the sequential sampling process is terminated. Otherwise, an objective-oriented sequential sampling procedure will be applied to pick new sampling points of HF simulations. In the proposed framework, only one sampling point of HF simulation is added at each iteration or ‘stage’.

7.5 Case Study

In this section, we will go through two examples of variable fidelity optimization problems to illustrate the proposed objective oriented sequential experimentation approach.

7.5.1 Computer Experiment: One Dimensional Problem

We first look at a one dimensional problem, which was already used in Chapter 4. From Stages 1 to 5, additional 5 sampling points are sequentially collected following the PSC strategy we proposed in section 2.3. Using the Bayesian Gaussian process modeling approach described in Chapter 2, the posterior mean and the interpolation uncertainty (95% prediction interval (PI)) of $y^s(\mathbf{x})$ are shown in Figure 7.5, with all 5 sequential points annotated with the stage number besides. It is noted that although two local minimums exist in the HF model, only one of the 5 samples is used to explore the secondary local minimum region, the other four are all located around the global minimum. Therefore the created surrogate model is much more accurate in the

neighborhood of the global minimum than that of the secondary local minimum. In Stages 4 and 5, the sequential sampling points are very close to the global minimum. The sequential sampling process is objective-oriented, addressing both needs of global search and local search.

In Figure 7.5, points in the local region (0.215~0.253) surrounding \mathbf{x}^* ($=0.2330$) is identified as indifferentiable to \mathbf{x}^* with certain design tolerance H ($=0.023$) and confidence C_{x^0} ($=99\%$). The design point $\mathbf{x}=0.746$, shown with large interpolation uncertainty, is identified as the most competing point \mathbf{x}^{mc} (marked with triangle). The \mathbf{x}^{mc} point is considered as the most competing point to \mathbf{x}^* among all design points outside the indifferentiable region X^0 because its lower bound of the prediction interval is very close to the performance at \mathbf{x}^* .

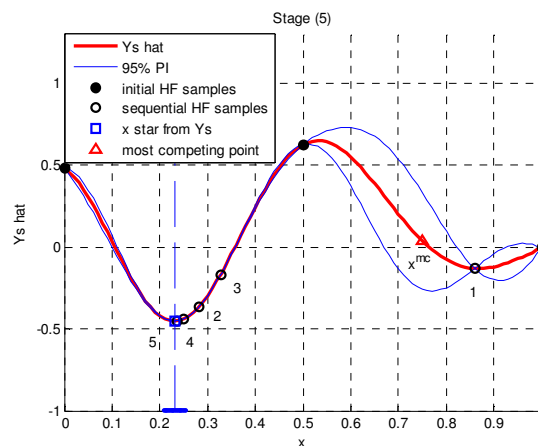


Figure 7.6 The plots of $\hat{y}^s(x)$ and the HF samples (Stage 5)

7.5.2 Computer Experiment: Two Dimensional Problem (the Modified Branin Function)

This example was also used in Chapter 4. The effectiveness of the proposed sequential approach is demonstrated through a modified Branin function. Optimizing the Branin function (Leary et al. 2004) is challenging because it has three global minima with exactly equal performance values. The problem has been studied in literature for various purposes. In this work

we modified the original Branin function by adding an additional small ‘tip’ term so that it has only one global minimum, while the other two become local minima but stay competing to the global one. The modified Branin function is used as the HF model, while we hypothetically construct the LF model (see in Appendix for mathematical details). The 3-D plots of the HF and the LF models are shown in Figure 7.7, and the contour plot of the HF model with the global optimal point indicated as \mathbf{x}^*_{HF} is shown in Figure 7.8, with the two local minima marked with * and the global minimum marked with a star. Note the ranges of \mathbf{x}_1 and \mathbf{x}_2 are normalized to 0~1.

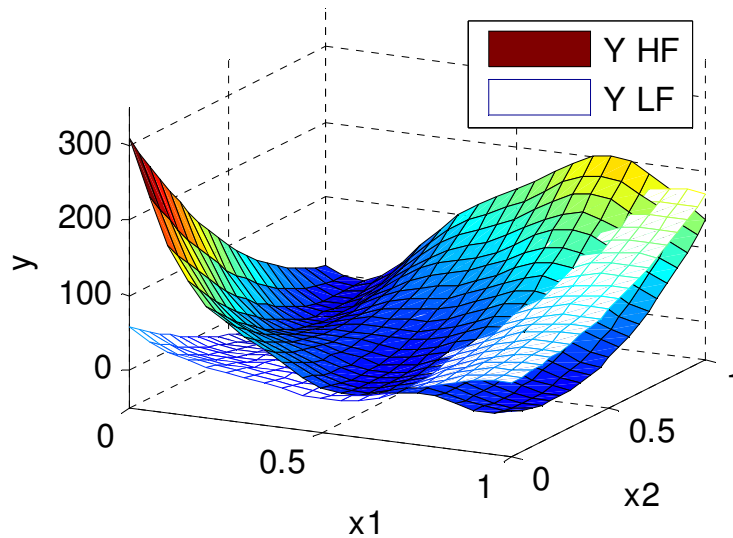


Figure 7.7 The 3-D plots of HF and LF models

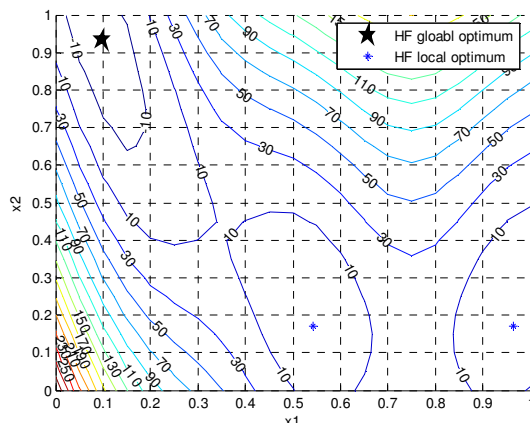


Figure 7.8 The contour plot of HF model marked with \mathbf{x}_{HF}^*

$$= [0.0912 \ 0.9325], y^h(\mathbf{x}_{HF}^*) = -19.142.$$

At the initial stage (Stage 0) (see Figure 7.9), only 5 sampling points are available which are generated with the Optimal Latin-Hypercube (OLH) algorithm (Jin et al. 2005). The contour plot of the obtained surrogate model at this stage is shown in Figure 7.9. It is clear that the optimal design ($\mathbf{x}^* = [0.6094, 0.3012]$, marked with a square) from the surrogate model is very different from the true optimal design ($\mathbf{x}_{HF}^* = [0.0970, 0.9344]$, marked with a star).

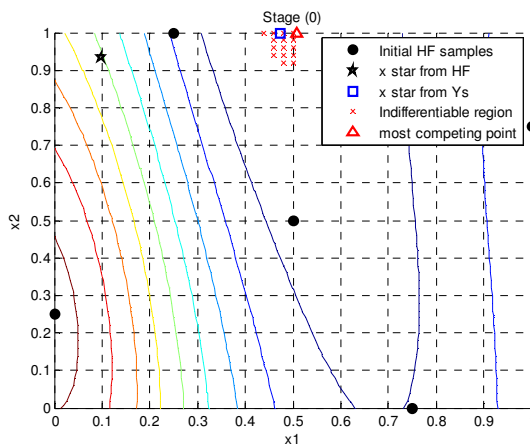


Figure 7.9 The plot of $\hat{y}^s(\mathbf{x})$ at Stage 0 (5 points) with $\mathbf{x}^* = [0.694, 0.001]$

In order to demonstrate the effectiveness of the proposed PSC strategy in the sequential sampling, we compare the result from using the EI criterion with that from the PSC strategy using the same amount of sampling data. The plots of the resulted surrogate models from EI and PSC at Stage 10 (i.e., after 10 sequential points are added) are shown in Figure 7.10 and Figure 7.11, respectively for comparison.

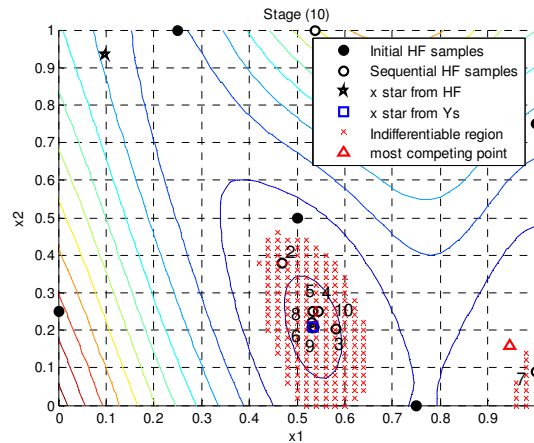


Figure 7.10 The plot of $\hat{y}^s(\mathbf{x})$ at Stage 10, with $\mathbf{x}^* = [0.5276, 0.2132]$: sequential sampling points generated by EI criterion

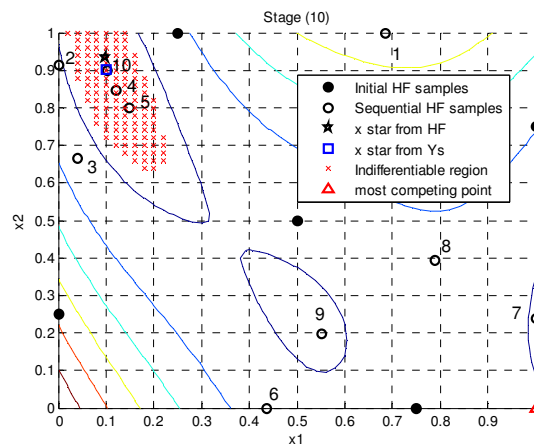


Figure 7.11 The plot of $\hat{y}^s(\mathbf{x})$ at Stage 10, with $\mathbf{x}^* = [0.1011, 0.9156]$: sequential sampling points generated by PSC strategy

In Figure 7.10, where the EI is applied, it is found that the optimal design \mathbf{x}^* (marked by square) is erroneously identified at a sub-optimal region. The number marked beside each sequential point indicates the stage they belong to. It is found that the sequential points via EI criterion (marked by solid circles) fails to discover the region sufficiently before it converges to the local minimum. Similar drawbacks of the EI criterion are also observed in Sasena (2002) and Sekishiro et al. (2006).

In Figure 7.11, where the PSC is applied, \mathbf{x}^* (marked by square) is identified at [0.1011, 0.9156], fairly close to \mathbf{x}^*_{HF} . From the locations of the sequential points (marked by solid circles), it is found that most of the sampling points are placed in the local region around the global minimum, while the rest of them are placed elsewhere to reduce the interpolation uncertainty of the surrogate model. It is found that at the early stages when the uncertainty of the surrogate model is large, the sampling procedure explores the model space more rather than focusing on any local promising region. After sufficient samples have been accumulated and the uncertainty of a surrogate model is reduced, more samples are used for local refinement of the global surrogate model in the region that is in favor of the design objective.

The most competing point (\mathbf{x}^{mc}) w.r.t. the optimal \mathbf{x}^* obtained from the surrogate model, is marked as a triangle in both plots in Figures 7.10 and 7.11, where the indiffereniable region X^0 is depicted by a collection of '+' markers. \mathbf{x}^{mc} and X^0 are determined based on the definitions given in the previous section. In essence, with the consideration of model uncertainty, the designs in the indiffereniable region are considered as equivalent to the optimal \mathbf{x}^* within certain tolerance. The design tolerance value H selected for this example is 12, which is about 3% of the range of y . Note that in Figure 7.10, since the local sub-optimal regions have similar y values, the indiffereniable region X^0 w.r.t. \mathbf{x}^* are located in both the neighborhood of \mathbf{x}^* and a

disjoint region centered around the other sub-optimal region extreme. In Figure 7.11, since \mathbf{x}^* is already correctly identified within the true global optimal region, X^0 is a continuous region surrounding \mathbf{x}^* . The most competing point \mathbf{x}^{mc} w.r.t. \mathbf{x}^* is marked with a triangle in both Figures 7.10 and 7.11. It is noted that \mathbf{x}^{mc} is always located outside of X^0 and represents the most competing design w.r.t. \mathbf{x}^* . The design confidence $DC(\mathbf{x}^*)$ achieved using the EI criterion and the proposed PSC strategy is 87.12% and 99.99%, respectively.

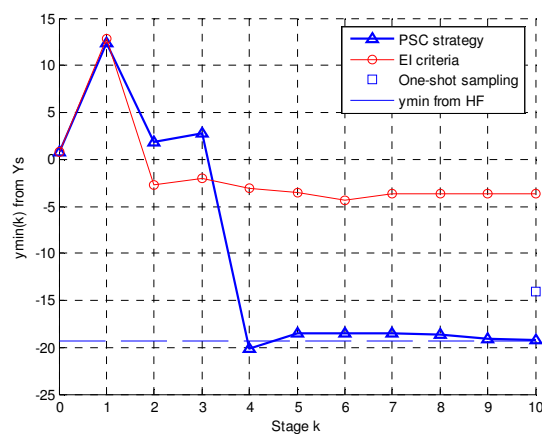


Figure 7.12 The comparison of the history plots of y^*

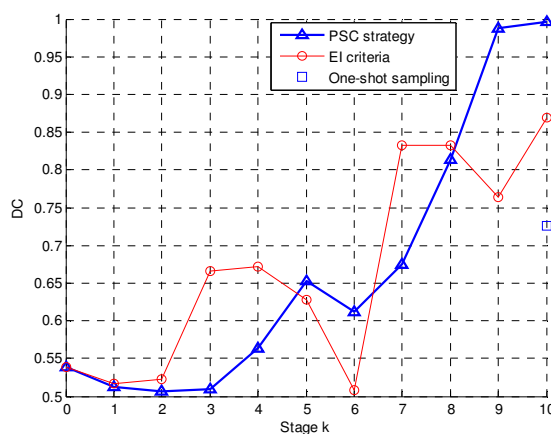


Figure 7.13 The comparison of the history plots of $DC(\mathbf{x}^*)$

$$(H = 12 \text{ (3\% of } y_{\text{range}}) \text{ and } C_{X^0} = 0.95)$$

Figures 7.12 and 7.13 show the history plots of the response value y^* and design confidence value $DC(\mathbf{x}^*)$ from the surrogate models at different stages. The results from using the EI criterion and the PSC strategy are compared in both Figures. It is observed that the DC level consistently increases with more sample points when using the PSC strategy which yields a high DC level (close to 100%) in Stages 9 and 10, much better than that (87.4%) from the EI with the same amount of sampling points. Besides, in terms of y^* , from the true y^*_{HF} indicated by the horizontal dashed line in Figure 7.13, it is observed that the PSC generates a more accurate value than the EI. These facts imply that the proposed PSC strategy holds much advantage over the EI approach.

From the history plot of y^* in Figure 7.13, it is found that y^* from both EI and PSC appears to be stabilized after a few stages. However, only examining the history of y^* is not sufficient in determining if the sequential process should be terminated, because the DC level could still be low like the case with using the EI method. This implies that the use of the design confidence (DC) as a termination criterion is more effective which offers more information for design decision making than simply examining the convergence behavior of y^* .

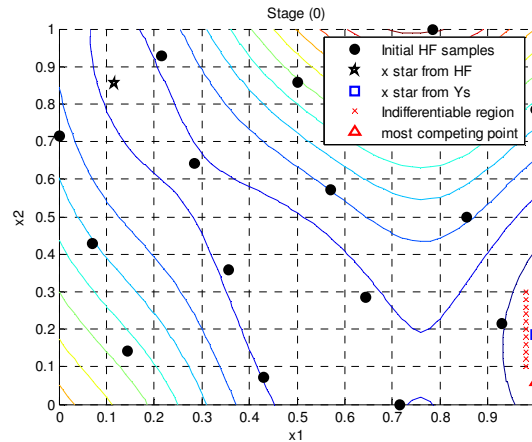


Figure 7.14 The plots of $\hat{y}^s(\mathbf{x})$ with $\mathbf{x}^* = [1.0000, 0.2103]$

(One-shot sampling of 5+10=15 points)

To demonstrate the advantage of using sequential sampling over a one-shot (single stage) sampling, we generate the same amount of data (5+10=15 points) using the space-filling criterion (OLH) as a comparison to the sequential sampling above. Figure 7.14 shows the settings of the evenly-spaced 15 points and the contour plot of the surrogate model $\hat{y}^s(\mathbf{x})$ built using the HF data. Even though this surrogate model might be more accurate in a global sense than those built based on sequential sampling, the model fails to capture the local details of the three local minimum regions, and the optimal design $\mathbf{x}^* = [1.000, 0.2103]$ (marked by square) is erroneously identified at the local minimum region far away from the true global minimum. It is found that $DC(\mathbf{x}^*)$ (=72.81%) achieved by the one-shot sampling is lower than the sequential sampling by both the EI criterion and the PSC strategy.

7.6 A Framework of Sequential Physical Experimentation

When combining the computer simulations with physical experiments for model updating, the accuracy of a predictive model is generally expected to be improved by adding more physical experiments, as well as more computer experiments (in the case that the computer model $\hat{y}^m(\mathbf{x})$ is approximated based on computer experiments). Since the cost of computer experiments is relatively much cheaper compared to that of physical experiments, the interest in this work is to develop appropriate strategies for guiding physical experiments.

Despite the difference between physical experiments and computer experiments, the strategy of sequential physical experimentation may share some similarities with that of sequential computer experimentation. In a design-driven model validation framework, the design of sequential physical experiments should be objective-oriented, instead of uniformly distributed. Three objectives for selecting the new experiment point(s) are identified in this work as follows:

Objective A, to improve the design objective;

Objective B, to improve the accuracy of a model and explore potential design space;

Objective C, to improve the confidence level of claiming the optimal solution

(measured by the proposed M_D metrics).

In the approach by Jones et al. (1998), the formulation of maximizing the Expected Improvement essentially embodies the objectives A and B. It should be noted that using Object A alone is not sufficient because the optimal design location is identified based on the predictive model with error and uncertainty. Object B is applied to select points in those regions with large prediction uncertainty to the accuracy of a predictive model, which potentially may lead to a better design solution. In Apley et al. (2005), the prediction interval plot is applied to narrow

down the potential design region for further sequential experiments, excluding an inferior design region with certain confidence. Similar to Jones' approach, the concept of inferior region implies the balance between Objectives A and B. Note that the two approaches are both under the computer experiment scenario.

It should be noted that, unlike computer experiments, the design of physical experiments has some restrictions on the location of experimentation, e.g., certain regions in a design space cannot be considered due to the physical restrictions or unaffordable cost associated with them. In summary, the question of the sequential physical experiments considered in this work is *where to conduct the next one site or group of physical experiment(s) subject to certain constraints towards simultaneously achieving the objectives A, B, and C*. Some strategies are proposed next. These strategies are intended to accommodate both scenarios, namely, 1) finite design alternatives, and 2) continuous design space.

Strategy A. Locate the Next Site for a Single Experiment

Unlike computer experiments, it is much more practical to sequentially add one experiment at a time due to the high cost of physical experiments. Although multiple sample points might be applicable in some cases, one could extend the single-point method to a multiple-point method by repeating the former.

To find the next one site of experiment, an optimization problem is defined as

$$\begin{aligned}
 & \textit{Find } \mathbf{x}_{N+1}, \\
 & \textit{Maximize } E_{y_{N+1}^e} [M_D | \mathbf{x}_{N+1}], \\
 & \textit{Subject to } \mathbf{x}_{N+1} \in \Omega_d,
 \end{aligned} \tag{7.10}$$

$$\mathbf{x}_{N+1} \notin \Omega_n .$$

where Ω_d denotes the intended (given) design region; Ω_n denotes the forbidden region(s) in which physical experiments are not allowed. The objective is to find the optimal location of the next experiment point \mathbf{x}_{N+1} , to maximize the confidence level (M_D) when the new experimental data $y^e(\mathbf{x}_{N+1})$ is included in the model. However, the future observation of $y^e(\mathbf{x}_{N+1})$ is never known unless the experiment has been done. $M_D | \mathbf{x}_{N+1}$ is uncertain as a result of the uncertainty of $\hat{y}^e(\mathbf{x}_{N+1})$. Expectation of $M_D | \mathbf{x}_{N+1}$ w.r.t. $\hat{y}^e(\mathbf{x}_{N+1})$, denoted as $E_{y_{N+1}^e} [M_D | \mathbf{x}_{N+1}]$, referred to as the ‘Expected M_D ’, is used as an objective in Eq. (7.10). Recall the basic model

$$y^e(\mathbf{x}) = y^r(\mathbf{x}) + \varepsilon(\mathbf{x}),$$

from which $y^e(\mathbf{x}_{N+1})$ could be predicted upon the predictive model $\hat{y}^r(\mathbf{x})$ plus an additional ε term representing the experiment error (Figure 7.15). The variance of ε [assumed as $\varepsilon \square NID(0, \sigma_\varepsilon^2)$] could be calculated by $\hat{\sigma}_\varepsilon^2 = \hat{\tau} \cdot \hat{\sigma}_\delta^2$. Therefore, assumed as following Gaussian,

$\hat{y}^e(\mathbf{x}_{N+1})$ is characterized by

$$\hat{y}^e(\mathbf{x}_{N+1}) \sim N\{E[y^r(\mathbf{x})], \text{Var}[y^r(\mathbf{x})] + \hat{\sigma}_\varepsilon^2\}.$$

Monte Carlo simulation can be applied to sample the distribution of $\hat{Y}^e(\mathbf{x}_{N+1})$ to evaluate the Expected M_D .

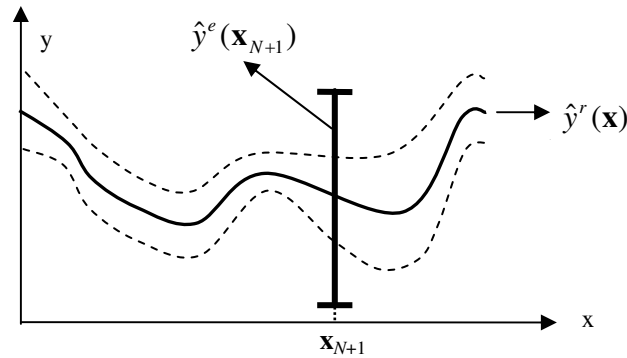


Figure 7.15 The distribution of $\hat{y}^r(\mathbf{x})$ and future experiment $\hat{y}^e(\mathbf{x}_{N+1})$

Since the physical experiment set $\{y^e(\mathbf{x}_i) | i=1, \dots, N\}$ (assuming $N \gg 1$) is augmented by adding a single new observation $y^e(\mathbf{x}_{N+1})$, it can be reasonably assumed that all the unknown parameters (i.e., $\phi_{m,k}$, $\phi_{\delta,k}$, and τ) underlying the Bayesian model will not change. Therefore there is no need to re-estimate all these parameters to include $y^e(\mathbf{x}_{N+1})$ into the Bayesian model in each iteration of the optimization.

One challenge for solving the above optimization lies in the high dimension, for which the search region for \mathbf{x}_{N+1} could be large. One feasible simplification could be to discretize the region by grid points or DOE techniques, or ruling out the inferior region, which is introduced next.

It is noted that the strategy proposed above is driven by the **Objective C** (and partially **Objective A**), because the objective function posed in Eq. (7.10) only considers the improvement of M_D . For discrete design space scenario, where only finite design alternatives are considered, there is no need to explore potential design region. In such scenario, the strategy is deemed sufficient for guiding the sequential experiment. However, for the scenario of continuous

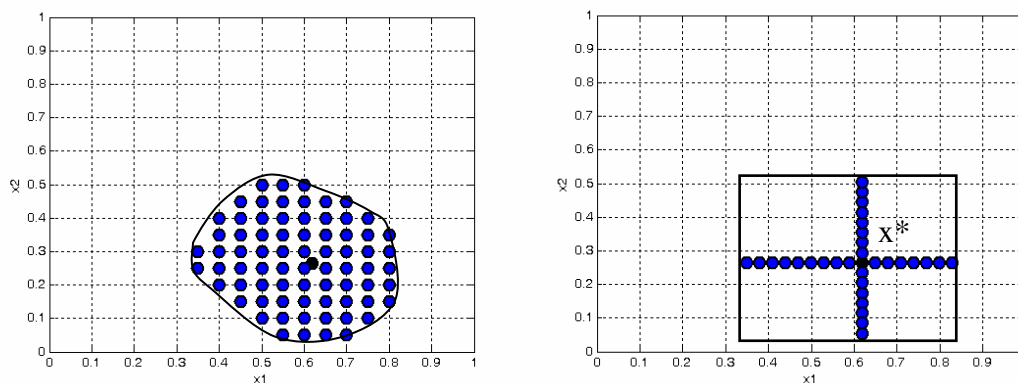
design space, **Objective B** needs to be considered as well. In such scenario, the strategy may not provide an effective guidance to explore potential design region. To solve this problem, strategies similar to Jones' need be considered together with the proposed strategy. Two possible ways are proposed in this work: 1) to apply different strategies towards different objectives in a hybrid or stepwise manner; 2) to formulate a multiobjective optimization problem, which incorporates the objectives A, B and C.

Strategy B. Region Ruling-Out

An indifferentiable *design region* w.r.t. optimal design \mathbf{x}^* can be conceptually be formulated as the collection of design \mathbf{x} such that

$$\Omega_{ind} = \left\{ \mathbf{x} \mid P\{\hat{U}(\mathbf{x}^*) > \hat{U}(\mathbf{x})\} < C \right\}, \quad (7.11)$$

where Ω_{ind} denotes the indifferentiable design region under certain desired confidence level represented by C . Two types of methods could be used to identify Ω_{ind} , namely, the space grid point method in Figure 7.16 (a), and the coordinate intervals method in Figure 7.16 (b). For the former method, the boundary could be represented using classical classification method, based on the binary training data (Hastie et al., 2001). For the latter method, the boundary is constructed as a hyper-rectangle.



(a) Space grid point method

(b) Coordinate intervals method

Figure 7.16 Region ruling-out strategy: identifying indifferentiable

region Ω_{ind} w.r.t. the optimal design x^*

The indifferentiable design region Ω_{ind} may suggest one way of guiding the sequential physical experiment design. Because one has at least 95% confidence to claim that the points outside Ω_{ind} is differentiated with the optimal design x^* , there is no need to add physical experiments outside Ω_{ind} , in other words, regions that exclude Ω_{ind} are ruled out. To add additional points to the identified region Ω_{ind} , certain criteria can be applied, such as the space-filling criterion.

Another application of the region ruling-out strategy could be to substitute the design region Ω_d for Ω_{ind} in the first constraint of the optimization problem defined by Eq. (7.10), thus the updated constraint is $\mathbf{x}_{N+1} \in \Omega_{ind}$. Such treatment facilitates the optimization, because the search region is largely reduced from the design region Ω_d to a smaller region Ω_{ind} .

7.7 Summary

In this chapter, we developed a new objective oriented sequential sampling approach for computer experiment, with a proposed periodical switching criteria which is shown to be effective in guiding the sequential sampling towards improving a design objective as well as reducing the interpolation uncertainty. A design confidence (DC) metric is proposed as the stopping criterion to facilitate design decision making against the interpolation uncertainty. As a demonstration of the proposed sequential sampling approach, we investigate the application of the method to variable fidelity optimization, which are further illustrated with two example problems.

For design optimization, an objective-oriented sequential sampling strategy is investigated. A periodical switching criterion (PSC) is employed to balance the search of optimum solution based on the current surrogate model and the exploration of regions with large interpolation uncertainty. Our empirical studies with the example problems show that this strategy is more effective compared to the expected improvement (EI) approach. We also propose to use design confidence (DC), a probabilistic measure of the confidence in employing the surrogate model for making a specific design choice, as the stopping criterion for the proposed framework. This proposed approach effectively facilitates decision making in engineering design, by taking into account the uncertainty associated with the use of surrogate models. Through a variable fidelity optimization example, we show that designers' preference has an impact on the decision of whether a solution can be accepted with sufficient confidence.

Based on the principles of our approach to sequential computer experiments, we also proposed a general framework that guides objective oriented sequential physical experimentation,

considering the uncertainty of physical experimentation and possible restrictions on experimentation settings.

Chapter 8. Conclusion

8.1 Contribution

The research presented in this dissertation represents efforts to develop methods, formulations, and solution strategies in metamodeling, uncertainty quantification, and model validation that are critical to the use of predictive models in engineering design. The overall contribution of this dissertation is the development of new approaches that facilitate the use of predictive models in engineering design to help designers make informed decisions while acknowledging uncertainties associated with the use of predictive models. The contributions are reflected in the following aspects:

(1) A new Kriging method with non-stationary covariance structure is developed. While most of the prior work in non-stationary covariance modeling has focused on low-dimensionality and is limited to physical experimental data, the proposed approach can be applied to computer experiments in high dimensionality. The proposed Kriging modeling not only captures the changing smoothness behavior of a response, but also provides more accurate qualifications of prediction uncertainty. Through testing multiple functions under different sampling situations, the robustness of the proposed non-stationary Kriging method was clearly demonstrated.

(2) A bias-correction approach that compensates the original computer model with a quantified bias function based on Bayesian analysis is investigated for updating a predictive model. This approach can be applicable to two scenarios, i.e., bias-correction of computer model against physical experiment data, and bias-correction of a low fidelity computer model against a high fidelity computer model. By using the Bayesian approach, the method offers much

flexibility as additional design knowledge and information can be easily incorporated through prior distributions, and also possesses advantages in engineering applications where it is too expensive to obtain experimental data. With the derived closed form posterior distribution of parameters, the approach is expected to be more accurate and economically sound compared to the conventional numerical approach to Bayesian analysis.

(3) A better understanding of the various model updating strategies is achieved by examining different model updating formulations, e.g., calibration and bias-correction, as well as different solution methods. Traditional approaches to calibration treat certain computer model parameters as fixed over the physical experiment, but unknown, and the objective is to infer values for the so-called calibration parameters that provide a better match between the physical and computer data. In many practical applications, however, certain computer model parameters vary from trial to trial over the physical experiment, in which case there is no single calibrated value for a parameter. We pay particular attention to this situation and develop a maximum likelihood estimation (MLE) approach for estimating the distributional properties of the randomly varying parameters which, in a sense, calibrates them to provide the best agreement between physical and computer observations.

(4) A design driven model validation procedure is developed for the purpose of using predictive models in engineering design. With the quantified uncertainty of Bayesian prediction models, decision validation metrics are developed to provide confidence measures in making a design choice for a given design objective. The implications of using such metrics are examined and the computational requirements are discussed for cases with either discrete or continuous design alternatives.

(5) A new objective oriented sequential sampling approach is developed for sampling computer experiments in the process of using predictive models for design optimization. The proposed approach employs a periodical switching criterion for balancing the needs of optimizing a design objective versus reducing interpolation uncertainty. A design confidence metric is proposed as the stopping criterion to facilitate design decision making. The approach is demonstrated through the variable fidelity optimization problem in which both high-fidelity and low-fidelity simulations are integrated.

8.2 Future work

In Chapter 3, we demonstrated that the proposed non-stationary covariance function employs as few hyperparameters as possible, the total size of hyperparameters could still be large when the problem dimension is high or larger degree of freedom (d.o.f.) is desired. In the tested example problems, density functions with smaller d.o.f. are used to limit the total number of hyperparameters. Further efforts are needed in identifying the critical dimension where larger d.o.f. is desired and developing more efficient optimization strategies for estimating the hyperparameters to allow for larger d.o.f.

One problem associated with the Bayesian approach for bias correction (Chapter 4) is the numerical difficulty in estimating the unknown parameters. In current implementations, the maximum likelihood estimation (MLE) and the cross validation method (CV) are the two major methods utilized for estimating these unknown parameters. It is found that in some cases these approaches fail to yield reasonable estimations. Therefore, future effort is needed to research approaches that could provide reasonable and stable estimations for parameters, especially by examining a few typical patterns of model error.

Another future research opportunity lied in the verification of the validity of uncertainty estimation by the Bayesian approach developed in this work against the conventional Kriging approach. Although it is argued in this work that, in lack of sampling data the proposed Bayesian approach can better quantify the parameter uncertainty of the underlying Gaussian process model and therefore better quantify the overall surrogate model uncertainty, how sensitive the posteriors is to the prior specification is worth further investigation.

In Chapter 5, we proposed a theoretically sound model updating approach that account for the experimental uncertainty with model parameter uncertainty through MLE estimation. However, due to the nature of the MLE method, its effectiveness and accuracy may be downgraded when the data amount is extremely small. In our test with the ‘low level’ data sufficiency for the thermal challenge problem, it is found that the bandwidth of the prediction uncertainty could be degenerated to fairly small values. To mitigate this problem, prior knowledge may be used to specify more conservative bounds of model updating parameters to prevent them from running into ‘absurd’ values. Future research is to investigate how we may quantify the impact of lack of data in the model updating formulation, by separating the uncertainty caused by lack of data with the experimental uncertainty. This will not only benefit the modeling accuracy in terms of the prediction and uncertainty quantification, but also will help decision support to resource allocation in planning physical experiments.

Another potential weakness of the MLE based model updating approach might be associated with the numerical instability when optimizing the likelihood function, especially when a complex model updating formulation that involves many parameters is considered. To mitigate this issue, sensitivity analysis could be performed prior to MLE optimization to leave out parameters that are insensitive to model output and the likelihood function.

In Chapter 6, we developed a design driven model validation framework together with decision validation metrics and procedures. Future research is planned for particularizing the proposed Bayesian procedure and statistical inferences for specific engineering applications where the natures of available experimental and computational data vary. Methods for incorporating designers' belief into Bayesian modeling based on prior knowledge and experience will be further examined. The role of decision validation metrics in engineering design will be further extended by introducing not only product design decisions but also decisions in allocating the resources for physical and computer experiments. This will require the incorporation of decision analysis techniques to study the tradeoffs involved in model refinement and uncertainty reduction.

In Chapter 7, a new objective oriented sequential sampling approach is developed. However, it is noted that the approach is limited to unconstrained optimization, in other words, the constraint functions need to be first converted into the objective function before this approach can be applied. On future research topic is to treat the constraint responses and the objective response separately in the sequentially sampling approach. In design under uncertainty, sampling strategies that treat design variables differently from noise variables are worth further investigation. In this work, we only provided a general framework of sequential physical experimentation without providing specific examples. Future research effort should be taken in developing practical examples to demonstrate the allocation of resources in sequential physical experimentation.

Physics-based predictive models are playing an increasingly important role in designing complex "engineered" systems. This research represents an attempt of providing the theoretical

framework and developing practical mathematical techniques for combining data from different sources and enhancing the confidence of using predictive models in engineering design.

References

- Abramowitz, M. and I. A. Stegun (1972). Handbook of mathematical functions (10th ed.). New York, Dover.
- Alexandrov, N. M., R. M. Lewis, et al. (1999). Optimization with variable-fidelity models applied to wing design. The 38th AIAA Aerospace Sciences Meeting and Exhibit, Reno, NV.
- Apley, D., J. Liu, et al. (2006). "Understanding the Effects of Model Uncertainty in Robust Design with Computer Experiments." ASME Journal of Mechanical Design 128(945): 745-958.
- Aughenbaugh, J. M. and J. W. Herrmann (2007). Updating uncertainty assessments: A comparison of statistical approaches. ASME International Design Engineering Technical Conferences & Computers and Information in Engineering Conference, Las Vegas, Nevada.
- Bandler, J. W., Q. S. Cheng, et al. (2004). "Space mapping: the state of the art." IEEE Transactions on Microwave Theory and Techniques 52(1): 337-361.
- Barthelemy, J. F. and R. T. Haftka (1993). "Approximation Concepts for Optimum Structural Design - A Review." Structural Optimization. 5: 129-144.
- Bates, D. M. and D. G. Watts (1988). Nonlinear Regression Analysis and Its Application. New York, Wiley.

- Bayarri, M. J., J. O. Berger, et al. (2002). A Framework for Validation of Computer Models, Foundations for Verification and Validation in 21st Century Workshop, Johns Hopkins University.
- Brandyberry, M. D. (2008). "Thermal Problem Solution Using A Surrogate Model Clustering Technique." *Computer Methods in Applied Mechanics and Engineering* 197(29–32): 2390–2407.
- Chen, C. H., J. Lin, et al. (2000). "Simulation Budget Allocation for Further Enhancing the Efficiency of Ordinal Optimization." *Discrete Event Dynamic Systems* 10(3): 251-270.
- Chen, W., L. Baghdasaryan, et al. (2004). "Model Validation via Uncertainty Propagation and Data Transformations." *AIAA Journal* 42(7): 1406-1415.
- Chen, W., Y. Xiong, et al. (2006). Some Metrics and a Bayesian Procedure for Validating Predictive Models in Engineering Design. ASME Design Technical Conference, Design Automation Conference, Philadelphia, PA.
- Cox, D. D. and S. John (1997). SDO: A Statistical Method for Global Optimization Multidisciplinary design optimization: state of the art, SIAM, Philadelphia.
- Dasgupta, T. (2007). Robust Parameter Design for Automatically Controlled Systems and Nanostructure Synthesis. School of Industrial and Systems Engineering, Georgia Institute of Technology.
- Dowding, K. J., M. Pilch, et al. (2008). "Formulation of the thermal problem." *Computer Methods in Applied Mechanics and Engineering* 197: 2385–2389.
- Easterling, R. G. and J. O. Berger (2002). Statistical Foundations for The Validation of Computer Models. presented at Computer Model Verification and Validation in the 21st Century Workshop. Johns Hopkins University.

- Farhang-Mehr, A. and S. Azarm (2005). "Bayesian Meta-Modeling of Engineering Design Simulations: A Sequential Approach with Adaptation to Irregularities in the Response Behavior." *International Journal for Numerical Methods in Engineering* 62(15): 2104-2126.
- Ferson, S., W. L. Oberkampf, et al. (2008). "Model Validation and Predictive Capability for the Thermal Challenge Problem." *Computer Methods in Applied Mechanics and Engineering* 197(29–32): 2408–2430.
- Gano, S. E., J. E. Renaud, et al. (2006). "Update strategies for kriging models used in variable fidelity optimization." *Structural and Multidisciplinary Optimization* 32(4): 287-298.
- Gano, S. E., J. E. Renaud, et al. (2004). Variable Fidelity Optimization Using a Kriging Based Scaling Function. 10th AIAA/ISSMO Multidisciplinary Analysis and Optimization Conference, Albany, New York.
- Ghanem, R. and A. Doostan (2006). "On the construction and analysis of stochastic models: Characterization and propagation of the errors associated with limited data." *Journal of Computational Physics*(217): 63-81.
- Haftka, R. T., E. P. Scott, et al. (1998). "Optimization and Experiments: A Survey." *Applied Mechanics Reviews* 51(7): 435-448.
- Hasselmann, T., K. Yap, et al. (2005). A case study in model improvement for vehicle crashworthiness simulation. 23rd International Modal Analysis Conference, Orlando, Florida.
- Hastie, T., R. Tibshirani, et al. (2001). *The Elements of Statistical Learning, Data Mining, Inference and Prediction*, Springer, New York.

- Hastings, W. K. (1970). "Monte Carlo sampling methods using Markov chains and their applications." *Biometrika* (57): 97–109.
- Hazelrigg, G. A. (2003). *Thoughts on Model Validation for Engineering Design*. ASME Design Technical Conference, Chicago, IL.
- Higdon, D., M. Kennedy, et al. (2004). "Combining Field Observations and Simulations for Calibration and Prediction." *SIAM Journal of Scientific Computing*(26): 448-466.
- Higdon, D., C. Nakhleh, et al. (2008). "A Bayesian Calibration Approach to the Thermal Problem." *Computer Methods in Applied Mechanics and Engineering* 197(29–32): 2431–2441.
- Hills, R. G. and K. J. Dowding (2008). "Multivariate Approach To The Thermal Challenge Problem." *Computer Methods in Applied Mechanics and Engineering* 197(29–32): 2442–2456.
- Hills, R. G., K. J. Dowding, et al. (2008). "Thermal challenge problem: Summary." *Computer Methods in Applied Mechanics and Engineering* 197: 2490–2495.
- Hills, R. G., M. Pilch, et al. (2008). "Model validation challenge problems: tasking document." *Computer Methods in Applied Mechanics and Engineering*.
- Hills, R. G., M. Pilch, et al. (2008). "Validation Challenge Workshop." *Computer Methods in Applied Mechanics and Engineering* 197: 2375–2380.
- Hoffman, R. M., A. Sudjianto, et al. (2003). *Robust Piston Design and Optimization Using Piston Secondary Motion Analysis*. SAE World Congress, Detroit, Michigan.
- Huang, D., Allen, T.T., Notz, W.I. , Miller, R.A. (2006). "Sequential Kriging Optimization Using Multiple-Fidelity Evaluations." *Structural and Multidisciplinary Optimization* 32(5): 369-382.

- Jin, R. (2005). Enhancements of Metamodeling Techniques on Engineering Design. Mechanical Engineering. Chicago, University of Illinois Ph.D.
- Jin, R., W. Chen, et al. (2002). On Sequential Sampling for Global Metamodeling in Engineering Design. The 2002 ASME IDETC Conferences, Montreal, Quebec, Canada.
- Jin, R., W. Chen, et al. (2005). "An Efficient Algorithm for Constructing Optimal Design of Computer Experiments." *Journal of Statistical Planning and Inference* 134(1): 268-287.
- Jones, D. R. (2001). "A Taxonomy of Global Optimization Methods Based on Response Surfaces." *Journal of Global Optimization* 21(4): 345-383.
- Jones, D. R., M. Schonlau, et al. (1998). "Efficient global optimization of expensive black-box functions." *Journal of Global Optimization* 13(4): 455-492.
- Kennedy, M. C. and A. O'Hagan (2001). "Bayesian calibration of computer models." *Journal of the Royal Statistical Society Series B*(63): 425-464.
- Leary, S. J., A. Bhaskar, et al. (2004). "A Derivative Based Surrogate Model for Approximating and Optimizing the Output of an Expensive Computer Simulation." *Journal of Global Optimization* 30: 39-58.
- Lee, S. H., H. S. Choi, et al. (2007). "Multi-Level Design of Experiments for Statistical Moment and Probability Calculation." *Structural and Multidisciplinary Optimization*.
- Leoni, N. and C. H. Amon (2000). "Bayesian Surrogates for Integrating Numerical, Analytical, and Experimental Data: Application to Inverse Heat Transfer in Wearable Computers." *IEEE Transactions On Components And Packaging Technologies* 23(1): 23-32.
- Li, R. and A. Sudjianto (2003). Analysis of Computer Experiments Using Penalized Likelihood Gaussian Kriging Model. ASME International DETC & CIE, Chicago, IL.

- Lin, Y., F. Mistree, et al. (2004). A Sequential Exploratory Experimental Design Method: Development of Appropriate Empirical Models in Design. ASME 2004 Design Engineering Technical Conferences and Computers and Information in Engineering Conference, Salt Lake City, Utah.
- Lindgren, L.-E., H. Alberg, et al. (2003). Constitutive modelling and parameter optimization. 7th International Conference on Computational Plasticity, Barcelona, Spain, Barcelona.
- Liu, F., M. J. Bayarri, et al. (2008). "A Bayesian Analysis of the Thermal Challenge Problem." *Computer Methods in Applied Mechanics and Engineering* 197(29–32): 2457–2466.
- Liu, W. K., E. G. Karpov, et al. (2005). *Nano-Mechanics and Materials: Theory, Multiscale Methods and Applications*, Wiley, New York.
- Loeppky, L., J. Bingham, et al. (2006). "Computer Model Calibration or Tuning in Practice." Submitted to *Technometrics*.
- Mahadevan, S. and R. Rebba (2005). "Validation of Reliability Computational Models using Bayes Networks." *Reliability Engineering and System Safety*(87): 223-232.
- Martin, J. D. and T. W. Simpson (2002). Use of Adaptive Metamodeling for Design Optimization. 9th AIAA/ISSMO Symposium on Multidisciplinary Analysis and Optimization, Atlanta, GA.
- Martin, J. D. and T. W. Simpson (2004). A Monte Carlo Simulation of the Kriging Model.
- McFarland, J. and S. Mahadevan (2008). "Multivariate Significance Testing and Model Calibration under Uncertainty." *Computer Methods in Applied Mechanics and Engineering* 197: 2467–2479.

- McFarland, J. M., S. Mahadevan, et al. (2007). Calibration and Uncertainty Analysis for Expensive Computer Simulations with Multivariate Output. The Computer Science Research Institute at Sandia National Laboratories.
- McFarland, J. M., S. Mahadevan, et al. (2007). Bayesian Calibration of the QASPR Simulation. 48th AIAA/ASME/ASCE/AHS/ASC Structures, Structural Dynamics, and Materials Conference, Honolulu, Hawaii.
- McFarland, J. M. and L. P. Swiler (2005). Validation of the Thermal Challenge Problem Using Bayesian Belief Networks, Sandia National Laboratories.
- Mockus, J., V. Tiesis, et al. (1978). "The application of Bayesian Methods for Seeking the Extremum." *Towards Global Optimisation 2*: 117-129.
- Nocedal, J. and S. J. Wright (1999). *Numerical Optimization*, Springer Verlag.
- NSF (2006). *Revolutionizing Engineering Science through Simulation*, National Science Foundation.
- Oberkampf, W. and M. Barone (2006). Measures of Agreement between Computation and Experiment: Validation Metrics. *Journal of Computational Physics*, 217(1): 5-36.
- Oberkampf, W. L., T. G. Trucano, et al. (2003). *Verification, Validation, and Predictive Capability in Computational Engineering and Physics*, Sandia National Laboratories.
- Oberkampf, W.L., Trucano, T.G. and Hirsch, C (2004). *Verification, Validation, and Predictive Capability in Computational Engineering and Physics*. . *Applied Mechanics Reviews*, 57(5): 345-384.
- Panchal, J. H., H.-J. Choi, et al. (2005). A Strategy for Simulation-Based Design of Multiscale, Multi-Functional Products and Associated Design Processes. *ASME 2005 International*

- Design Engineering Technical Conferences & Computers and Information in Engineering Conference, Long Beach, CA.
- Qian, Z., C. C. Seepersad, et al. (2006). "Building Surrogate Models Based on Detailed and Approximate Simulations." *Journal of Mechanical Design* 128: 668.
- Qian, Z. and C. F. J. Wu (2005). Bayesian Hierarchical Modeling for Integrating Low-Accuracy and High Accuracy Experiments. Twelfth Annual International Conference on Statistics, Combinatorics, Mathematics and Applications, Auburn, AL.
- Qian, Z. and C. F. J. Wu (2006). "Bayesian Hierarchical Modeling for Integrating Low-accuracy and High-accuracy Experiments." tentatively accepted by *Technometrics*.
- Rasmussen C. E., Williams, C.K.I.(2006), *Gaussian Processes for Machine Learning*, MIT Press,. ISBN 0-262-18253-X.
- Rai, R. and M. Campbell (2008). "Q2S2: A New Methodology for Merging Quantitative and Qualitative Information in Experimental Design." *Journal of Mechanical Design* 130(3): 031103-1 - 031103-12.
- Rebba, R. and S. Mahadevan (2006). Probabilistic Assessment of CAE Models. SAE World, Congress, Detroit, MI.
- Rodriguez, J. F., V. M. Pérez, et al. (2001). "Sequential Approximate Optimization Using Variable Fidelity Response Surface Approximations." *Structural and Multidisciplinary Optimization* 22: 24-34.
- Romero, D. A., C. H. Amon, et al. (2006). On Adaptive Sampling for Surrogate Models in Simulation-based Design and Optimization. ASME 2006 International Design Engineering Technical Conferences and Computers and Information in Engineering Conference, Philadelphia, PA.

- Romero, V. J. (2007). A Paradigm of Model Validation and Validated Models for Best-Estimate-Plus-Uncertainty Predictions in Systems Engineering. Soc. Automotive Engineers 2007 World Congress, Detroit, Michigan.
- Romero, V. J. (2007). Validated Model? Not So Fast. The Need for Model “Conditioning” as an Essential Addendum to Model Validation. 48th AIAA/ASME/ASCE/AHS/ASC Structures, Structural Dynamics, and Materials Conference, Honolulu, Hawaii.
- Rutherford, B. M. (2008). "Computational Modeling Issues and Methods for The 'Regulatory Problem' in Engineering - Solution to The Thermal Problem." *Computer Methods in Applied Mechanics and Engineering* 197(29–32): 2480–2489.
- Sacks, J., W. J. Welch, et al. (1989). "Design and Analysis of Computer Experiments." *Statistical Science* 4(4): 409-423.
- Sacks, J., W. J. Welch, et al. (1989). "Design and analysis of computer experiments." *Statistical Science*(4): 409–423.
- Santner TJ, Williams BJ, Notz WI. (2003) *The Design and Analysis of Computer Experiments*. Springer: New York,
- Sasena, M. J. (2002). Flexibility and Efficiency Enhancements for Constrained Global Design Optimization with Kriging Approximations. Mechanical Engineering, University of Michigan.
- Seber, G. A. F. and C. J. Wild (1989). *Nonlinear Regression*. New York, John Wiley and Sons.
- Sekishiro, M., G. Venter, et al. (2006). Combined Kriging and Gradient-Based Optimization Method. 11th AIAA/ISSMO Multidisciplinary Analysis and Optimization Conference, Portsmouth, Virginia.

- Smith, R. L. and Z. Zhu (2004). "Asymptotic Theory for Kriging with Estimated Parameters and Its Application to Network Design." Preliminary version, available from <http://www.stat.unc.edu/postscript/rs/supp5.pdf>.
- Stein, M. L. (1999). *Interpolation of Spatial Data: Some Theory of Kriging*. New York, Springer Verlag.
- Tamhane, A. C. and D. D. Dunlop (2000). *Statistics and Data Analysis: From Elementary to Intermediate*, Prentice Hall.
- Trucano, T. G., L. P. Swilera, et al. (2006). "Calibration, validation, and sensitivity analysis: What's what." *Reliability Engineering and System Safety*(91): 1331–1357.
- Turner, C. J., M. I. Campbell, et al. (2003). Generic sequential sampling for meta-model approximations. ASME 2003 Design Engineering Technical Conferences and Computers and Information in Engineering Conference, Chicago, Illinois.
- Wang, S., W. Chen, et al. (2008). "Bayesian Validation of Computer Models." resubmitted to *Technometrics*.

Appendix

Appendix A. Example and Tested Functions used in Non-stationary Kriging methods

(Chapter 3)

Function 1

$$f(x_1, x_2) = \sin(30(x-0.9)^4) \cos(2(x-0.9)) + (x-0.9)/2 \quad x_1, x_2 \in [0,1] \quad (\text{A1})$$

Function 2 ('Mystery Function', Sasena, 2002)

$$f(x_1, x_2) = 2 + 0.01(x_2 - x_1^2)^2 + (1 - x_1) + 2(2 - x_2)^2 + 7 \sin(0.5x_1) \sin(0.7x_1x_2) \quad x_1, x_2 \in [0,1] \quad (\text{A2})$$

Function 3 (Paciorek, 2003)

$$f(x_1, x_2) = \sin(1/(x_1 * x_2)) \quad x_1, x_2 \in [0.3,1] \quad (\text{A3})$$

Function 4

$$f(x_1, x_2) = x_1 \exp(-x_1^2 - x_2^2) \quad x_1, x_2 \in [-2.5, 2.5] \quad (\text{A4})$$

Function 5 (Jin, et al., 2002)

$$f(x_1, x_2) = \cos(6(x_1 - 0.5)) + 3.1|x_1 - 0.7| + 2(x_1 - 0.5) + 7 \sin(1/(|x_1 - 0.5| + 0.31)) + 0.5x_2 \quad x_1, x_2 \in [0,1] \quad (\text{A5})$$

Function 6

$$f(x_1, x_2) = \cos(5(x_1 - 0.5)) + 3.1|x_2 - 0.7| + 2(x_1 - 0.5) + 7 \sin(1/(|0.5x_2 + 0.31|)) \quad x_1, x_2 \in [0,1] \quad (\text{A6})$$

Function 7 (Paciorek, 2003)

$$f(x_1, x_2) = 1.9(1.35 + \exp(x_1) \sin(13(x_1 - 0.6)^2) \exp(-x_2) \sin(7x_2)) \quad x_1, x_2 \in [0,1] \quad (\text{A7})$$

Function 8 ('Six-hump Function', Sasena, 2002)

$$y = (4 - 2.1x_1^2 + x_1^4/3)x_1^2 + x_1x_2 + (-1 + 4x_2^2)x_2^2 \quad x_1 \in [-2, 2] \quad x_2 \in [-1, 1] \quad (\text{A8})$$

Function 9 ('Branin Function', Jin et al, 2002)

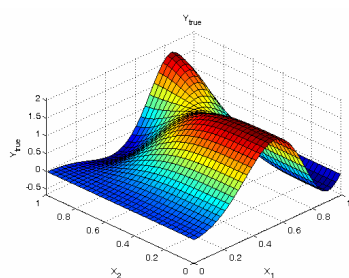
$$y = (x_2 - 5.1x_1^2 / (4\pi^2) + 5x_1 / \pi - 6)^2 + 10(1 - 1/(8\pi)) \cos(x_1) + 10 \quad x_1 \in [-5, 10] \quad x_2 \in [0, 15] \quad (\text{A9})$$

Function 10 ('Goldstein-Price Function', Jin et al, 2002)

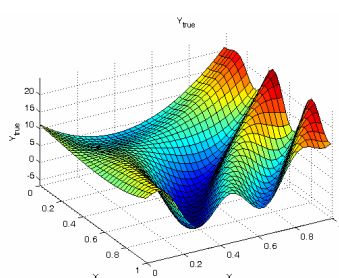
$$y = [1 + (x_1 + x_2 + 1)^2(19 - 14x_1 + 3x_1^2 - 14x_2 + 6x_1x_2 + 3x_2^2)] \cdot [30 + (2x_1 - 3x_2)^2(18 - 32x_1 + 12x_1^2 + 48x_2 - 36x_1x_2 + 27x_2^2)] \quad x_1, x_2 \in [-2, 2] \quad (\text{A10})$$

Function 11

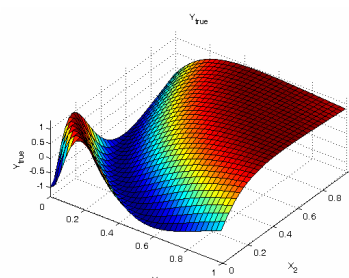
$$f(x) = \sin(30(x - 0.9)^4) \cos(2(x - 0.9)) + (x - 0.9)/2 \quad x \in [0, 1] \quad (\text{A11})$$



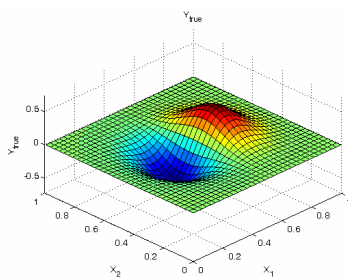
(a) Function 1



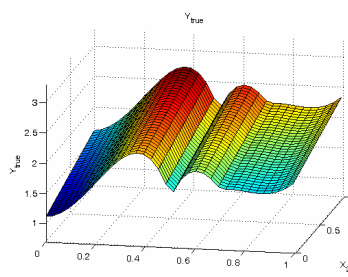
(b) Function 2



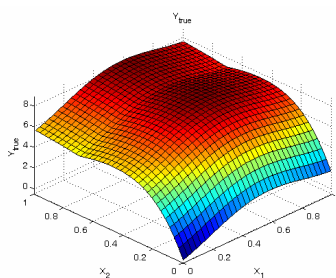
(c) Function 3



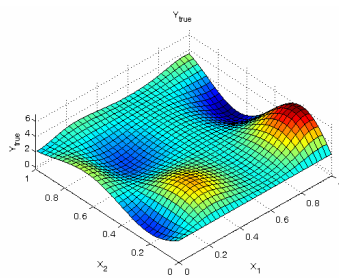
(d) Function 4



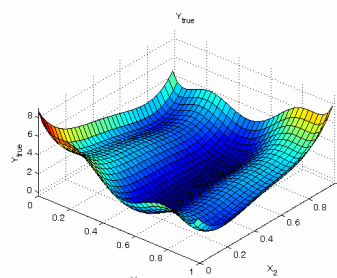
(e) Function 5



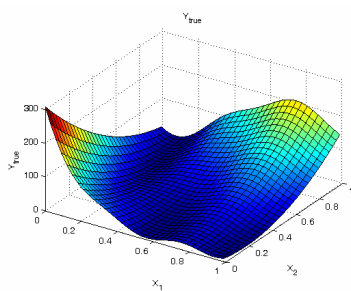
(f) Function 6



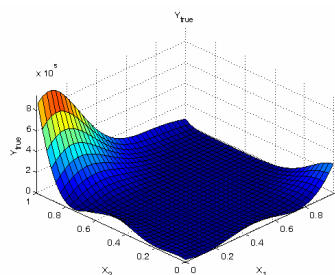
(g) Function 7



(h) Function 8



(i) Function 9



(j) Function 10

Figure A1 The 3-D plots of Function 1 ~ Function 10

(a~e: there are obvious non-stationary behavior;

f~j: there are no obvious non-stationary behavior)

Appendix B. Derivations of Eqs. (4.7-4.13) (Chapter 4, see also in Wang et al. 2008)

(1) The Posteriors of β_δ and σ_δ^2

The posteriors of β_δ and σ_δ^2 are

$$\beta_\delta | \mathbf{y}^e, \mathbf{y}^m, \theta_{-(\beta_\delta)} = \beta_\delta | \mathbf{y}^e, \mathbf{y}_{n_e}^m, \sigma_\delta^2, \phi_\delta, \sigma_\varepsilon^2 \propto N(\mathbf{A}_\delta \mathbf{v}_\delta, \sigma_\delta^2 \mathbf{A}_\delta)$$

and

$$\begin{aligned} \sigma_\delta^2 | \mathbf{y}^e, \mathbf{y}^m, \theta_{-(\beta_\delta, \sigma_\delta^2)} &= \sigma_\delta^2 | \mathbf{y}^e, \mathbf{y}_{n_e}^m, \phi_\delta, \tau \\ &\propto IG\left(\alpha_\delta + \frac{n_e}{2}, \gamma_\delta + \frac{1}{2} \left[(\mathbf{y}^e - \mathbf{y}_{n_e}^m)^T (\mathbf{R}_\delta + \tau \mathbf{I}_{n_e})^{-1} (\mathbf{y}^e - \mathbf{y}_{n_e}^m) + \mathbf{b}_\delta \mathbf{V}_\delta^{-1} \mathbf{b}_\delta - \mathbf{v}_\delta^T \mathbf{A}_\delta \mathbf{v}_\delta \right] \right), \end{aligned}$$

where

$$\begin{aligned} \mathbf{A}_\delta^{-1} &= \mathbf{F}_\delta^T (\mathbf{R}_\delta + \tau \mathbf{I}_{n_e})^{-1} \mathbf{F}_\delta + \mathbf{V}_\delta^{-1}, \\ \mathbf{v}_\delta &= \mathbf{F}_\delta^T (\mathbf{R}_\delta + \tau \mathbf{I}_{n_e})^{-1} (\mathbf{y}^e - \mathbf{y}_{n_e}^m) + \mathbf{V}_\delta^{-1} \mathbf{b}_\delta, \\ \tau &= \sigma_\varepsilon^2 / \sigma_\delta^2. \end{aligned}$$

and \mathbf{I}_{n_e} is an $n_e \times n_e$ identity matrix.

(2) The posterior of $\delta(\mathbf{x})$

It can be shown that

$$\delta(\mathbf{x}) | \mathbf{y}^e, \mathbf{y}^m, \theta$$

$$\propto N(\mathbf{f}_\delta^T(\mathbf{x}) \beta_\delta + \mathbf{r}_\delta^T(\mathbf{x}) (\mathbf{R}_\delta + \tau \mathbf{I}_{n_e})^{-1} (\mathbf{y}^e - \mathbf{y}_{n_e}^m - \mathbf{F}_\delta \beta_\delta), \sigma_\delta^2 \left[1 - \mathbf{r}_\delta^T(\mathbf{x}) (\mathbf{R}_\delta + \tau \mathbf{I}_{n_e})^{-1} \mathbf{r}_\delta(\mathbf{x}) \right]),$$

and the posterior of $\delta(\mathbf{x})$ given ϕ_δ and τ is

$$\begin{aligned} p(\delta(\mathbf{x}) | \mathbf{y}^e, \mathbf{y}^m, \phi_\delta, \tau) \\ = \iint_{\beta_\delta, \sigma_\delta^2} p(\delta(\mathbf{x}) | \mathbf{y}^e, \mathbf{y}^m, \theta) \cdot p(\beta_\delta | \mathbf{y}^e, \mathbf{y}_{n_e}^m, \sigma_\delta^2, \phi_\delta, \tau) \cdot p(\sigma_\delta^2 | \mathbf{y}^e, \mathbf{y}_{n_e}^m, \phi_\delta, \tau) d\beta_\delta d\sigma_\delta^2 \end{aligned}$$

where

$$p(\delta(\mathbf{x}) | \cdot) \propto (\sigma_\delta^2)^{-\frac{1}{2}} \cdot \exp \left\{ -\frac{\left[\delta(\mathbf{x}) - \mathbf{r}_\delta^T(\mathbf{x}) \mathbf{B} (\mathbf{y}^e - \mathbf{y}_{n_e}^m) - \mathbf{h}^T \beta_\delta \right]^2}{2\sigma_\delta^2 (1 - \mathbf{r}_\delta^T(\mathbf{x}) \mathbf{B} \mathbf{r}_\delta(\mathbf{x}))} \right\},$$

$$p(\beta_\delta | \cdot) \propto (\sigma_\delta^2)^{-\frac{p+1}{2}} \cdot \exp \left\{ -\frac{(\beta_\delta - \mathbf{A}_\delta \mathbf{v}_\delta)^T \mathbf{A}_\delta^{-1} (\beta_\delta - \mathbf{A}_\delta \mathbf{v}_\delta)}{2\sigma_\delta^2} \right\},$$

$$p(\sigma_\delta^2 | \cdot) \propto (\sigma_\delta^2)^{-\alpha_\delta - \frac{n_e}{2} - 1} \cdot \exp \left\{ -\frac{\gamma_\delta + \frac{1}{2} \left[(\mathbf{y}^e - \mathbf{y}_{n_e}^m)^T \mathbf{B} (\mathbf{y}^e - \mathbf{y}_{n_e}^m) + \mathbf{b}_\delta \mathbf{V}_\delta^{-1} \mathbf{b}_\delta - \mathbf{v}_\delta^T \mathbf{A}_\delta \mathbf{v}_\delta \right]}{\sigma_\delta^2} \right\},$$

where $\mathbf{B} = (\mathbf{R}_\delta + \tau \mathbf{I}_{n_e})^{-1}$, and $\mathbf{h} = \mathbf{f}_\delta(\mathbf{x}) - \mathbf{F}_\delta^T \mathbf{B} \mathbf{r}_\delta(\mathbf{x})$. Collecting all terms involving β_δ together gives

$$\exp\left\{-\frac{1}{2\sigma_\delta^2}[\beta_\delta^T \mathbf{A}^{-1} \beta_\delta + \mathbf{v}^T \beta_\delta]\right\},$$

where

$$\mathbf{A}^{-1} = \mathbf{A}_\delta^{-1} + \frac{\mathbf{h}\mathbf{h}^T}{1 - \mathbf{r}_\delta^T(\mathbf{x})\mathbf{B}\mathbf{r}_\delta(\mathbf{x})},$$

$$\mathbf{v} = \mathbf{v}_\delta + \frac{\delta(\mathbf{x}) - \mathbf{r}_\delta^T(\mathbf{x})\mathbf{B}(\mathbf{y}^e - \mathbf{y}_{n_e}^m)}{1 - \mathbf{r}_\delta^T(\mathbf{x})\mathbf{B}\mathbf{r}_\delta(\mathbf{x})} \cdot \mathbf{h}.$$

Hence,

$$\int_{\beta_\delta} \exp\left\{-\frac{1}{2\sigma_\delta^2}[\beta_\delta^T \mathbf{A}^{-1} \beta_\delta + \mathbf{v}^T \beta_\delta]\right\} d\beta_\delta \propto (\sigma_\delta^2)^{\frac{p+1}{2}} \cdot \exp\left\{\frac{\mathbf{v}^T \mathbf{A} \mathbf{v}}{2\sigma_\delta^2}\right\}.$$

Collecting all terms involving σ_δ^2 gives

$$(\sigma_\delta^2)^{-\frac{1}{2} - \alpha_\delta - \frac{n_e}{2} - 1} \cdot \exp\left\{-\frac{\gamma}{\sigma_\delta^2}\right\},$$

where

$$\gamma = \gamma_\delta + \frac{(\mathbf{y}^e - \mathbf{y}_{n_e}^m)^T \mathbf{B}(\mathbf{y}^e - \mathbf{y}_{n_e}^m) + \mathbf{b}_\delta \mathbf{V}_\delta^{-1} \mathbf{b}_\delta}{2} + \frac{[\delta(\mathbf{x}) - \mathbf{r}_\delta^T(\mathbf{x})\mathbf{B}(\mathbf{y}^e - \mathbf{y}_{n_e}^m)]^2}{2(1 - \mathbf{r}_\delta^T(\mathbf{x})\mathbf{B}\mathbf{r}_\delta(\mathbf{x}))} - \frac{\mathbf{v}^T \mathbf{A} \mathbf{v}}{2}.$$

Performing the integration over σ_δ^2 yields

$$\int_{\sigma_\delta^2} (\sigma_\delta^2)^{-\frac{1}{2} - \alpha_\delta - \frac{n_e}{2} - 1} \exp\left(-\frac{\gamma}{\sigma_\delta^2}\right) d\sigma_\delta^2 \propto \gamma^{-\frac{1+2\alpha_\delta+n_e}{2}}.$$

Therefore,

$$p(\delta(\mathbf{x}) | \mathbf{y}^e, \mathbf{y}^m) \propto \gamma^{-\frac{1+2\alpha_\delta+n_e}{2}}.$$

If we can write γ in the form of

$$\gamma = C \cdot \left(1 + \frac{1}{2\alpha_\delta + n_e} \cdot \frac{(\delta(\mathbf{x}) - \mu_{\delta|e,m}(\mathbf{x}))^2}{\sigma_{\delta|e,m}^2(\mathbf{x})}\right),$$

where C is any constant, then

$$p(\delta(\mathbf{x}) | \mathbf{y}^e, \mathbf{y}^m) \propto \left(1 + \frac{1}{2\alpha_\delta + n_e} \cdot \frac{(\delta(\mathbf{x}) - \mu_{\delta|e,m}(\mathbf{x}))^2}{\sigma_{\delta|e,m}^2(\mathbf{x})}\right)^{-\frac{1+2\alpha_\delta+n_e}{2}},$$

which implies that $\delta(\mathbf{x}) | \mathbf{y}^e, \mathbf{y}^m$ has a noncentral t distribution with degree of freedom $2\alpha_\delta + n_e$, noncentrality parameter $\mu_{\delta|e,m}(\mathbf{x})$, and scale parameter $\sigma_{\delta|e,m}(\mathbf{x})$.

Expanding γ gives

$$\begin{aligned}
\gamma &= \gamma_\delta + \frac{1}{2} \left[(\mathbf{y}^e - \mathbf{y}_{n_e}^m)^T \mathbf{B} (\mathbf{y}^e - \mathbf{y}_{n_e}^m) + \mathbf{b}_\delta \mathbf{V}_\delta^{-1} \mathbf{b}_\delta \right] \\
&+ \frac{\delta^2(\mathbf{x}) - 2\mathbf{r}_\delta^T(\mathbf{x}) \mathbf{B} (\mathbf{y}^e - \mathbf{y}_{n_e}^m) \cdot \delta(\mathbf{x}) + [\mathbf{r}_\delta^T(\mathbf{x}) \mathbf{B} (\mathbf{y}^e - \mathbf{y}_{n_e}^m)]^2}{2[1 - \mathbf{r}_\delta^T(\mathbf{x}) \mathbf{B} \mathbf{r}_\delta(\mathbf{x})]} \\
&- \frac{\mathbf{h}^T \mathbf{A} \mathbf{h} \cdot \delta^2(\mathbf{x})}{2[1 - \mathbf{r}_\delta^T(\mathbf{x}) \mathbf{B} \mathbf{r}_\delta(\mathbf{x})]^2} - \left[\frac{\mathbf{h}^T \mathbf{A} \mathbf{v}_\delta}{1 - \mathbf{r}_\delta^T(\mathbf{x}) \mathbf{B} \mathbf{r}_\delta(\mathbf{x})} - \frac{\mathbf{h}^T \mathbf{A} \mathbf{h} \cdot \mathbf{r}_\delta^T(\mathbf{x}) \mathbf{B} (\mathbf{y}^e - \mathbf{y}_{n_e}^m)}{[1 - \mathbf{r}_\delta^T(\mathbf{x}) \mathbf{B} \mathbf{r}_\delta(\mathbf{x})]^2} \right] \delta(\mathbf{x}) \\
&- \frac{\mathbf{v}_\delta^T \mathbf{A} \mathbf{v}_\delta}{2} - \frac{\mathbf{h}^T \mathbf{A} \mathbf{h} \cdot [\mathbf{r}_\delta^T(\mathbf{x}) \mathbf{B} (\mathbf{y}^e - \mathbf{y}_{n_e}^m)]^2}{2[1 - \mathbf{r}_\delta^T(\mathbf{x}) \mathbf{B} \mathbf{r}_\delta(\mathbf{x})]^2} + \frac{\mathbf{h}^T \mathbf{A} \mathbf{v}_\delta \cdot \mathbf{r}_\delta^T(\mathbf{x}) \mathbf{B} (\mathbf{y}^e - \mathbf{y}_{n_e}^m)}{1 - \mathbf{r}_\delta^T(\mathbf{x}) \mathbf{B} \mathbf{r}_\delta(\mathbf{x})}.
\end{aligned}$$

As

$$\begin{aligned}
\mathbf{A} &= \mathbf{A}_\delta - \frac{\mathbf{A}_\delta \mathbf{h} \mathbf{h}^T \mathbf{A}_\delta}{\mathbf{h}^T \mathbf{A}_\delta \mathbf{h} + 1 - \mathbf{r}_\delta^T(\mathbf{x}) \mathbf{B} \mathbf{r}_\delta(\mathbf{x})}, \\
\mathbf{h}^T \mathbf{A} \mathbf{h} &= \frac{1 - \mathbf{r}_\delta^T(\mathbf{x}) \mathbf{B} \mathbf{r}_\delta(\mathbf{x})}{\mathbf{h}^T \mathbf{A}_\delta \mathbf{h} + 1 - \mathbf{r}_\delta^T(\mathbf{x}) \mathbf{B} \mathbf{r}_\delta(\mathbf{x})} \cdot \mathbf{h}^T \mathbf{A}_\delta \mathbf{h}, \\
\mathbf{h}^T \mathbf{A} \mathbf{v}_\delta &= \frac{1 - \mathbf{r}_\delta^T(\mathbf{x}) \mathbf{B} \mathbf{r}_\delta(\mathbf{x})}{\mathbf{h}^T \mathbf{A}_\delta \mathbf{h} + 1 - \mathbf{r}_\delta^T(\mathbf{x}) \mathbf{B} \mathbf{r}_\delta(\mathbf{x})} \cdot \mathbf{h}^T \mathbf{A}_\delta \mathbf{v}_\delta, \\
\mathbf{v}_\delta^T \mathbf{A} \mathbf{v}_\delta &= \mathbf{v}_\delta^T \mathbf{A}_\delta \mathbf{v}_\delta - \frac{(\mathbf{h}^T \mathbf{A}_\delta \mathbf{v}_\delta)^2}{\mathbf{h}^T \mathbf{A}_\delta \mathbf{h} + 1 - \mathbf{r}_\delta^T(\mathbf{x}) \mathbf{B} \mathbf{r}_\delta(\mathbf{x})},
\end{aligned}$$

we have

$$\begin{aligned}
\gamma &= \gamma_\delta + \frac{1}{2} \left[(\mathbf{y}^e - \mathbf{y}_{n_e}^m)^T \mathbf{B} (\mathbf{y}^e - \mathbf{y}_{n_e}^m) + \mathbf{b}_\delta \mathbf{V}_\delta^{-1} \mathbf{b}_\delta - \mathbf{v}_\delta^T \mathbf{A}_\delta \mathbf{v}_\delta \right] \\
&+ \frac{1}{2} \frac{[\mathbf{h}^T \mathbf{A}_\delta \mathbf{v}_\delta + \mathbf{r}_\delta^T(\mathbf{x}) \mathbf{B} (\mathbf{y}^e - \mathbf{y}_{n_e}^m) - \delta(\mathbf{x})]^2}{\mathbf{h}^T \mathbf{A}_\delta \mathbf{h} + 1 - \mathbf{r}_\delta^T(\mathbf{x}) \mathbf{B} \mathbf{r}_\delta(\mathbf{x})}.
\end{aligned}$$

Therefore,

$$\begin{aligned}
\mu_{\delta|e,m}(\mathbf{x}) &= \mathbf{h}^T \mathbf{A}_\delta \mathbf{v}_\delta + \mathbf{r}_\delta^T(\mathbf{x}) \mathbf{B} (\mathbf{y}^e - \mathbf{y}_{n_e}^m) \\
\sigma_{\delta|e,m}^2(\mathbf{x}) &= \frac{Q_\delta^2}{2\alpha_\delta + n_e} \cdot [\mathbf{h}^T \mathbf{A}_\delta \mathbf{h} + 1 - \mathbf{r}_\delta^T(\mathbf{x}) \mathbf{B} \mathbf{r}_\delta(\mathbf{x})]
\end{aligned}$$

where

$$Q_\delta^2 = 2\gamma_\delta + (\mathbf{y}^e - \mathbf{y}_{n_e}^m)^T \mathbf{B} (\mathbf{y}^e - \mathbf{y}_{n_e}^m) + \mathbf{b}_\delta \mathbf{V}_\delta^{-1} \mathbf{b}_\delta - \mathbf{v}_\delta^T \mathbf{A}_\delta \mathbf{v}_\delta$$

Substituting \mathbf{B} and \mathbf{h} into above equations for $\mu_{\delta|e,m}$ and $\sigma_{\delta|e,m}^2$, we have

$$\begin{aligned}
\mu_{\delta|e,m}(\mathbf{x}) &= \mathbf{f}_\delta^T(\mathbf{x}) \mathbf{A}_\delta \mathbf{v}_\delta + \mathbf{r}_\delta^T(\mathbf{x}) (\mathbf{R}_\delta + \tau \mathbf{I}_{n_e})^{-1} (\mathbf{y}^e - \mathbf{y}_{n_e}^m - \mathbf{F}_\delta \mathbf{A}_\delta \mathbf{v}_\delta) \\
\sigma_{\delta|e,m}^2(\mathbf{x}) &= \frac{Q_\delta^2}{2\alpha_\delta + n_e} \cdot \left(1 - \begin{bmatrix} \mathbf{f}_\delta(\mathbf{x}) \\ \mathbf{r}_\delta(\mathbf{x}) \end{bmatrix}^T \begin{bmatrix} -\mathbf{V}_\delta^{-1} & \mathbf{F}_\delta^T \\ \mathbf{F}_\delta & \mathbf{R}_\delta + \tau \mathbf{I}_{n_e} \end{bmatrix}^{-1} \begin{bmatrix} \mathbf{f}_\delta(\mathbf{x}) \\ \mathbf{r}_\delta(\mathbf{x}) \end{bmatrix} \right)
\end{aligned}$$

where

$$Q_\delta^2 = 2\gamma_\delta + (\mathbf{y}^e - \mathbf{y}_{n_e}^m)^T (\mathbf{R}_\delta + \tau \mathbf{I}_{n_e})^{-1} (\mathbf{y}^e - \mathbf{y}_{n_e}^m) + \mathbf{b}_\delta \mathbf{V}_\delta^{-1} \mathbf{b}_\delta - \mathbf{v}_\delta^T \mathbf{A}_\delta \mathbf{v}_\delta.$$

Appendix C. Material characterization data of the Thermal Challenge problem (Chapter

5)

Table C.1 Prior Material characterization data of κ

20°C	250°C	500°C	750°C	1000°C
0.0496	0.0628	0.0602	0.0657	0.0631
0.0530	0.0620	0.0546	0.0713	0.0796
0.0493	0.0537	0.0638	0.0694	0.0692
0.0455	0.0561	0.0614	0.0732	0.0739
0.0483	0.0563	0.0643	0.0684	0.0806
0.0490	0.0622	0.0714	0.0662	0.0811

Table C.2 Prior Material characterization data of ρ

20°C	250°C	500°C	750°C	1000°C
3.76E+05	3.87E+05	4.52E+05	4.68E+05	4.19E+05
3.38E+05	4.69E+05	4.10E+05	4.24E+05	4.38E+05
3.50E+05	4.19E+05	4.02E+05	3.72E+05	3.45E+05
4.13E+05	4.28E+05	3.94E+05	3.46E+05	3.95E+05
4.02E+05	3.37E+05	3.73E+05	4.07E+05	3.78E+05
3.53E+05	3.77E+05	3.69E+05	3.99E+05	3.77E+05

Appendix D. High Fidelity and Low Fidelity models (Chapter 4 and Chapter 7)

Example 1:

HF Model

$$y_1^h(x) = 0.5 \sin[4\pi \sin(x + 0.5)] + (x + 0.5)^2 / 3,$$

$$x \in [0, 1].$$

LF Model

$$y_1^l(x) = 0.5 \sin[4\pi \sin(1.1x + 0.4)] + (1.1x + 0.4)^2 / 3 - 0.2,$$

$$x \in [0, 1].$$

Example 2: (Modified Branin Function)

HF Model

$$y_2^h(x_1, x_2) = y_{branin}(x_1, x_2) - 22.5x_2,$$

$$x_1 \in [-5, 10] \quad x_2 \in [0, 15].$$

LF Model

$$y_2^l(x_1, x_2) = y_{branin}(0.7x_1, 0.7x_2) - 15.75x_2 + 20 \cdot (0.8 + x_1)^3 - 50,$$

$$x_1 \in [-5, 10] \quad x_2 \in [0, 15].$$

where

$$y_{branin}(x_1, x_2) = 10 + [x_2 - 5.1x_1^2 / (4\pi^2) + 5 / (\pi x_1) - 6]^2 + 10 \cos(x_1) [1 - 1 / (8\pi)].$$

Appendix E. Engine Piston Design (Chapter 4 and Chapter 7)

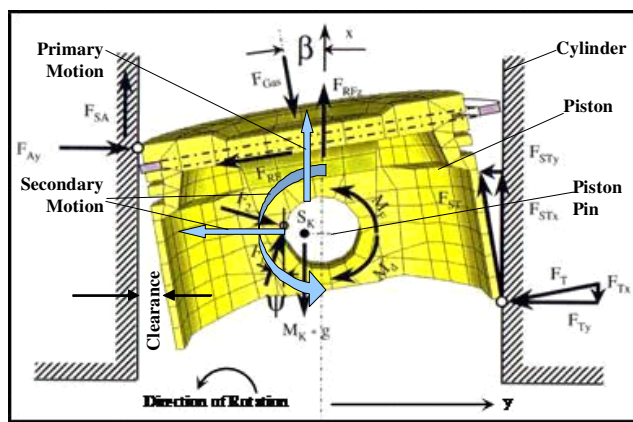


Figure E.1 Engine Piston Design: Piston Secondary Motion and Piston In-Cylinder Forces

Table E.1 Design Variables in Engine Piston Design

Variable	Description	Nominal Value	Lower Bound	Upper Bound	Unit
SL	Skirt Length	23.07	21	25	millimeter
SP	Skirt Profile	3	1	3	/
SO	Skirt Ovality	2	1	3	/
PO	Pin Offset	0.9	0.5	1.3	millimeter

Table E.2 Noise Variables in Engine Piston Design

Variable	Description	Distribution	Mean	STD	Unit
CL	Piston-to-bore Clearance	Normal	50	11	micrometer
LP	Location of Combustion Peak Pressure	Normal	14.5	1	degree

VITA

EDUCATION

Ph.D. Northwestern University, Evanston, IL, USA, 2008

M.S. Huazhong University of Science & Technology, Wuhan, China, 2001

B.S. Huazhong University of Science & Technology, Wuhan, China, 1998

EXPERIENCE

Bank of America, Sept 2008 - present

Researcher and Developer, Fiberhome Telecom Technology Co., China, 2001 – 2004

JOURNAL PUBLICATIONS

Xiong, Y., Chen, W., Tsui, K-L., and Apley, D., “A Better Understanding of Model Updating Strategies in Validating Engineering Models,” *Computer Methods in Applied Mechanics and Engineering*, accepted, 2008.

Xiong, Y., Chen, W., and Tsui, K-L., “A New Variable Fidelity Optimization Framework Based on Model Fusion and Objective-Oriented Sequential Sampling,” *ASME Journal of Mechanical Design*, accepted, 2008.

Chen, W., Xiong, Y., Tsui, K-L., and Wang, S., “Decision Validation Metrics and a Bayesian Procedure for Validating Predictive Models in Engineering Design”, *ASME Journal of Mechanical Design*, 130, 1-9, 2008.

Xiong, Y., Chen, W., Apley, D., and Ding, X., “A Nonstationary Covariance-Based Kriging Method for Metamodeling in Engineering Design”, *International Journal for Numerical Methods in Engineering*, 71(6), 733-756, August 2007.

Xiong, Y., Hu, Y., and Zhao, J., “An Algorithm of Surface Triangulation Based on Mapping and Delaunay Method”, *Journal of Computer-Aided Design & Computer Graphics*, 14, 56-60, 2002.

CONFERENCE PUBLICATIONS

Xiong, F, Xiong Y, Chen, W, “Quasi-LHD Sequential Sampling Method for Computer Experiments with Extension to Multidisciplinary Design”, 12th AIAA/MAO, Sept 10-12, Victoria, Canada, 2008.

Chen S, Xiong Y, Chen, W, “A Level-Set-Based Multistage Metamodeling Approach for Design Optimization”, 49th AIAA/ SDM, Schaumburg, IL, Apr 7-10, 2008.

Xiong, Y., Chen, W., and Tsui, K-L., “A Better Understanding of Model Updating Strategies in Validating Engineering Models,” 49th AIAA/ SDM, Schaumburg, IL, Apr 7-10, 2008.

Xiong, Y., Chen, W., and Tsui, K-L., “A New Variable Fidelity Optimization Framework Based on Model Fusion and Objective-Oriented Sequential Sampling,” DETC2007-35782, ASME Design Technical Conference, Design Automation Conference, Sept 4-7, Las Vegas, NV, 2007.

Xiong, Y., Chen, W., “A New Variable Fidelity Optimization Approach,” 7th World Congresses of Structural and Multidisciplinary Optimization, Seoul, Korea, May 21-25, 2007.

Chen, W., Xiong, Y., and Tsui, K-L., and Wang, S., “Some Metrics and a Bayesian Procedure for Validating Predictive Models in Engineering Design,” DETC2006-99599, ASME Design Technical Conference, Design Automation Conference, Philadelphia, PA, Sept 10-13, 2006.

Xiong, Y., Chen, W., Apley, D., and Ding, X., “A Nonstationary Covariance Based Kriging Method for Metamodeling in Engineering Design,” AIAA-2006-7050, AIAA/ISSMO Multidisciplinary Analysis and Optimization Conference, Portsmouth, VA, Sept 6-8, 2006.

MEMBERSHIPS

American Society of Mechanical Engineering

American Institute of Aeronautics and Astronautics